

Rowan University

Rowan Digital Works

Theses and Dissertations

9-1-2016

Structural and dynamic analysis of wild and splice variants human μ -opioid receptors in complex with Morphine and IBNtxA and human topoisomerase II alpha mutational basis of Amsacrine resistance

Safaa Sader
Rowan University

Follow this and additional works at: <https://rdw.rowan.edu/etd>



Part of the [Pharmacy and Pharmaceutical Sciences Commons](#)

Recommended Citation

Sader, Safaa, "Structural and dynamic analysis of wild and splice variants human μ -opioid receptors in complex with Morphine and IBNtxA and human topoisomerase II alpha mutational basis of Amsacrine resistance" (2016). *Theses and Dissertations*. 2151.

<https://rdw.rowan.edu/etd/2151>

This Thesis is brought to you for free and open access by Rowan Digital Works. It has been accepted for inclusion in Theses and Dissertations by an authorized administrator of Rowan Digital Works. For more information, please contact graduateresearch@rowan.edu.

**STRUCTURAL AND DYNAMIC ANALYSIS OF WILD AND SPLICE
VARIANTS HUMAN μ -OPIOID RECEPTORS IN COMPLEX WITH
MORPHINE AND IBNTXA AND HUMAN TOPOISOMERASE II ALPHA
MUTATIONAL BASIS OF AMSACRINE RESISTANCE**

by

Safaa Zahi R. Sader

A Thesis

Submitted to the
Department of Chemistry and Biochemistry
College of Science and Mathematics
In partial fulfillment of the requirement
For the degree of
Master of Science in Pharmaceutical Sciences
at
Rowan University
July 1, 2016

Thesis Chair: Chun Wu, Ph.D.

© 2016 Safaa Zahi R. Sader

Dedication

I would like to dedicate my thesis work to my uncle Bassam who was my mainstay during Master degree years. He was my source of inspiration throughout my study period and his persistent encouragement pushed me toward achieving my goals through hard work and perseverance.

Acknowledgments

I would like to express my deep appreciation to my research advisor Dr. Chun Wu. The time and efforts he dedicated had had a great impact on my success and performance. His continuous encouragement and insightful comments contributed to build my critical thinking skills and build nascent skills to be future scientist. In addition, I would like to thank my thesis committee Dr. Subash Jonnalagadda and Dr.Lark Perez for their valuable insights on my thesis content and format. Finally, I would like to thank Rowan University department of chemistry and biochemistry faculty members for the opportunity they provided to audit some of their valuable classes.

This work was supported by Rowan Startup and SEED grant and the National Science Foundation under Grant NSF ACI-1429467 and XSEDE MCB160004.

Abstract

Safaa Zahi R. Sader

STRUCTURAL AND DYNAMIC ANALYSIS OF WILD AND SPLICE VARIANTS
HUMAN μ -OPIOID RECEPTORS (G1 & G2) AND AMSACRINE RESISTANCE IN
HUMAN TOPOISOMERASE II ALPHA MUTANTS

2015-2016

Dr. Chun Wu, Ph.D.

Master of Science in Pharmaceutical Sciences

Morphine prescribing is limited by its high addiction tendency and other serious effects. Recent animal's biological studies on Mu 6TM splice variants, which mainly include G1, G2 and Mu3, supported a high safety and potency profiles of IBNtxA as potential alternative of Morphine. Nevertheless, there is no high-resolution structures of these 6TM variants, and the detailed structural features and dynamic characteristics of these splice variants remain elusive. We applied homology modeling and MD simulation to probe the structural, dynamic and ligand binding differences between the wild type (7TM) and two major truncated 6TM variants (G1 and G2). MD results underscored important structural and dynamic differences between these receptors as well as prioritized ligand affinity toward each receptor. The second project in this thesis involves in silico analysis of mutational basis of Amsacrine resistance. Both R487K and E571K mutations were studied. MD results indicated significant weakening of Amsacrine affinity in two mutants in a consistent manner with the previous biological degree of resistance of two mutants. Additionally, the intercalation loss and ligand ternary complex coordinate changes were also revealed by MD simulation as possible causes of resistance.

Table of Contents

Abstract	v
List of Figures	ix
List of Tables	x
Chapter 1: Introduction to Computational Drug Design.....	1
1.1. Computational Methods Used in This Thesis	2
1.1.1. Bioinformatics	2
1.1.2. Homology Modeling and Sequence Alignment.....	2
1.1.3. Molecular Docking	2
1.1.4. Binding Energy Calculations	4
1.1.5. Molecular Dynamic Simulations	6
Chapter 2: Structural and Dynamic Analysis of Wild and Splice Variants μ -Opioid Receptors in Complex with Morphine and IBNtxA by Homology Modeling, Docking and All Atoms Molecular Dynamic Simulation with Explicit Membrane.....	8
2.1 Introduction.....	8
2.2 Computational Methods.....	14
2.2.1 Homology Modeling of Receptors	14
2.2.2 Glide Docking	15
2.2.3 Molecular Dynamic Simulations	16
2.2.4 Binding Energy Calculations and Decompositions Methods	18
2.3 Results.....	19
2.3.1 Homology Modeling.....	19
2.3.2 XP Glide Docking.....	20
2.3.3 Ligand Binding Energy Calculations.....	21

Table of Contents (Continued)

2.3.4 Morphine and IBNtxA Binding Poses	23
2.3.5 Morphine and IBNtxA Ligand 2D Interaction Data	24
2.3.6 Receptors Secondary Structures Data	27
2.3.7 Receptors Dynamic Responses for the Same Ligand	29
2.3.8 Ligand Fluctuation (L-RMSF)	32
2.4 Discussion and Conclusion	33
Chapter 3: Computational Analysis of Amsacrine Resistance in htop2 α Enzyme Mutation Using Homology Modeling and Molecular Dynamic Simulation	41
3.1 Introduction	41
3.2 Computational Materials and Methods	44
3.2.1 Human Topoisomerase II α Structure Homology Modelling	44
3.2.2 Molecular Dynamic (MD) Simulations	44
3.2.3 Binding Energy Calculations and Decompositions	46
3.3 Results	47
3.3.1 Amsacrine Binding Energy Calculations	47
3.3.2 Amsacrine Binding Poses and 2D Interaction Diagram	48
3.3.3 Amsacrine-DNA Intercalation Changes	51
3.3.4 Enzyme Protein C α RMSF Analysis	54
3.3.5 Ligand Conformational Change (L-RMSF)	55
3.4 Discussion and Conclusion	56
References	61
Appendix A: Supporting Material (Chapter 2)	69

Appendix B: Supporting Material (Chapter 3)89

List of Figures

Figure	Page
Figure 1. (A) Definition of Core and Rotamer Groups (B) Ligand Diameter and Center Definitions (C) Glide Docking “Funnel”, Showing the Glide Docking Hierarchy.	3
Figure 2. Chemical Structures of Morphine and IBNtxA.....	9
Figure 3. Abbreviated Sequences of Human MOR-1 (hMOR-1) Splicing Variants	11
Figure 4. Homology Models of (A) Full Length 7TM hMOR-1 Receptor, (B) Truncated hMOR-1G2 and (C) hMOR-1G1.....	20
Figure 5. Superposition of the Most Abundant Complexes from the Simulations	24
Figure 6. Protein Secondary Structure Profile of Three Receptors Complexes with IBNtxA.....	28
Figure 7. RMSF Diagrams of Receptor Protein C- α	31
Figure 8. RMSF Diagrams of Receptor Protein C- α	32
Figure 9. Ligand RMSF Diagrams of Morphine Binding to Three Different Receptors.....	33
Figure 10. A Schematic Detailed Atom Interaction with Protein Residues Comparison.....	37
Figure 11. Structure of Amsacrine (A), Amsacrine-Top2 α Complex (B) and Amsacrine-DNA Complex(C)	43
Figure 12. Representatives of the Most Abundant Structure Families of the Three Complexes.....	51
Figure 13. Amsacrine-DNA Intercalation Changes of the R487 (B1, B2) and E571K(C) Mutations Compared to Wild Type (A).	53
Figure 14. Protein C α RMSF Diagrams of hTop2 α WT and Mutants upon Amsacrine Binding.....	54
Figure 15. Average Ligand RMSF for the Three Complexes.....	56

List of Tables

Table	Page
Table 1. MOR-1 Knockout Mouse Models and Opioid Analgesia	13
Table 2. MMGB-SA Binding Energies for Both Morphine and IBNtxA Complexes with the Three Receptors	22
Table 3. Morphine 2D Interaction Table with Three Different Receptors.....	26
Table 4. Average MM-GBSA Binding Energies of Amsacrine with hTOP2a WT and Mutants (kcal/mol).....	48
Table 5. Interacting Residues with Amsacrine	50

Chapter 1

Introduction to Computational Drug Design

Currently, developing new drug can cost approximately US 1.0 -1.9 billion.(1) This cost mainly because the company need to synthesize and make thousands of compounds to find the desired hit compound. Computational drug design and molecular modelling offers enormous opportunity in pharmaceutical research due to precision and cost effectiveness of algorithms used in these methods. The recent burst in bioinformatics, genomics and structural information data had discovered plethora of new targets and ligands. Considering the rapidly emerging new diseases and the cost and effort imposed by traditional drug design and development, computational tools can provide fast and reliable prediction of the pharmacological properties pertaining to ligand and target.(2)

Drug discovery process is research intensive, time consuming and required exorbitant funding resources. (2)Traditionally, the HTS is the widely used screening method used by pharmaceutical companies where compounds synthesized and screened against certain target via assay based tests. However, when it comes to testing millions of compounds and the fact that many hits get stalled during clinical trials due to poor pharmacokinetics profile or unwanted side effects, this traditional process becomes heavy financial burden endured by the company and the cost of this research often transferred to the patient.

Computer aided drug design employs different methodologies to explore the biological processes and most importantly the ligand –protein binding. Some of methods involves Bioinformatics tools, which provides the sources of data, required to start computational jobs. For instance, homology modeling and sequence alignment of new

and existing targets is of pivotal importance in target validation and characterization. Other tools involve ligand –protein binding energy determination and visualization which will be discussed in this chapter.

1.1 Computational Methods Used in this Thesis

1.1.1 Bioinformatics. Bioinformatics combines computer science, statistics and mathematics, to analyze and interpret biological data. It has several applications in drug design such as sequence alignment and analysis and homology modeling.

1.1.2. Homology modeling and sequence alignment. This technique is extremely important in predicting the protein structure if the experimental X-ray crystallography is not available. Furthermore, it is useful in refining the experimental structure obtained through the crystallography or NMR to provide more precise structure coordinates that can be further used for docking and simulation. Example tool is *Prime (Schrodinger)* is a powerful and complete tool for generating accurate receptor models for structure based drug design. Another function of Prime is sequence alignment of two or multiple protein sequences and gives an accurate prediction of degree of homology between the sequences from different species. This is crucial in structural modelling of new target when desired species' crystal structure is only available for other species. For example modelling desired human receptor based on experimentally available crystal structure of Mouse receptor.

1.1.3. Molecular docking. Considered is essential tool in computer aided drug design that aims to generate an accurate ligand-receptor complex structure especially when the crystal structure is not resolved. Successful protein-ligand docking depends on exhaustive exploration of space and effective scoring. Glide docking conducts complete

systematic search of conformational, orientational and positional space of the docked ligand as can be seen in (figure 1).

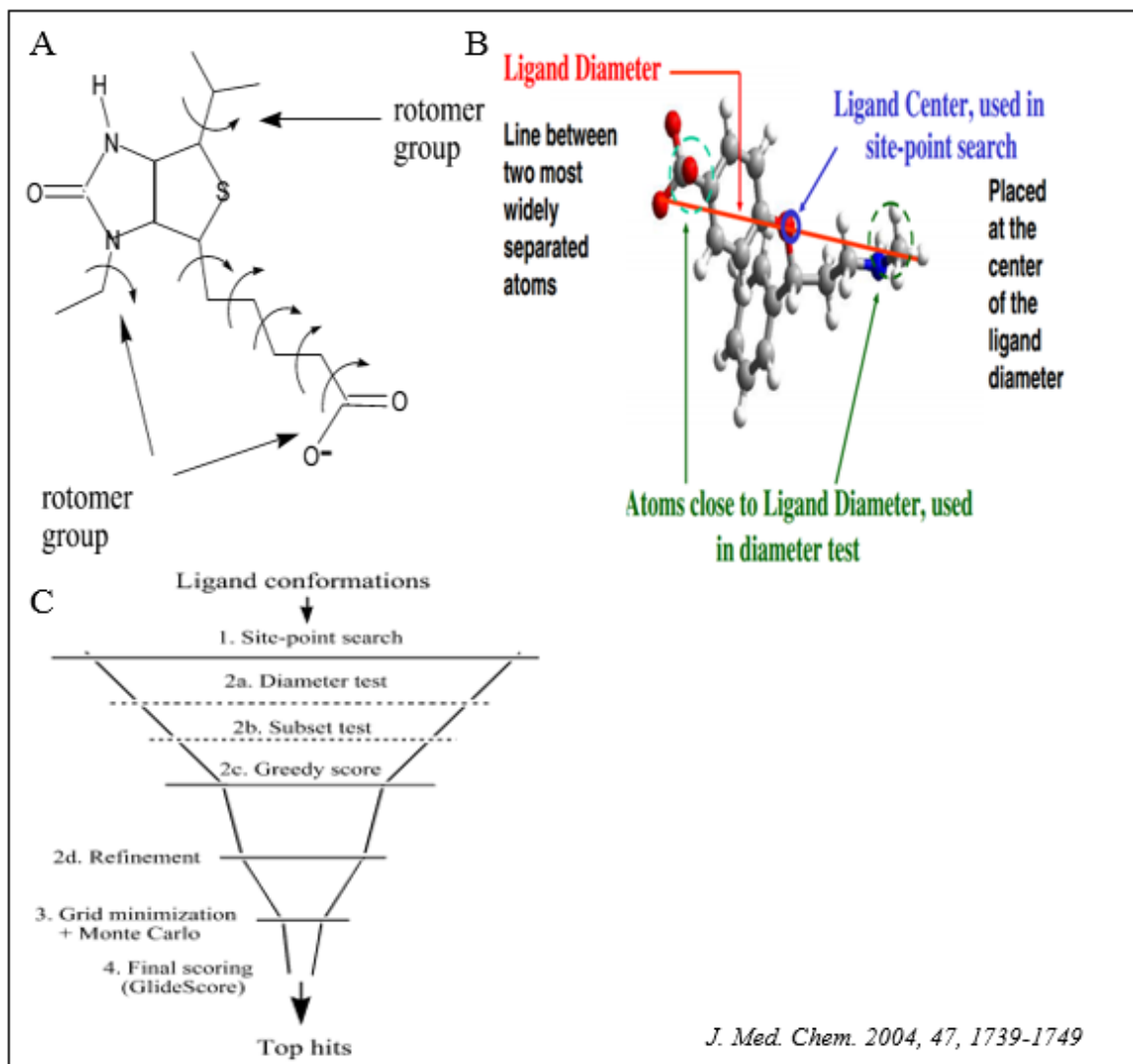


Figure 1. (A) Definition of core and rotamer groups (B) Ligand diameter and center definitions (C) Glide docking “funnel”, showing the Glide docking hierarchy.

Applications.

1. Ligand-protein complex construction.
2. Binding affinity calculations.
3. Drug discovery and lead optimization.
4. Virtual high throughput screening.

1.1.4 Binding energy calculations. In biological systems, ligands are continuously binding and dissociating from the proteins as indicated by the following chemical equation:



There are many methods to measure the ligand –protein binding affinity .Most or all depends on measuring the binding as function of concentration of ligand or protein. For example enzyme inhibition essays, Isothermal titration calorimetry (ITC) and other essays. The binding reaction can also be analyzed in thermodynamics terms involving free energy, enthalpy and entropy. For binding reaction at constant pressure, the standards Gibbs free energy is given by:

$$\Delta G^\circ = -RT \ln K_B$$

Moreover, this energy change can be broken down into energetic and entropic terms as follow:

$$\Delta G^\circ = \Delta H - T\Delta S^\circ$$

Since ($H=E+PV$) and P & V hardly change at biological systems:

$$\Delta G^\circ \approx \Delta E - T\Delta S$$

ΔE can be averaged over the range of molecular conformations that the free and bound molecules explore due to thermal motions. Thus, the energy can be broken into number of

contributions including, electrostatic interactions among charged and dipolar chemical groups, hydrophobic interactions and intrinsic energetics of rotatable bonds.

Developing an effective binding-free energy scoring function.

(OPLS-AA) Force fields development and parameterizations(3). Force field calculates the molecular system potential energy as a sum of individual energy terms:

$$E = E_{\text{covalent}} + E_{\text{noncovalent}}$$

$$E_{\text{covalent}} = E_{\text{bond (Stretching)}} + E_{\text{angle (Bending)}} + E_{\text{(dihedral)}}$$

$$E_{\text{noncovalent}} = E_{\text{electrostatic}} + E_{\text{van der Waals}}$$

Force field based scoring function with implicit solvent (MM-GBSA). MM-GBSA(4) stands for the Molecular Mechanics Generalized Born Surface Area. It is fastest force-field based energy calculation obtained from energy difference between complex and unbound ligand and protein. It combines the molecular mechanics terms from force field with the solvation energy terms (implicit solvent), however, it lacks the entropy term as follows:

$$\begin{aligned} \Delta G &= \Delta E_{MM}^1 + \Delta G_{\text{solv}}^2 - T \Delta S \\ &= \Delta E_{\text{bat}}^3 + \Delta E_{\text{vdW}} + \Delta E_{\text{coul}} + \Delta G_{\text{solv}, p} \\ &\quad + \Delta G_{\text{solv}, np} - T \Delta S \end{aligned}$$

¹ ΔE_{MM} : gas phase molecular mechanics energy

² ΔG_{solv} : polar and nonpolar terms

³ E_{bat} : covalent energy (bonds, angle, torsion).

XP Glide docking and scoring. XP glide score (5) is a novel semi empirical scoring function that uses unique water desolvation energy terms. Furthermore, new protein-ligand structural binding terms to enhance prediction. The scoring function and docking protocol were developed to reproduce the experimental binding affinities for a set of 198 complexes (RMSD of 2.26 and 1.73 Kcal/mol) over all and well docked ligands respectively.

$$XP\ Glide\ Score = \Delta E_{coul} + \Delta E_{vdW} + E_{bind} + E_{penalty}$$

$$E_{bind} = E_{hyd_enclosure}^4 + E_{hb_nn_motif}^5 + E_{hb_cc_motif}^6 + E_{pi}^7 +$$

$$E_{hb_pair} + E_{phobic_pair}$$

$$E_{penalty} = E_{desolv} + E_{ligand_strain}$$

1.1.5 Molecular dynamic simulations. This is one of the principal tools in theoretical Biological activity. It measures time dependent interaction between biological molecules such as protein-protein ligand-protein and ligand-DNA. MD simulation generates information at the microscopic level including atomic positions and velocities. Thus, it helps to visualize the macroscopic properties of system via microscopic simulation. For example, to calculate changes in the binding free energy of a particular drug, or to examine the energetics and mechanisms of conformational change.

Biological Applications includes:

- Protein stability
- Conformational changes
- Protein folding

⁴ $E_{hyd_enclosure}$: hydrophobic Enclosure

⁵ $E_{hb_nn_motif}$: is the hydrogen bonds neutral-neutral motifs

⁶ $E_{hb_cc_motif}$: hydrogen bonds charged-charged motif

⁷ E_{pi} : pi stacking and pi-cation interactions

- Molecular recognition: protein, DNA membrane.
- Ion transport
- Drug design and structure determination of X-ray and NMR structures.

The molecular dynamics simulation method is based on Newton's second law or the equation of motion, $F_i = m_i \cdot a_i$. From a knowledge of the force on each atom, it is possible to determine the acceleration of each atom in the system. Integration of the equations of motion then yields a trajectory that describes the positions, velocities and accelerations of the particles as they vary with time. From this trajectory, the average values of properties can be determined. Once the positions and velocities of each atom are known, the state of the system can be predicted at any time in the future or the past. Molecular dynamics simulations can be time consuming and computationally expensive. However, computers are getting faster and cheaper. Simulations of solvated proteins are calculated up to the nanosecond time scale; however, simulations into the millisecond regime have been reported.

Chapter 2

Structural and Dynamic Analysis of Wild and Splice Variants μ -Opioid Receptors in Complex with Morphine and IBNtxA by Homology Modeling, Docking and All Atoms Molecular Dynamic Simulation with Explicit Membrane

2.1 Introduction

Opioid drugs are a critical class of medications to treat acute and chronic pain, a serious and costly public health issue (6-9). The prototypical opioid analgesic morphine (Fig. 1A) is on the WHO Model List of Essential Medicines, the most important medications needed in a basic health system. However, the safety and tolerability of opioid analgesics is severely restricted due to side effects including sedation, constipation, abuse liability and respiratory depression (10-14). The constipating effects (15) in particular are common with chronic opioid use and can be dose-limiting, resulting in inadequate pain relief (16), particularly in cancer pain management. Opioid misuse and abuse is currently recognized as a major public health emergency, often referred to as the “opioid epidemic” (17-19). Thus, based on the very large public health need for effective analgesics, and substantial limitations confronting current prescription opioids, there is pressing need for the development of novel opioid analgesics with more precisely targeted mechanisms of action.

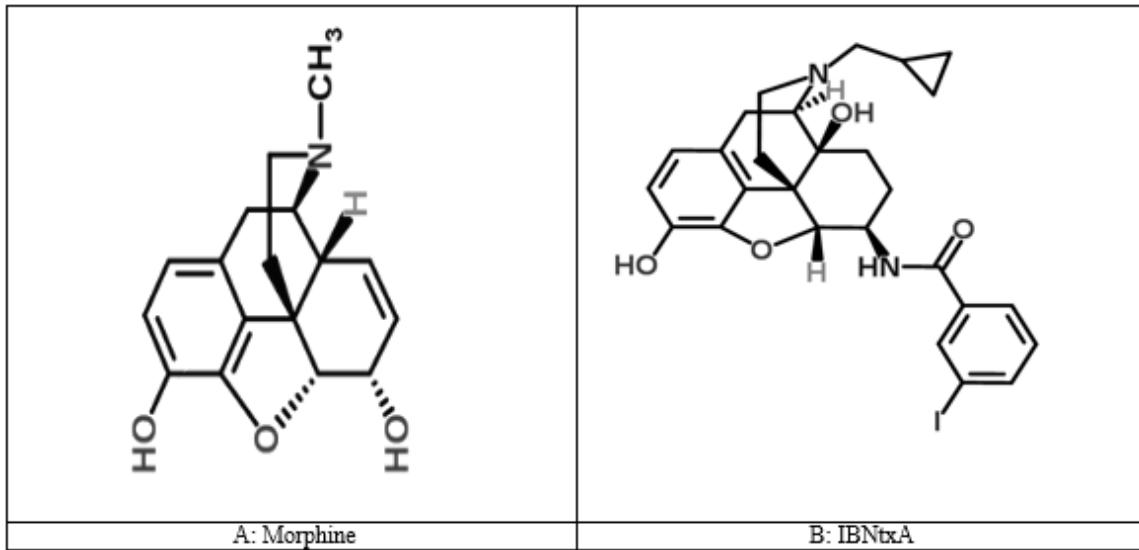


Figure 2. Chemical structures of morphine and IBNtxA.

Mu opioid receptor (MOR) are selectively activated by morphine, and most opioid analgesics exert their effects via MOR signaling (20). MOR is a member of the G-protein coupled receptor (GPCR) family, which is the largest and most diverse group of membrane receptors, targets for a large proportion of drugs currently used in medicine. Structurally, GPCRs all contain seven transmembrane (TM) domains with an extracellular N-terminus and an intracellular C-terminus. Classically, once an agonist binds, a conformational change in the receptor activates the α subunit of G-protein, which exchanges GTP in place of GDP, causing the dissociation of the α subunit, the $\beta+\gamma$ dimer, and the receptor. Agonist binding to MOR-1 (e.g., by morphine), a $G_{\alpha i/o}$ -coupled GPCR (21), induces suppression of adenylyl cyclase activity via the activated $G_{\alpha i/o}$ subunit, thereby reducing intracellular cyclic AMP (cAMP) concentrations. The free $\beta+\gamma$ dimer can activate G protein-coupled inwardly rectifying potassium (GIRK) channels, altering

cell membrane potentials. Additionally, MOR-1 has a dissociable signaling mechanism via β -arrestin (22-26).

Since the cloning of the MOR gene, *Oprm1*, multiple splice variants have been discovered. (27-31) The primary MOR variant, MOR-1, has been widely studied and its high-resolution crystal structure has been obtained (32). In MOR-1, the TM domains form a circular structure with the opioid-binding pocket located deep within the TM region of the receptor (Fig. 3). *Oprm1* splice variants include a variety of 3' and 5' splicing modifications, with similar patterns seen across a wide range of species, including humans, rats, and mice (10). Three major sets of splice variants have been identified. The first set are classical full-length variants, with all 7 TM domains, in which 3' splicing leads to changes in only the tip of the intracellular tail; these modifications may play important role in biased agonism (33). Because the remainder of these full-length variants is the same, including all 7 TM domains, they should contain nearly identical ligand-binding pockets. The second set of splice variants involves exon skipping, producing only final protein products that contain a single TM domain. Although these variants do not bind opioids directly, they help modulate opioid analgesia by increasing expression of the full-length 7 TM variants through a chaperone-like action (34). The final set of splice variants—and the focus of this research involves exon 11 and its promoter, located about 30 k bases upstream of exon 1. These variants include exon 11 to the exclusion of exon 1, and thus are presumed to lack the first TM (TM1) domain that exon 1 encodes, resulting in a truncated N-terminus (Fig. 2). Due to this truncation, these MOR variants have been described as containing only 6 TM domains (35-37). Three MOR variants (G1/1K/Mu3) completely lack the putative TM1 sequence, while the

G2 variant retains only a small segment of the TM1 domain sequence. The complete or partial absence of TM1 may change the ligand-receptor interaction, and thus opioid analgesics. Indeed, the opioid analgesics profile of these truncated 6 TM/exon 11 (6TM/E11) variants is quite different from the full-length MOR-1, providing a target for new agents with unique pharmacologic properties.

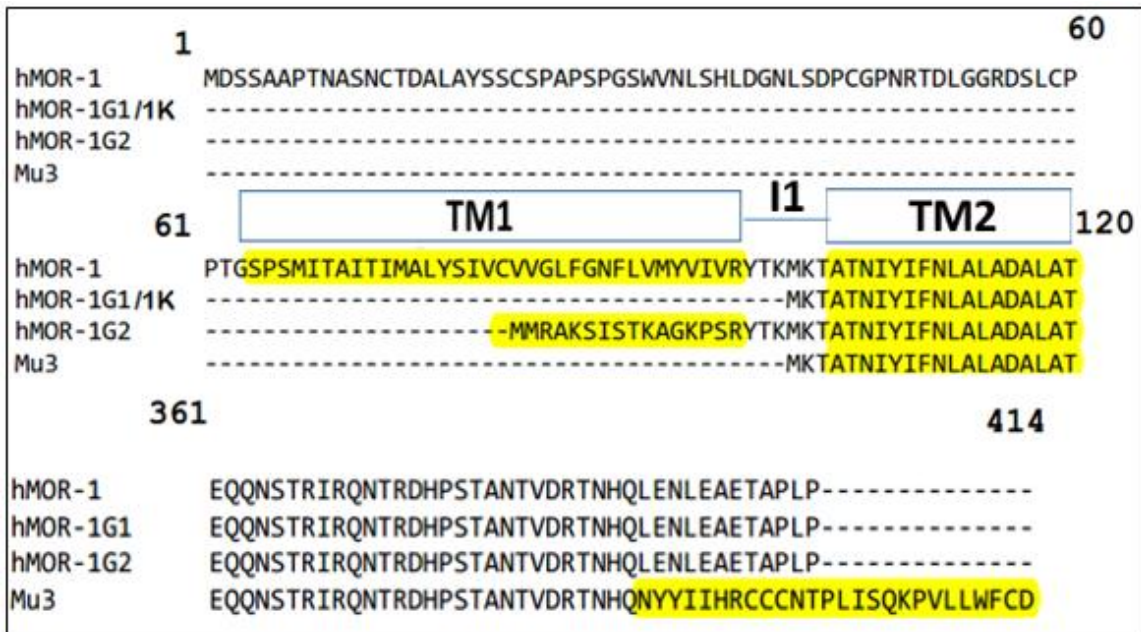


Figure 3. Abbreviated sequences of human MOR-1 (hMOR-1) splicing variants. Transmembrane domains (TM1 and TM2) are highlighted in yellow. Residues 121-360 are not shown, as they are identical for all variants (see supporting info).

Various MOR-1 knockout mice models have provided important insights into pharmacological profiles of the different splice variants (10). Two models in particular are valuable: one MOR-1 knockout targeting exon 1, but still expressing exon 11-containing

6 TM truncated variants (38), and an exon 11 knockout that lacks the 6TM variants without appreciable changes in the expression levels of the full-length variants (39). These two knockout models reveal different profiles of activity for different opioids (Table 1). Based on the results of these studies, the analgesic effects of morphine are totally dependent on the full-length MOR-1 and but unaffected by loss of the 6-TM variants. Alternatively, the experimental drug 3-iodobenzoyl-6-naltrexamide (IBNtxA; Fig. 1), a potent analgesic in wild-type mice (40), is unaffected by the loss of the full-length MOR-1 splice variants (or delta and kappa1 receptors), but loss of the exon 11 variants removes its activity. This indicates that IBNtxA activity is primarily mediated through its binding to 6TM/E11 MOR variants. Furthermore, IBNtxA is a potent analgesic with an unusual pharmacologic profile. It is not only 10-fold more potent than that of morphine (40,41), but also active in neuropathic/inflammatory pain models, which is unusual for opioids (10). This is particularly useful in cancer pain management since much of it is neuropathic in nature. Its adverse effect profile is also very attractive: IBNtxA shows limited respiratory depression, reduced gastrointestinal slowing, and no measurable abuse liability in a conditioned place preference experiment, and does not produce physical dependence with chronic administration. These results raise the hope that it might be possible to dissociate opioid analgesia from side effects and abuse liability. Thus, targeting 6TM variants may yield important new analgesics in the future. However, there is no high-resolution receptor/complex structure of the 6TM/E11 MOR variants with morphine/IBNtxA, and it is not clear how the receptor truncation alters the ligand binding properties of these receptors. In this study, we aim to decipher the

structural and dynamic differences between splice variants and wild type when binding to morphine and IBNtxA.

Table 1

MOR-1 knockout mouse models and opioid analgesia.

Properties	Exon 1 knockout ^a	Exon 11 knockout ^b
Mu receptor		
7 TM variants	Lost	Retained
6 TM variants	Retained	Lost
Analgesia		
Morphine	Lost	Retained
IBNtxA	Retained	Lost

^a Schuller *et al.* (38) ^b Pan *et al.* (39)

We applied homology modeling and MD simulations to understand the how truncated and wild type receptors responded to Morphine and IBNtxA activations. Our model was based on crystal structure of Mu-receptor bound to Morphinan antagonist (2.8 Å) as a template to construct the two splice variants G1 and G2 receptors as well as Mu receptor wild type . The final homologs were obtained from GPCR-I-TASSER server (42). Furthermore, we utilized Glide XP docking to dock Morphine and IBNtxA into wild type and splice variants. Using the complexes from Xp docking, we constructed six model systems of morphine and IBNtxA docked into three receptors and performed 100 ns MD simulations using consistent conditions for all six complexes. Results of 2D interactions, protein C α RMSFs and RMSDs data where supporting the premise that

morphine and IBNtxA have completely different binding pockets and each one activated its native wild type and related splice variant receptors differently. Predicted binding energy calculations showed Morphine prioritize its wild type Over G1 and G2 .On the other hand, IBNtxA showed higher affinity toward its wild type (G1) and 7TM compared to G2. The 2D interaction comparisons among the three receptors complexes provided additional evidence that splice variants interact with each ligand using different binding pocket as indicated by genetic numbering. Collectively, truncated splice variants responded differently from canonical Mu receptor, which provided new opportunities of developing safe and effective morphine alternatives as indicated by in vivo and computational results of G1 receptor modeling and IBNtxA pharmacological characterizations data.

2.2 Computational Methods

2.2.1 Homology modeling of receptors. The FASTA sequences files of hMOR-1, hMOR-1G1 and hMOR-1G2 were obtained from the Uniprot website(43). GPCR-I-TASSER online service(42)was used to build their homology models . Out of five homology models for each receptor obtained from the GPCR-I-TASSER online service, the top 1 model was used in this study. The following PDB structures were used as templates for building homology models by GPCR-I-TASSER: human delta opioid 7TM receptor (PDB ID: 4N6H), Mu-opioid receptor in complex with a Morphinan antagonist (PDB ID: 4DKL), chimeric protein of 5-HT1B-BRIL in complex with ergotamine (PDB ID: 4IAR) and human delta opioid 7TM receptor (PDB ID: 4N6H).

2.2.2 Glide docking.

Ligand preparation. The 3D structure of morphine and IBNtxA were prepared using Maestro Elements. The 2D structures of morphine and IBNtxA were drawn using the 2D sketcher. Then after, the ionization/tautomeric states were generated at pH=7 using the Epik which is based on the more accurate Hammett and Taft methodologies(44). Only lowest ionization/tautomeric states were selected. Restrained minimization was used to relax the ligand structure.

Protein structure preparation. Protein structures were prepared using Schrodinger maestro protein preparation Wizard.(44) The charge state of preprocessed protein was optimized at pH=7. Finally restrained minimization was performed to relax the protein structure using OPLS3 force field (45).

Ligand docking. The binding sites of the prepared receptors were identified using “binding site detection” module of Maestro. The site that is close to the N-terminal binding pocket was used for docking, and the prepared ligands were docked into the N-terminal pocket using Glide XP scoring function with default procedures and parameters (5,46). In details, the receptor grid required for docking process was generated using Van der Waals scaling factor of 1 and partial charge cutoff 0.25. Docking was performed using a ligand-centered grid using OPLS3 force field. Glide XP Dock performed a comprehensive systematic search for the best receptor conformations and orientations to fit the ligand. The docking results are included in Figure S2 of the supporting material.

2.2.3 Molecular dynamic simulations. All six molecular dynamic simulation systems were constructed using the prepared receptor-ligand complexes from the XP docking. Each system was placed in a membrane of POPC lipids (47), and solvated in an orthorhombic water box with a buffer distance of 8Å using SPC water model (48). System was neutralized using Na⁺ ions, and was added with a salt concentration of 0.15 M NaCl. OPLS3 force field (45) was used to represent the receptor-ligand.

Relaxation and production runs. Using Desmond module, the system was first relaxed using the default relaxation protocol for membrane proteins (49). This relaxation protocol consists of eight stages: 1). Minimization with restraints on solute heavy atoms; 2) Minimization without any restraints; 3). Simulation with heating from 0 K to 300 K, H₂O barrier and gradual restraining; 4). Simulation under the NPT ensemble (constant number of particles, constant pressure of 1 bar and constant temperature of 300 K, Martyna-Tuckerman-Klein Nosé-Hoover chain coupling scheme (50) with H₂O barrier and with heavy atoms restrained; 5) Simulation under the NPT ensemble with equilibration of solvent and lipids; 6). Simulation under the NPT ensemble with protein heavy atoms annealing from 10.0 kcal/mol to 2.0 kcal/mol; 7). Simulation under the NPT ensemble with Ca atoms restrained at 2 kcal/mol; and 8). Simulation for 1.5 ns under the NPT ensemble with no restraints. After the relaxation, a 100.0 ns production run was conducted under the NPT ensemble for each of the six systems using the default protocol. M-SHAKE (51) was applied to constrain all bonds connecting hydrogen atoms, enabling a 2.0 fs time step in the simulations. The k-space Gaussian split Ewald method (52) was used to treat long-range electrostatic interactions under periodic boundary conditions (charge grid spacing of ~1.0 Å, and direct sum tolerance of 10⁻⁹). The cutoff distance for

short-range non-bonded interactions was 9 Å, with the long-range van der Waals interactions based on a uniform density approximation. To reduce the computation, non-bonded forces were calculated using an r-RESPA integrator (53) where the short range forces were updated every step and the long range forces were updated every three steps. Temperature was controlled using the Martyna-Tuckerman-Klein Nosé-Hoover chain-coupling scheme with a coupling constant of 1.0 ps. The trajectories were saved at 40.0 ps intervals for analysis.

Convergence of simulation. Convergence of simulation were inspected using the root mean square deviation (RMSD) of the protein C α atoms as a measure of system equilibration. Protein RMSD is calculated as an average change of displacement of selection of atoms for particular frame with respect to particular frame relative to the initial frame structure. RMSD plots are shown in Figure S3 of the supporting material.

Receptor-ligand interaction analysis. Detailed receptor-ligand interaction was analyzed using Simulation Interaction Diagram module of Maestro. The results are included in Figure S7-S15 of the supporting material.

Trajectory clustering analysis. Protein backbone RMSD matrix was used in hierarchical cluster average linkage method (54) to group the complex structures of the simulation trajectory for each system. The merging distance cutoff used was set to be 2Å. The centroid structure (i.e. the structure having the largest number of neighbors in the structural family) was used to represent the family. The centroid structures of populated structural families (>1% of total structure population) are shown in Figure S5-S6 of the supporting material.

2.2.4 Binding energy calculations and decompositions methods. Molecular Mechanism-General Born Surface Area (MM-GBSA) binding energies were calculated for frames of the last 20ns of trajectory. VSGB 2.0 with implicit membrane model (4) was used based on OPLS3 force field. The stepwise energy calculations as follows: (1) Receptor alone (minimization). (2) Ligand alone (minimization). (3) Receptor-ligand complex (minimization) (4) Ligand extracted from optimized receptor-ligand complex (energy calculation) (5) Receptor extracted from optimized receptor-ligand complex (energy calculation). MMGBSA binding energy decompositions in this study, we merge the original terms (Coulombic + H-bond + GB solvation + van der Waals + pi-pi packing + self-contact + lipophilic) (55) into three components: $E_{\text{electrostatics}}$, E_{vdW} , and $E_{\text{Lipophilic}}$, where $E_{\text{electrostatics}} = (E_{\text{bond}} + E_{\text{coulomb}} + E_{\text{GB_solvation}})$, $E_{\text{vdW}} = (E_{\text{vdW}} + E_{\text{pi-pi}} + E_{\text{self-contact}})$ and $E_{\text{lipophilic}}$.

2.3 Results

2.3.1 Homology modelling. Using the X-ray solved complex structure of mouse MOR1 with a ligand (32), the homology models of the full length and truncated human MOR-1 were obtained. The cartoon representations are shown in (Figure 3) from top viewpoints. Clearly, the TM1 is completely missed in G1 receptor. It is interesting that TM1 in 1G2 is only partially missed, because the protein sequence encoded by exon 11 in hMOR-1G2 is predicted to be helical. However, this partial truncation should not change much the ligand interaction with hMOR-1G2 from that with 1G1/K1/Mu3, because the partially helix is located at intracellular part and not at extracellular part where ligands bind to. It appears that TM1 is next the binding pocket, and thus its action on ligand-receptor interactions may come from indirect allosteric/chaperone-like effect. Nonetheless, the partial or complete missing of TM1 can significantly change ligand-receptor interaction and dynamics, and thus changing the response of the receptors in comparison to full-length version. The differences provide the base for designing more selective ligands toward specific variant. These homology models can be good starting structures for long time scale (μ s) convention and replica exchange molecular dynamics simulations to inspect these ligand-protein interaction and dynamics (56-61).

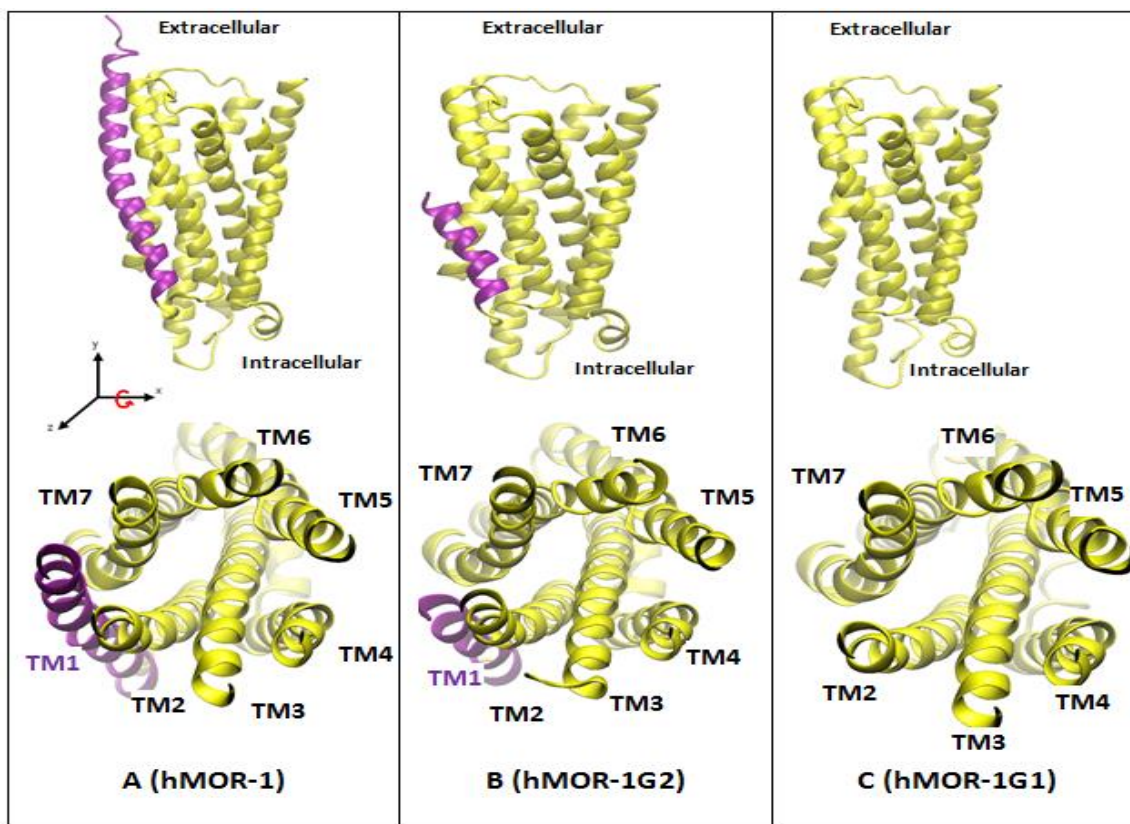


Figure 4. Homolog models of (A) full length 7TM hMOR-1 receptor, (B) truncated MOR-1G2 and (C) hMOR-1G1.

2.3.2 XP Glide docking. In order to build the Mu receptors complexes with morphine and IBNtxA, we used Glide XP docking implemented in Schrodinger (methodology). Each ligand (IBNtxA and morphine) was docked into three receptors and binding poses were utilized as input structure to perform MD simulations. In addition, we recorded the XP scores to get initial insight into the binding affinities of each ligand to wild type and truncated variants (scores table is not shown). Morphine showed binding energy of (-3.4 kcal) to full-length hMOR-1 which is slightly stronger than its binding to the truncated G2 (-2.7 kcal/mol) and G1 (-3.0 kcal/mol). While the binding pose to the full-length hMOR-1 is similar to hMOR-1G2 with a partial truncation of TM1, its

binding pose is significantly different from its binding pose to hMOR-1G1 with a full truncation TM1. In contrast, IBNtxA binds more strongly to hMOR-G2 and hMOR-G1 than to hMOR-1. The binding poses on hMOR-G2 and hMOR-G1 are different from its binding pose to hMOR-1. It is also clear the binding energy of IBNtxA on G2/G1 is stronger than the binding energy of morphine on the full-length hMOR1.

2.3.3 Ligand binding energy calculations. To characterize ligand binding affinities toward different receptors, we performed the MMGBSA calculation (4) as described in the method section and results are tabulated in (table 2). Morphine binding to its wild type receptor 7TM showed ΔG of -73.6 kcal/mol compared to -66.4 kcal/mol and -54.9 kcal/mol in case of G2 and G1 respectively. The order is 7TM>G2>G1, morphine binds more favorable to 7TM than to G2 and G1 by -7.2 kcal/mol and -18.7 kcal/mol respectively. In contrast, IBNtxA binding to its wild type (G1) receptor possessed the highest affinity ($\Delta G = -134.9$ kcal) compared to -102.6/mol kcal and -118.9 kcal/mol for G2 and 7TM receptors respectively. The order is G1>7TM>G2, IBNtxA binds more favorable to G1 than 7TM and G1 by -15.9 kcal/mol and -32.3 kcal/mol, respectively. The ligand-receptor binding order from our MMGBSA binding energy data is consistent with that of our XP scores, except that IBNtxA binds stronger to 7TM than to G2. Therefore, MMGBSA data generally supports our early speculation that the activity differences between morphine and IBNtxA might be caused by the differences in the binding affinity. Our decomposition results indicated that, with all six complexes, ΔVDW and $\Delta LIPO$ have the highest contribution compared to $\Delta GBELE$. However, significant variations observed were as follows: (1) with Morphine, 7TM has higher contribution from ΔVDW and $\Delta LIPO$ compared to those in

G1 and G2 .Whereas in G2, Δ GBELE contribution was the highest. (2)With IBNtxA , Δ VDW and Δ LIPO contributions was proportionate in all three receptors .However, Δ GBELE contribution in G1 was significantly higher than 7TM which in turn was higher than G2.These inter receptors variations in energy decomposition components can be utilized to design effective future G1 and G2 candidates .Above results are tabulated in table 2.

Table 2

MMGB-SA binding energies for both Morphine and IBNtxA complexes with the three receptors.

LIGAND RECEPTOR	Morphine			IBNtxA		
	7TM	G2	G1	7TM	G2	G1
Δ G ¹	-73.6±4	-66.4±6.5	-54.9±5.3	-119.0±5.4	-102.6±4.6	-134.9±6.6
$\Delta\Delta$ G ²	0.0	7.2	18.7	15.9	32.3	0.0
Δ VDW ³	-35.9±1.6	-27.9±8.4	-28.6±2.2	-53.4±2.3	-49.5±2.7	-52.9±1.7
$\Delta\Delta$ VDW	0.0	8.1	7.3	-0.5	3.4	0.0
Δ GBELE ⁴	-2.5±3.6	-8.7±4.5	-2.2±2.5	-13.2±3.8	-6.9±3	-27.9±3.8
$\Delta\Delta$ GBELE	0.0	-6.2	0.3	14.7	21.1	0.0
Δ LIPO ⁵	-35.1±1.0	-29.8±3.2	-24.0±1.6	-52.4±2.8	-46.3±2.3	-54.1±3.1
$\Delta\Delta$ LIPO	0.0	5.3	11.1	1.7	7.8	0.0

¹ Δ G: MM-GBSA binding energy (Complex – Receptor – Ligand).

² $\Delta\Delta$ G: relative binding energy with reference to active complex (wide type/G1).

³ Δ VDW: Change of van der Waals energy (vdW + Pi-pi stacking +Self-contact correction) in gas phase upon complex formation

⁴ Δ GBELE: Change of electrostatic interactions (GB/Generalized Born electrostatic solvation energy+ ELE/Coulomb energy +Hydrogen-bonding) upon complex formation.

⁵ Change of lipophilic term (Lipophilic energy) upon complex formation.

2.3.4 Morphine and IBNtxA binding poses. To identify the major binding pose, we clustered the trajectory (54) as described in the method section. The representative structure of the most abundance structure families are shown in Figure 4. Morphine binding to its wild type and two splice variants adopted three slightly different poses (Figure 4 A-C). IBNtxA binding to its wild type receptor and its splice variants structures (Figure 4 D-F) also showed three distinct binding poses. To facilitate the comparison, we superimpose the three complexes for the same ligand in Figure 5.

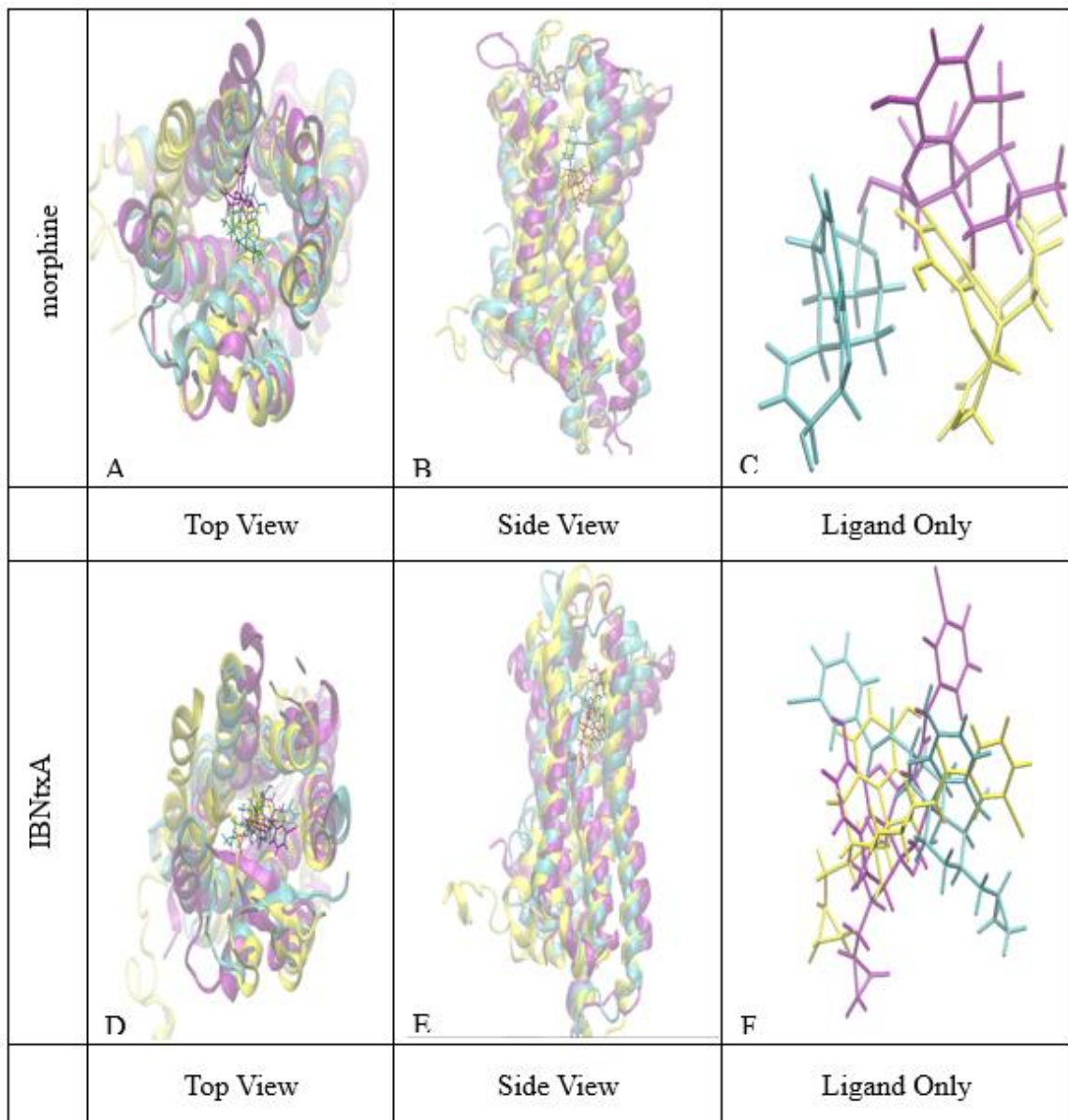


Figure 5. Superposition of the most abundant complexes from the simulations. The yellow, purple and cyan colors refer to wild type, G1 and G2 respectively.

2.3.5 Morphine and IBNtxA ligand 2D interaction data. To identify critical residues contributing to morphine and IBNtxA bindings in each receptor, we did the simulation interaction diagram analysis, which is implemented in DESMOND. The raw

data are included in Figure S7-12 and the key interacting residues for each ligand were tabulated in Table 3. For example, morphine-7TM 2D interaction conferred 18 different residues from transmembranes 2, 3, 5, 6, and 7. Polar Residues are: ASP116^{2.50}, ASP149^{3.32}, ASN152^{3.35}, TYR150^{3.33}, SER156^{3.39}, LYS235^{5.40}, TRP295^{6.48}, CYS294^{6.47}, HSD299^{6.52}, CYS323^{7.37}, TYR328^{7.42}, TRP320^{7.34}, and hydrophobic residues: ALA119^{2.53}, MET153^{3.36}, VAL238^{5.43}, LE298^{6.51}, VAL302^{6.55}, and ILE324^{7.38}. Morphine binding to other two splice variants confers slightly different binding residues compared to wild type. Similarly, IBNtxA binding to its wild type (G1) showed different residues contacting the ligand compared to wild type. Figure 5 shows residues contacting ligand more than 30% of simulation time. Clearly, we see there is no single interacting residue of 7TM, G1 and G2 is identical for morphine. For IBNtxA, TRP^{7.34} is conserved for 7TM and G2 and TYR^{7.42} is conserved for G2 and G1.

Table 3

Morphine 2D interaction table with three different receptors. The three receptors are aligned using Schrodinger maestro software, the genetic numbering was used to compare residues in different receptors.

Morphine				IBNtxA		
GEN_NO	7TM	G2	G1	7TM	G1	G2
2x50	ASP116					
2x53	ALA119			ALA119		
2x57						LEU42
2x60		GLN45	GLN26	GLN126	GLN26	GLN45
2x64				TYR130	TYR30	TYR49
e1				TRP135		TRP54
3X28		VAL64				
3x29		ILE65		ILE146	ILE46	ILE65
3x32	ASP149	ASP68	ASP49	ASP149	ASP49	ASP68
3x33	TYR150	TYR69		TYR150	TYR50	TYR69
e2		THR139				
3x35	ASN152	GLU150	ASN52	ASN152		
3x36	MET153		MET53	MET153	MET53	MET72
3x37						PHE73
3X39	SER156		SER56	ASP218		
E2					LEU121	THR139
E2					PHE123	LEU140
5X39				LEU234	LEU134	
5X36						GLU150
5x40	LYS235	LYS154		LYS235		LYS154
5x43	VAL238		PHE191	VAL238	VAL138	VAL157
6x47	CYS294		CYS194			
6x48	TRP295		TRP195	TRP295	TRP195	
6x51	ILE298	ILE217	ILE198	ILE298	ILE198	ILE217
6x52	HSD299	HSE218		HSD299	HSE199	HSE218
6x54		TYR220				TYR220
6x55	VAL302	VAL221		VAL302	VAL202	VAL221
6x58		LYS224		LYS305	LYS205	LYS224
E3						GLU231
7X34	TRP320	TRP239	TRP220	TRP320	TRP220	TRP239
7X37	CYS323	CYS242	CYS223			
7x38	ILE324	ILE243	ILE224	ILE324	ILE224	ILE243
7x41				GLY327		
7x42	TYR328	TYR247		TYR328	TYR228	TYR247
7x46			SER231			

2.3.6 Receptors secondary structures data. G2 maintains the partial TM1, the hairpin at extracellular loop2 of 7TM and G1 lost the hairpin when binding with morphine. To investigate the secondary structure of the receptors, the abundance over the trajectory is shown in (Figure 6). In the six complexes, 0TM helices maintains and subtle differences are identified. Notable features are as follows: A). the partial TM1 of G2 maintained in the two complexes with morphine and IBNtxA. B). Morphine-G2 complex showed a 4.02 % β -strand component compared to negligible values in case of G1 and wild type receptors, indicating the unfolding of the hairpin at the extracellular loop2 in these two systems. IBNtxA binding to its wild type and other two splice variants showed three closely related SS components with an average of 4.1%. C). For Morphine-G1 complex, a part of TM2 and TM6 is unfolded. These structural changes can contribute to the loss of activation by morphine on G1 receptor. D). For IBNtxA, the helical content at the intracellular loop 2 are different for the the receptors, in the order of G2>G1>7TM. For IBNtxA, the coil content at the intracellular loop3 are different for the three receptors, in the order of G1>G2>7TM.

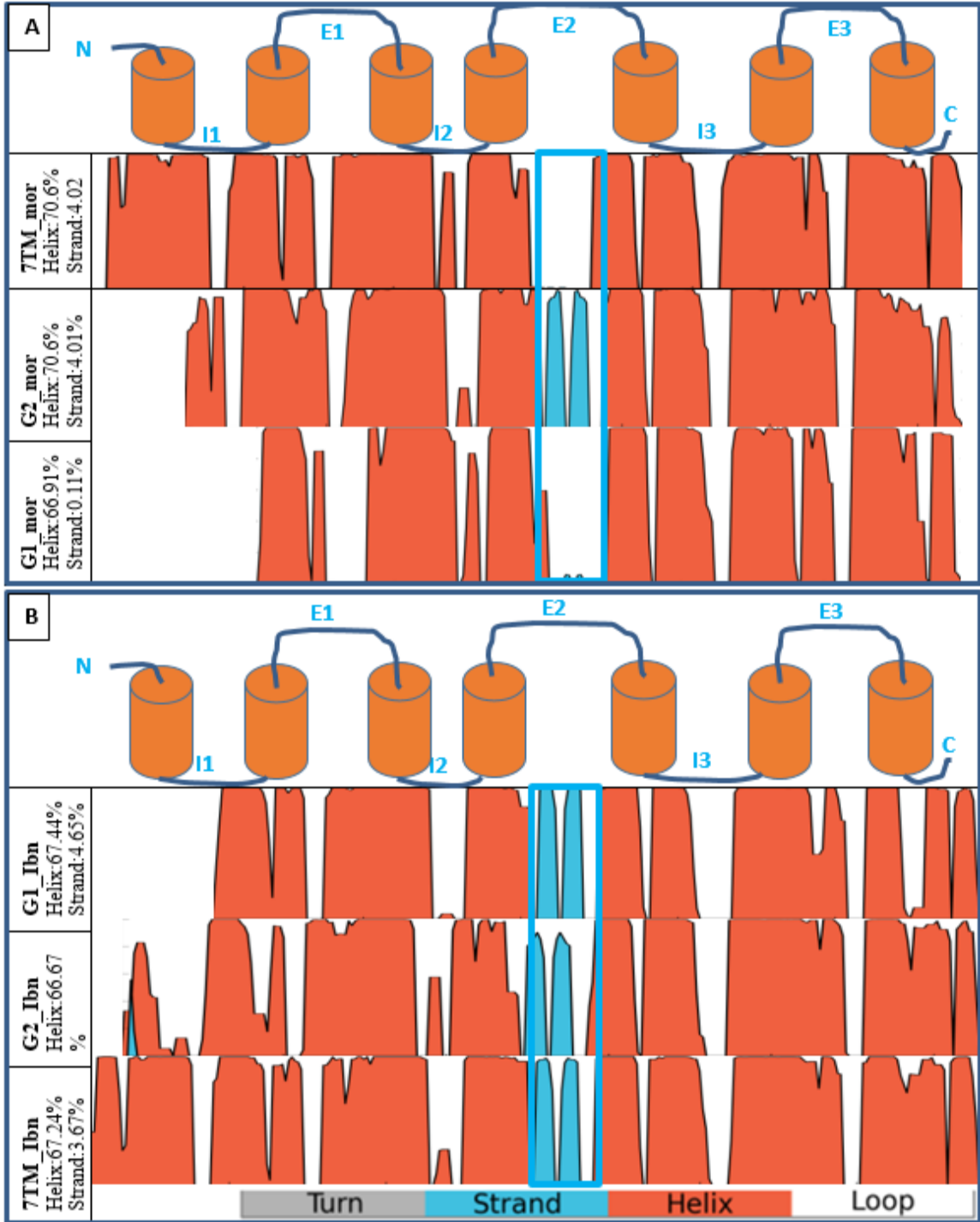


Figure 6. Protein Secondary structure profile of three receptors complexes with Morphine (A) and IBNtxA. (B).

2.3.7 Receptors dynamic responses for the same ligand. Receptor protein C α Root Mean Square Fluctuation (RMSF) values are shown in (Figure 7 A and B) for the Morphine and IBNtxA with G1 and 7TM complexes. We observe the general trend that the most rigid parts of the receptor (i.e. helices) exhibit lower RMSF values while loose structures such as the N and C terminals and intra and extra cellular loops show high RMSF values. In addition, subtle differences are identified for the different receptors in complex with the same ligand, these differences mainly located at the flexible part of the receptors. Given the different biological responses of the different receptors in response to the same stimulating ligand, these dynamic differences could contribute the different biological responses by modulating the interaction between the receptor and down-stream signal transduction proteins such as G-protein and or β -arrestin. Being major players in signal transduction, both the intracellular loop 3 and extracellular loop 2 receptor conformational changes were further scrutinized and compared. For the morphine-receptor complexes, intracellular loop 3 fluctuation intensities of three receptors were in the following order: G1>7TM; and similar order was observed for extracellular loop 2 fluctuation.

For the IBNtxA-receptor complexes, the intracellular loop 3 fluctuation intensities of the three receptors were in the following order: 7TM>G1; and similar order observed for extracellular loop 2 fluctuation. It appears that the lower the fluctuations are correlated with the receptor activation by morphine and IBNtxA.

We also inspect the different dynamic responses of the same receptor by the two different ligands in (Figure 8A and B). Where 7TM shows similar response to both

morphine and IBNtxA, G1 have larger fluctuation when binding with morphine than that with IBNtxA.

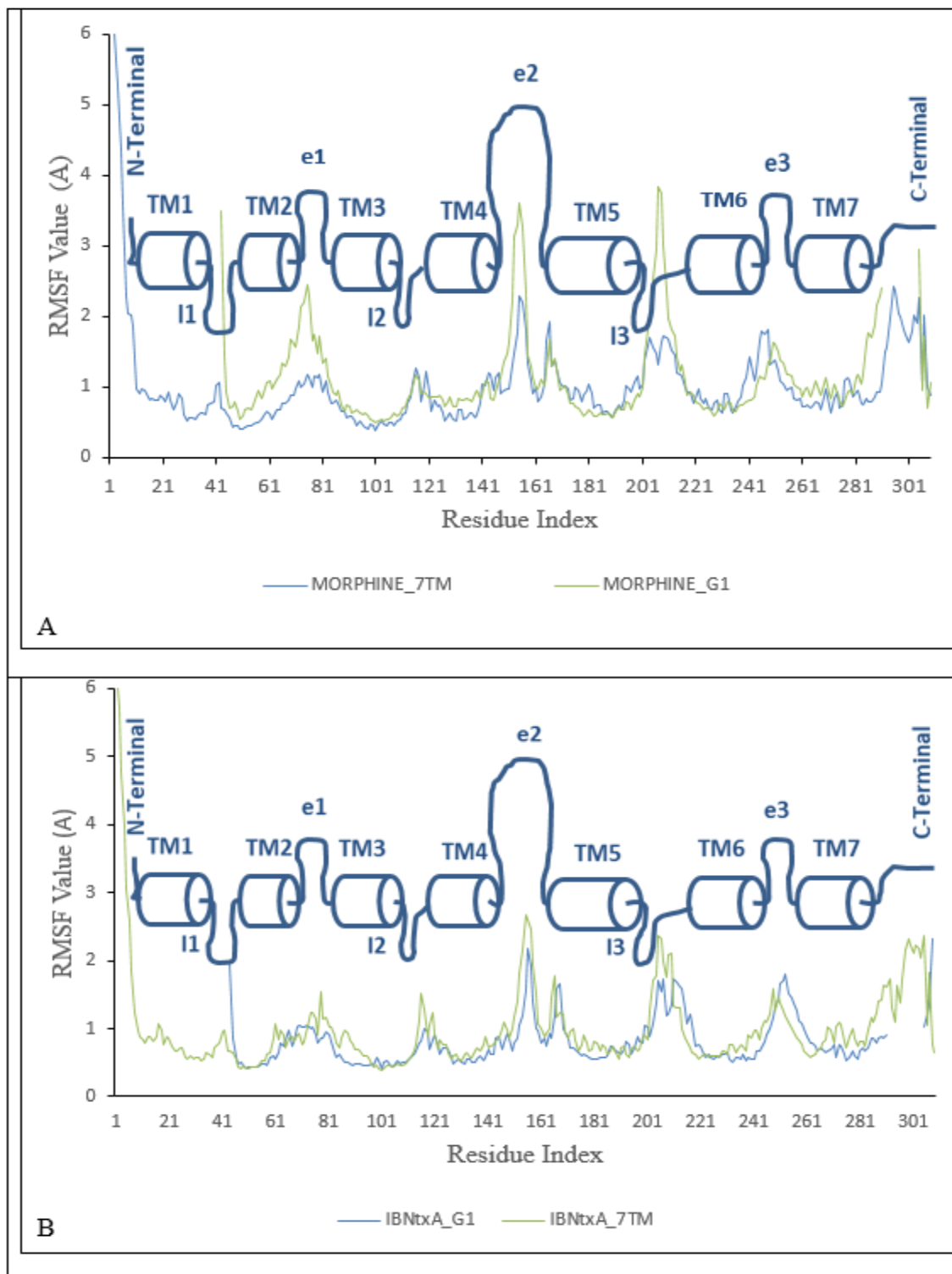


Figure 7. RMSF diagrams of receptor Protein C- α . Diagram (A): Morphine-7tm-G1 protein C- α RMSFs comparison. Diagram (B): IBNtxA-7TM-G1 protein C- α RMSFs comparison. The residue index is shown for the full-length wild type MOR-1 receptor. In case of G1 receptor, the RMSF diagram starts at the TM2 skipping TM1 as result of truncation.

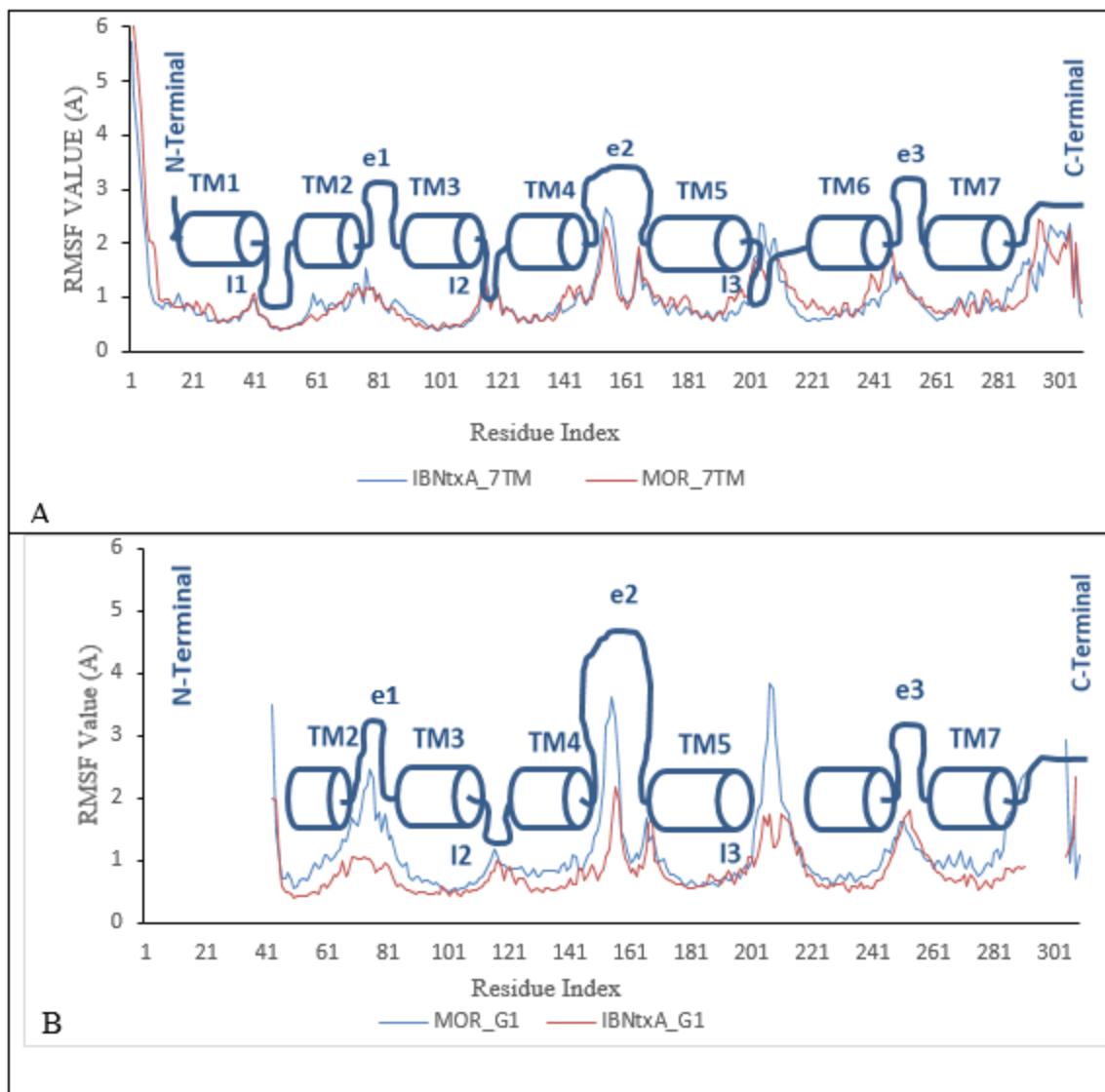


Figure 8. RMSF diagrams of receptor Protein C- α . Figures (A), (B) represent 7TM and G1 Receptors Interaction with both IBNtxA and Morphine Comparisons. Each receptors pairs were aligned using maestro alignment tool.

2.3.8 Ligand fluctuation (L-RMSF). When the same ligand binds to different receptors, its conformation dynamics might be different. To investigate this, the ligand RMSFs for morphine and IBNtxA are shown in (Figure 9). Interestingly, the RMSF profile of Morphine in the complex with 7TM significantly differs that with G1 and G2,

and the RMSF profiles of morphine with G1 and G2 are very similar. Likewise, IBNtxA L-RMSF plots differs between 7TM and both G1 and G2, and was similar for G1 and G2.

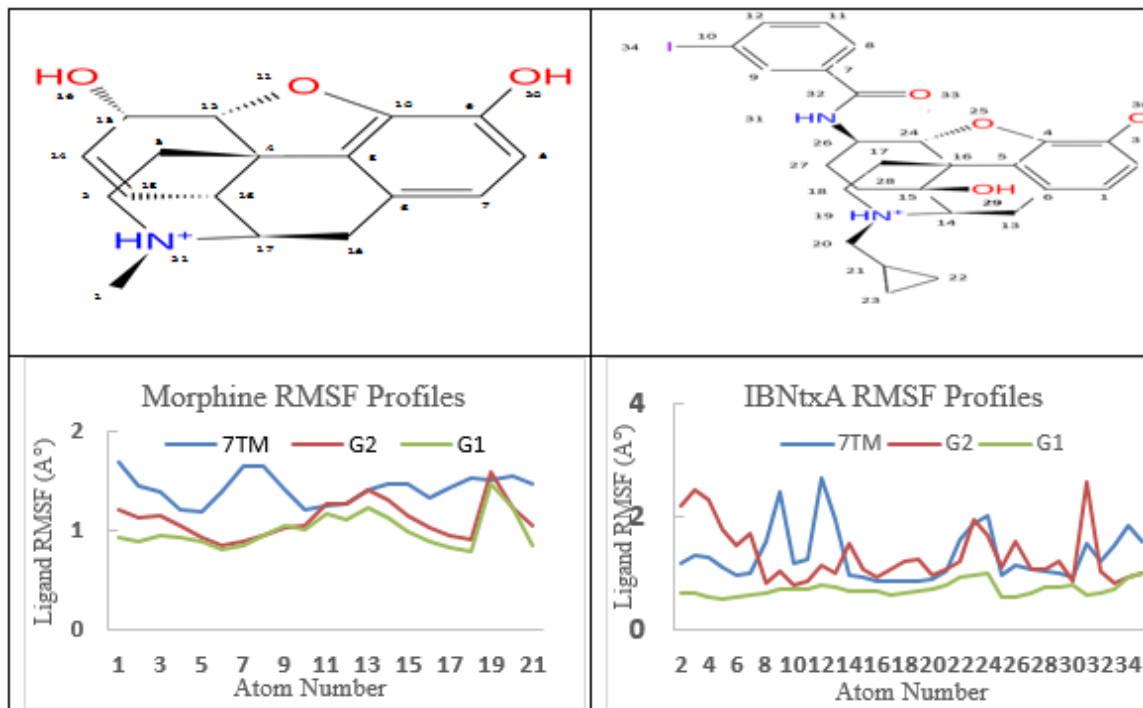


Figure 9. Ligand RMSF diagrams of Morphine binding to three different receptors.

2.4 Discussion and Conclusion

The compelling side effects and rising addiction rates of current opioids such as morphine necessitates more research to explore novel morphine replacement and μ -opioid receptors. Recent genetic study (62) has shown that the MOR-1 gene has alternative splicing leading to alternative 6TM receptors that lacks of TM1, including G1

and G2 and Mu3. Furthermore, recent in vivo studies (63) supports the pharmacological potency of synthetic Morphine analogue (IBNtxA) on mice 6TM alternatives. According to the mouse knockout model (64)Morphine analgesia is lost in exon 1 knock out model but reserved in exon 11 knockout. However, IBNtxA analgesia is retained in exon 1 knockout model and lost in exon 11 knockout. Therefore, the study on the structural, dynamics and interaction with ligand of 6TM will greatly advance IBNtxA analgesia. Although the crystal structures of 7TM with ligands are available, the high-resolution structures of 6TM with ligands are not available. A recent MD study have been recently performed on human Mu receptor wild type and G1 receptor in complex with morphine previously (65)While this study provided crucial information about the dynamics of the intracellular loop 3 in both G1 and wild type Mu receptors, other structural and dynamic differences were not illuminated. Additionally, the G2 receptor characteristic and IBNtxA binding properties was not explored previously. In this study, we probe the dynamic and structural properties of G1, G2 and 7TM in complex with morphine and IBNtxA. Because the interaction between morphine and 7TM has been widely studied experimentally and computationally. We want to validate our results on the morphine-7TM complex against several early studies. Most recently, resolved crystal structure of murine receptor in complex with BU72 is coincided with our most abundant structure after doing alignment with human sequence equivalents. Being a small and compacted molecule, morphine could adopt different binding poses within the pocket; however, the key residues involved in our binding pose have been consistent with most of previous experimental and theoretical studies. For example, the most important interaction observed in early studies (66-69) was a salt bridge formed between morphine's cationic

moiety (the tertiary amine) with ASP147 of mouse which corresponds to (ASP149) in human MOR-1. Our model confirms that morphine's cationic moiety is interacting with the ASP149 in Human 7TM MOR-1 receptor. A second important interaction was hydrophobic interaction between the phenyl group of morphine with TYR298 and TYR 328 which is also consistent with previous experiments which reported TYR299 and TYR326 of mouse MOR-1 as interacting residues(69-71). Another important interaction was observed between the aromatic ring of morphine with the sidechain of ILE324 and ILE298, which was also consistent with most of the previous studies (68,70,72). Most of the residues contacting morphine molecule (including the most crucial residue ASP 149) from our study are consistent with previous experimental and computational studies (73-76).

Interestingly, these important interactions are not observed in our binding pose between morphine to hMOR-1G1. Therefore, the change of the binding pose might contribute to the loss of analgesia on the 6TM variants in the exon 11 knockout model. Similarly, the residues of hMOR-1 interacting with IBNtxA are quite different from the residues of hMOR-1G1 interacting with IBNtxA. Again, these differences might contribute to the loss of analgesia of IBNtxA on hMOR-1G1. Interestingly, the salt bridge between ASP149 and the cationic moiety of IBNtxA is retained for hMOR-1 and hMOR-1G1. This interaction might be necessary for activating the receptor. Those detailed interactions can help us design point mutations to decipher the interaction mechanism using experimental techniques in the future.

Our homology modeling indicated that G1 is completely missing the first TM1 while G2 is only partially truncated possessing extra 20 amino acids in N terminal region of protein (Fig 2). This raised interesting questions on whether the partial TM1 helix is stable, whether it cause G2 significantly different from G1 and 7TM in term of receptor activation. Our simulation data indicates this partial helix of TM1 of G2 is stable in the two simulations in complex with morphine and IBNtxA (Figure S13). Our energetic, structural and dynamic data strongly support G2 are different from 7TM and G1. First, our MMGBSA binding data indicates that G2 binding to morphine is weaker than 7TM by 7.2 kcal/mol but is stronger than G1 by 11.5 kcal/mol. When binding to IBNtxA, G2 is weaker than both 7TM and G1 by 16.4 kcal/mol and 32.3 kcal/mol, respectively. Therefore, G2 might not be activated potently by both morphine and IBNtxA. The former is support by the fact morphine do not activate 6TM variants. The latter requires further testing of IBNtxA on G2 separately rather than the 6TM mixtures in the original test (64). Second, our clustering data show the binding pose of morphine and IBNtxA on G2 is slightly different on 7TM and G1 (Figure 5 and 6). Third, our secondary structure data show that G2-morphine complex maintained the hairpin at the extracellular loop 2, while 7TM and G1 did not (Figure 7). For G2-IBNtxA complex, its intracellular loop 2 has slightly higher helical content than G1 and 7TM. Fourth, our protein Ca-RMSF data show that the G2 profile with morphine and IBNtxA differs significantly from G1 at the intra-cellular loops 2 and 3, and the extracellular loop 2 (Figure 8). Because these parts are critical in the signal transduction, different RMSF profiles may suggest different receptor activation profiles.

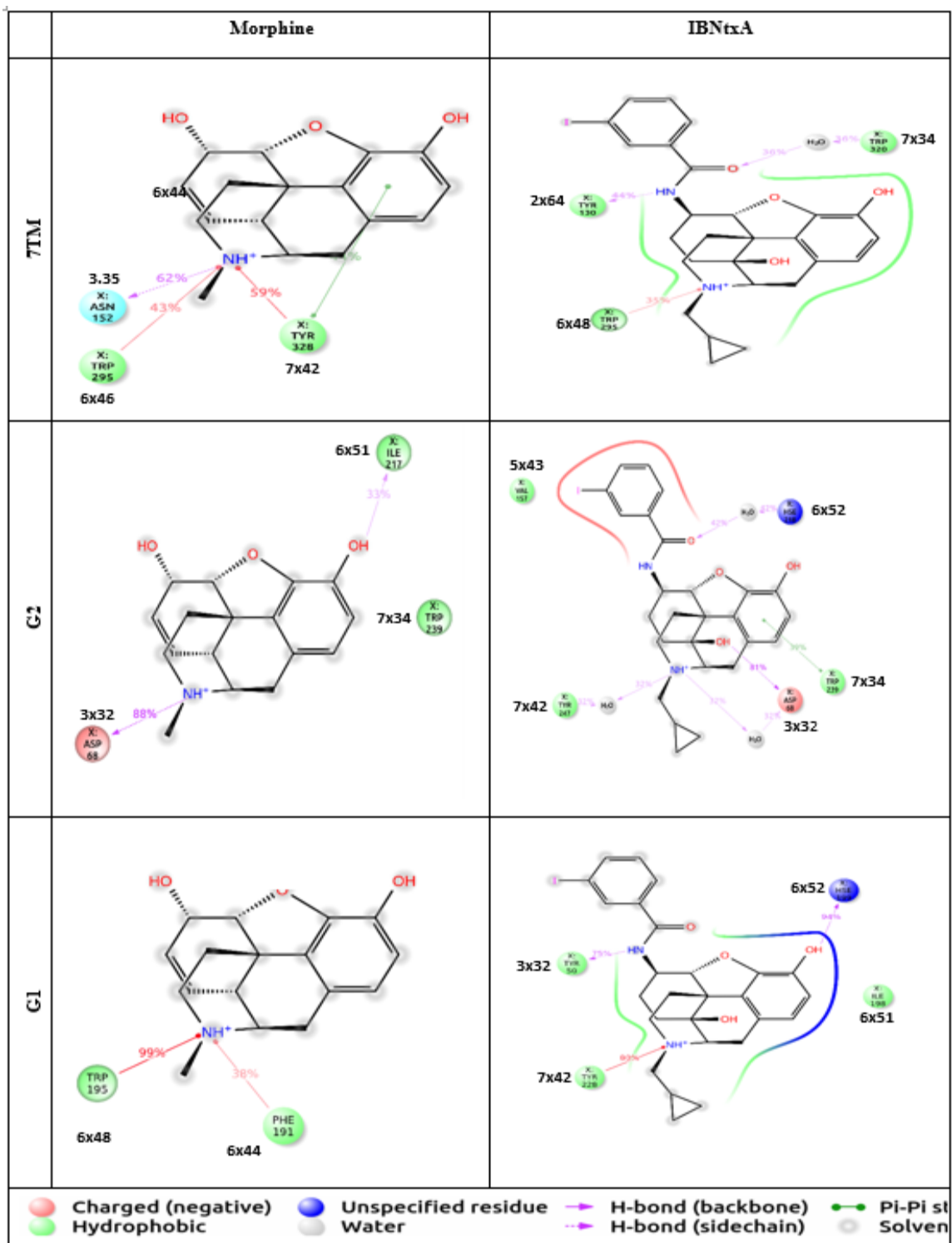


Figure 10. A schematic detailed atom interaction with protein residues Comparison. Interactions that persists more than 30% of simulation time are shown.

To understand the significant differences between 7TM and G1 in terms of ligand activation, and pharmacological actions, we performed both receptor and ligand based comparisons. Our MMGBSA binding data shows that IBNtxA binding affinity to G1 is significantly higher than 7TM; this is consistent with the *in vivo* data that IBNtxA can activate G1 in exon 1 knockout model while analgesia is lost in 7Tm, which contain exon 11 knockout. In contrast, as expected, morphine exhibited higher affinity to its wild type compared to G1. Our MD data shows that IBNtxA and Morphine exhibit significantly different binding poses as indicated from their most abundant structures (Fig 4). Moreover, when we aligned the complexes of the same ligand, it can vividly be seen that IBNtxA and Morphine have different binding pose on 7TM and G1 (Table 3). This evidence is further reinforced when we examine the 2D interaction profile of each ligand-receptor complex (Figure 6). Major interactions for morphine on 7TM are observed in TM 3 and TM6 which previously suggested to contain the ionic lock responsible for GPCR activation(77).However, when interacting with G1, morphine interacted with different residues (Figure 5). Likewise, IBNtxA 2D binding profile clearly indicated that IBNtxA interface differs significantly between G1 and 7TM receptor. More importantly, (Fig 5A) 2D interaction which monitors the highly interacting residues (more than 30% of the simulation time) clearly indicates that Morphine was able to make strong intermolecular forces with its surrounding lining 7TM pocket .These forces which including one pi-pi stacking and two cationic- can be better translated in term of binding energies which previously showed that both VDW and lipophilic are two major contributing components of the total binding energy Table 2. On the other hand, IBNtxA binding to same 7TM receptor was not only showing different residues from different

transmembrane, its binding forces were being mostly H-bonds, which might explain why it cannot activate this receptor.

Another important observation from the 2D interaction table is that secondary structures (E2) might influence IBNtxA receptor activation particularly in G1 receptors. Our MD simulation secondary structure analysis also indicated whereas the hairpin at extracellular loop 2 was stable in G1-IBNtxA Complex but was unfolded in 7TM-morphine complex. This leads us to speculation that this E2 plays important role in IBNtxA selectivity and binding .This is consistent with previous experimental studies of NMR and mutagenesis which confirmed the crucial role of E2 in ligand allosteric and orthostatic activations (78-80).Moreover, our IBNtxA MD trajectories movies clearly shows E2 persists as Cantilever umbrella capping the extracellular binding pocket .This was true most of the simulation time. This is supported by previous Rhodopsin research where N terminus and E2 were folding together forming a lid for ligand binding pocket. (63).

Morphine and IBNtxA induced different receptor responses (Figure 9). This is obvious from the pattern of RMSF fluctuations induced by morphine and IBNtxA on 7TM and G1 receptors. This reinforce our hypothesis that truncation has affected the conformational and structural priorities of spliced variants and eventually affected their ligand affinities preferences. The suggested mechanism of action of the GPCR including the opioids receptors involve the activation of the second and the third intracellular loops and the proximal portion of the C terminal(65,74,81). According to our protein C α RMSF data, I3 and I2 loops fluctuations distinctly different in G1 and 7TM. In case of Morphine bound G1 receptor, Although I3 loop was showing the highest flexibility compared to

7TM, it was incapable to influence the cAMP as robust manner as the Morphine effect on 7TM receptor even at higher doses as indicated by biological tests(65). This paradox is attributed to the fact that I3 activation is only one part of the total signal transduction pathway in GPCR. It still unclear whether G1 receptor will utilize the classical G-protein coupling or the B-arrestin in case of Morphine and IBNtxA. Previous research studies revealed that IBNtxA might exert even excitatory effect on G1 splice variant receptor contrary to the acknowledged fact of its high efficacy in triple KO mouse(36,65).

The results of partially or total absence of one transmembrane in wild type GPCR scaffold conferred structural and dynamic alterations in receptor capacity to interact different ligands .Although the differences between Mu receptors subtypes is subtle specially G1 and G2,MD simulation experiments could successfully provide evidence that truncated versions G1 and G2 are uniquely different from WT .Moreover, Morphine and IBNtxA preferential affinity toward their WT receptors was obviously noticeable from predicted energy calculations. .This encourages future attempts to design library of compounds selective to G1 and/or G2 receptors to achieve high efficacy and lowest side effects.

Chapter 3

Computational analysis of Amsacrine resistance in human Topoisomerase II alpha mutants (R487K and E571K) using homology modeling and all atom MD simulation in explicit membrane

3.1 Introduction

Amsacrine is an Acridine derivative and considered as the first topoisomerase II inhibitor effective in acute lymphatic leukemia and myeloid leukemia (82). It has relatively weak DNA binding affinity of 10^4 M^{-1} compared to other intercalates such as Adriamycin, Daunorubicin and Actinomycin -D with affinities range between 10^5 - 10^6 M^{-1} (83). Unlike etoposide which inhibit selectively topoisomerase Beta subtype, Amsacrine is equally effective in both subtype A and B of Topoisomerase II enzyme (84). Amsacrine molecule consists of two moieties; the intercalative Acridine moiety attached to 4'-amino-methanesulfon-m-anisidide head group (85) (Figure 11A). While intercalative part is important to anchor the molecule between the DNA base pairs, it is not sufficient to induce the enzyme inhibitory action by its self without the support of the second head group moiety. On the other hand, the head group have shown be effective in stimulating DNA session as standalone molecule without the help of intercalating body. Although this was happening at higher concentrations, it clearly indicates Amsacrine head group is critically important in its mechanism as inhibitor. (85) Overall, Amsacrine stabilizes cleavage complex with DNA via interaction of its head group with top2 residues (86) and DNA intercalation (87) Amsacrine intercalation pattern is shown in (figure 11C). However, cancer cells can circumvent the inhibitory mechanisms utilizing mutations, which ultimately confers resistance (88,89). Previous in vivo studies successfully analyzed two important point mutations (R487K and E571K) in leukemia

cell line(90) (Figure 11B). Results conferred Amsacrine Resistance was identified in vivo as >100-fold and >25-fold resistance in case of R487K and E571k respectively. Previous functional studies had confirmed the reduced cleavable complex formation as resistance mechanism for those two mutants (90). However, none of the previous studies illustrates how mutations reduced the stability of the cleavable ligand-DNA-protein complex. In this study, we sought to utilize the MD simulation method to study this mutational impact on the stability of the cleavable complex of human top2a homolog. We study top2a rather than top2b, because top2b is required for normal physiological function and its inhibition cause adverse effects (91). We constructed amsacrine-DNA-top2a complex based on the previously published crystal structure of top2beta (3Qx3). The wild type complex structure was used to introduce two mutants (R487K) and (E571K). The three complexes were subjected to 500 ns molecular dynamics simulation for each system. Our MM-GBSA binding energy calculations indicated a significant weakening of Amsacrine affinity toward its wild type compared to two mutants. Our clustering analysis indicates the changes of the binding poses upon the two point mutations. In particular, the DNA intercalation was completely and partially lost In R487K and E571K mutants structure respectively and a ligand was diffused away from its binding site in R487K. Additionally, the RMSF results for protein receptors were referring to higher structural and conformational changes in mutants protein structures compared with wild type.

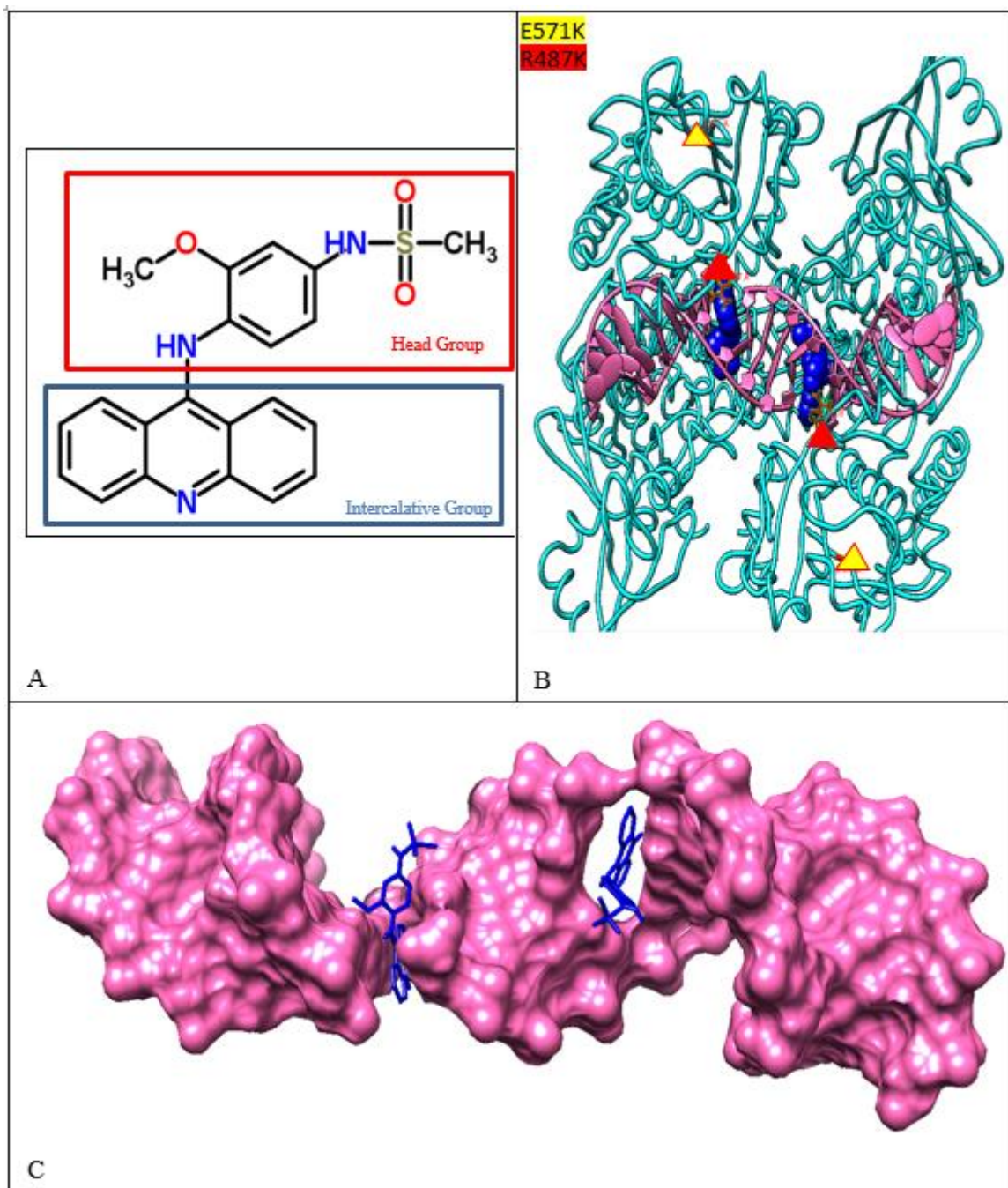


Figure 11. Structure of Amsacrine (A), amsacrine-Top2 α complex (B) and Amsacrine-DNA complex (C). Human Top2 α complex model was based on the crystal structure of Top2 β (PDB id: 3QX3). Two point mutations that cause drug resistance are indicated in red and yellow triangles (B).

3.2 Computational Materials and Methods

3.2.1 Human Topoisomerase II α structure homology modelling. Crystal structure of Human topoisomerase II β in complex with etoposide (pdb code 3QX3) (92) was used as template to build hTop2 α homology model. Prime utility (93,94) implemented in Maestro was used to build TOP2A structure homolog based on human hTop2 α FASTA sequence from Uniprot (43). The final homolog complex structure was obtained by docking two prepared Amsacrine molecules into hTop2 α using Glide XP implemented in Maestro(5,46) .The complex was prepared using maestro protein preparation wizard, optimized and minimized. The same structure was used as primary structure of hTopII α . This structure was used to introduce two mutants (R487K) and (E571K) in both A and B chains of hTop2 α homolog.

3.2.2 Molecular dynamic (md) simulations.

Simulation system setup. All three molecular dynamic simulation systems were built using the prepared and refined receptor-ligand complexes from the XP docking as input files. In each complex, System was built using SPC as solvent model (48) using orthorhombic solvent box .Buffer was used as the method of solvent box size calculation .System was neutralized using Na⁺ ions, and was added with a salt concentration of 0.15 M NaCl. After the system was successfully solvated, OPLS3 force field (45) (3) was used to represent the receptor-ligand.

Relaxation and simulation protocols. Desmond simulation package (3) was used to run all simulations, systems were first relaxed using the default Desmond relaxation protocol. After Simulation for 1.5 ns under the NPT ensemble with no restraints, the

relaxed systems were assigned a 400 ns production run conducted under the NPT ensemble for each of the three systems using the default protocol. M-SHAKE (51) was applied to constrain all bonds connecting hydrogen atoms, enabling a 2.0 fs time step in the simulations. The k-space Gaussian split Ewald method (52) was used to treat long-range electrostatic interactions under periodic boundary conditions (charge grid spacing of $\sim 1.0 \text{ \AA}$, and direct sum tolerance of 10^{-9}). The cutoff distance for short-range non-bonded interactions was 9 \AA , with the long-range van der Waals interactions based on a uniform density approximation. To reduce the computation, non-bonded forces were calculated using an r-RESPA integrator (53) where the short range forces were updated every step and the long range forces were updated every three steps. Temperature was controlled using the Martyna-Tuckerman-Klein Nosé-Hoover chain-coupling scheme with a coupling constant of 1.0 ps. The trajectories were saved at 40.0 ps intervals for analysis. All MD simulations were performed under 300 K and 1 bar conditions.

Molecular dynamic simulations convergence. To explore whether MD simulations trajectories were equilibrated toward the end of simulation time, we investigated the protein C α RMSD plots from the raw data for each trajectory (Figure S3). Clearly, plots indicate the convergence of C α RMSD diagram of all three complexes, which refers to the state of equilibrium of receptor proteins C alpha at the end of simulation time. This indicated a conformational stability of receptor throughout the simulation.

Trajectory clustering analysis. RMSD- based clustering was used to group Frames from Desmond trajectory (54) implemented in Schrodinger Software. The merging distance cutoff used was 2 \AA . This tool performs hierarchical clustering on

structures from a Desmond trajectory based on the RMSD matrix of a specified set of atoms [Schrodinger scripts]. The centroid structure (i.e. the structure having the largest number of neighbors in the structural family) was used to represent the family. The centroid structures of populated structural families (>1% of total structure population) are shown in (Figure S2) of the supporting material.

3.2.3 Binding energy calculations and decompositions. Binding energies were calculated as MMGB-SA using VSGB 2.0 solvation model (4). Frames from the last 20ns were used for this purpose. The net free binding energy calculation was performed for three complexes: (Ligand +Protein +DNA),(Ligand+ Protein) and (Ligand +DNA).For simplicity the previous terms were denoted LDP ,LD and LP respectively .In all three calculations , the same number of frames were selected to get consist binding free energy predictions . MM-GBSA calculation procedure consists of energy calculations and energy minimizations as follows: Receptor alone (minimization), Ligand alone (minimization), Receptor-ligand complex (minimization), Ligand extracted from optimized receptor-ligand complex (energy calculation), Receptor extracted from optimized receptor-ligand complex (energy calculation).The total binding free energy equation is:

$$\Delta G_{(bind)} = E_{complex (minimized)} - (E_{ligand(minimized)} + E_{receptor(minimized)}).$$

Decomposition of binding free energy values are also reported in each calculation. It includes electrostatic, van der Waals, hydrophobic, and composition interactions allows for a more detailed understanding of the effect that resistance places on each complex.

3.3 Results

Because hTop2a is a homodimer, we were expecting quantitative results from the MD simulation to be similar in two chains. However, in most parts, there were differences between the two subunits ranging from subtle to significant. Therefore, we sought to take the average value of the two chains to simplify the comparison between them.

3.3.1 Amsacrine binding energy calculations. Predicted binding energy of Amsacrine indicated significant affinity weakening in two mutants compared to wild type hTOP2A. hTOP2 α contains two binding DNA intercalation sites which required two separate binding energy Calculations to investigate the mutational impact on each site. The MMGB-SA results are charted in (table 4). The energy of binding ΔG of WT-LDP was calculated to be (-71.81 Kcal/mol) and (-60.93 Kcal/mol) in binding site A and B respectively. The E571K mutation impaired LDP binding affinity to be (-42.85 Kcal/mol) and (-53.5 Kcal/mol) in site A and B respectively. Moreover, R487K mutation attenuated binding affinities of LDP to be (-39.1 Kcal/mol) and (-34.8 Kcal/mol) in sites A and B respectively. To get more insight into the mutational impact of ligand on DNA and Protein interactions, additional MM-GBSA calculations for LD and LP were performed. As can be seen from the (table 4), In E571K mutant, the average cost of energy binding of Ligand-protein (LD) of was significantly higher than energy needed for Ligand-protein(LP) interaction (-20.85 Kcal/mol Vs -27 Kcal/mol). while the opposite was true for R487K where Ligand-DNA intercalation required less energy of binding compared to ligand –protein interaction (-21.5 Kcal/mol Vs -14.9 Kcal/mol). Another important result was gained from the MMGB-SA decomposition of complexes (Table 4) which clearly

indicated the significant contribution of both van der Waals forces and Lipophilic terms as major component of binding energy for all complexes. While, Δ GBELE contributed less favorably to total binding energy magnitude.

Table 4

Average MM-GBSA binding energies of Amsacrine with hTOP2a WT and Mutants (kcal/mol).

Δ G Type	WT			R487K			E571K		
	LDP	LD	LP	LDP	LD	LP	LDP	LD	LP
¹ Δ G	-66.4	-31.9	-32.7	-37.0	-21.5	-14.9	-48.2	-20.9	-27.1
² $\Delta\Delta$ G	0.0	0.0	0.0	29.4	10.4	17.7	18.2	11.1	5.6
³ Δ VDW	-56.3	-33.8	-22.1	-42.5	-27.5	-24.0	-46.4	-27.5	-18.9
$\Delta\Delta$ VDW	0.0	0.0	0.0	13.8	6.3	-1.9	10.0	6.3	3.2
⁴ Δ LIPO	-25.9	-7.9	-17.6	-8.6	-2.2	-6.4	-19.1	-2.7	-16.3
$\Delta\Delta$ LIPO	0.0	0.0	0.0	17.3	5.8	11.2	6.8	5.2	1.3
⁵ Δ GBELE	15.8	9.8	7.0	14.1	8.2	6.5	17.3	9.4	8.2
$\Delta\Delta$ GBELE	0.0	0.0	0.0	-1.7	-1.6	-0.6	1.4	-0.4	1.1

¹ Δ G: MM-GBSA binding energy (Complex – Receptor – Ligand).

² $\Delta\Delta$ G: Relative binding energy with reference to the WT complex.

³ Δ VDW: Change of van der Waals energy (vdW + Pi-pi stacking +Self-contact correction) in gas phase upon complex formation

⁴ Δ LIPO: Change of lipophilic term (Lipophilic energy) upon complex formation.

⁵ Δ GBELE: Change of electrostatic interactions (GB/Generalized Born electrostatic solvation energy+ ELE/Coulomb energy +Hydrogen-bonding) upon complex formation.

LD: Ligand-DNA only Interaction, LP: Ligand-Protein only Interaction, LPD: Ligand-Protein-DNA interaction

LD: Ligand-DNA complex, LP: Ligand-Protein complex, LPD: Ligand-Protein-DNA complex.

Note: Binding energy calculated based on average values from two subunits A and B.

3.3.2 Amsacrine binding poses and 2D interaction diagram. Two mutants

adopted different binding pockets and poses compared with wild type. To explore

mutational impact on Amsacrine binding pose and ligand interaction network change ,

we have extracted the most abundant structure of each complex and aligned them using prime implemented in maestro. The three ligands were superimposed according to the protein sequence alignments to visualize the nuance differences between the wild type and mutants structures. We formulated comparison table of all residues contacting the Amsacrine for three different complexes. Obviously, Amsacrine lost most of the interacting residues in case of two mutants as seen in (table 5) and sought to bind to residues significantly different from the wild type. This was clearly noticeable in R487K mutation which exhibited the highest binding affinity weakening. We noticed that Amsacrine in chain B in this mutations started forming new interactions in the 400 residue range of receptor which was absent in case of the wild type. This binding deviation was further verified by observing the significant change in binding poses of Amsacrine in two mutants (in both binding sites) compared with wild type (Figure 12 A,B,C,E).

Table 5

Interacting residues with Amsacrine.

WT-A	WT-B	R487K-A	R487K-B	E571K-A	E571K-B
			ARG 434		
			ILE 435		
LYS 436		LYS 436	LYS 436		
			GLY 437		
			ILE 438		
			PRO 439		
			LYS 440		LYS 440
			LEU 441		
GLH 461	GLH 461	GLH 461	GLH 461		GLH 461
			GLY 462		
ASP 463	ASP 463	ASP 463	ASP 463		ASP 463
	SER 464	SER 464	SER 464		SER 464
			PRO 485		
LEU 486	LEU 486	LEU 486	LEU 486		LEU 486
ARG 487	ARG 487			ARG 487	ARG 487
		LYS 487	LYS 487		
		GLY 488	GLY 488		
		LYS 489			
		ASN 504			
			ALA 505		
			GLH 506		
		GLU 506			
		LYS 743			
		TYR 757			
		HIS 759			
GLY 760		GLY 760			
GLU 761		GLU 761		GLU 761	
MET 762	MET 762	MET 762	MET 762	MET 762	MET 762
SER 763	SER 763	SER 763			SER 763
LEU 764					
MET 765	MET 765			MET 765	
ILE 766					
	MET 766	MET 766		MET 766	MET 766
	THR 767				
MET 769	ILE 769				
		LYS 798	LYS 798		
SER 800	SER 800			SER 800	
ALA 801	ALA 801			ALA 801	
SER 802	SER 802	SER 802	SER 802	SER 802	
PRO 803	PRO 803			PRO 803	
ARG 804	ARG 804	ARG 804		ARG 804	ARG 804
TYR 805		TYR 805	TYR 805	TYR 805	TYR 805

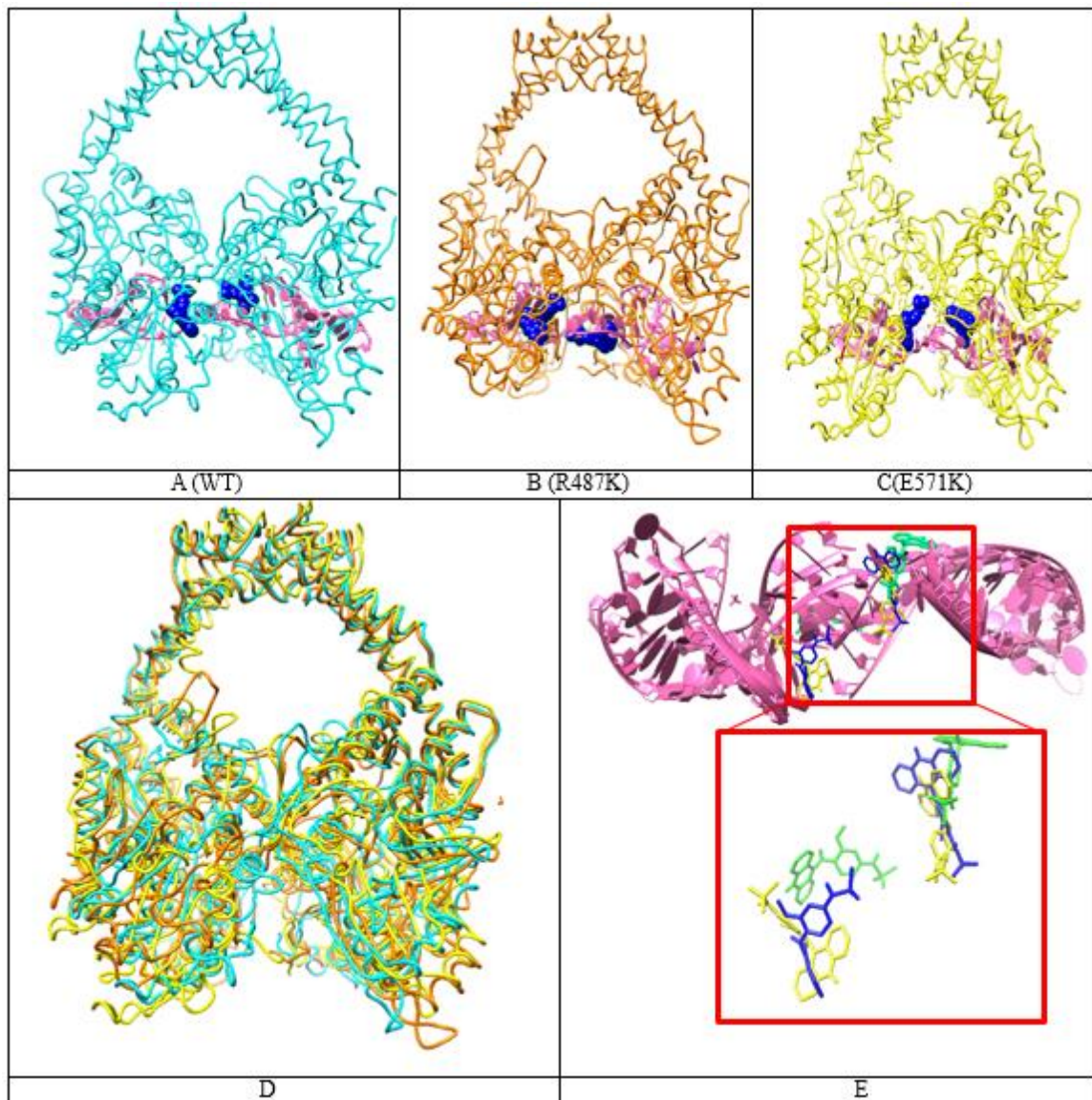


Figure 12. (A-C) Representatives of the most abundant structure families of the three complexes. (D) Superimposition of the three complex structures. (E) Superposition of ligand-DNA complexes (WT, E571K and R487K are in green, blue and yellow).

3.3.3 Amsacrine-DNA intercalation changes. Two mutants exhibited significant DNA intercalation changes compared with wild DNA. For each of the simulation system, the most abundant structure was extracted using clustering method which group frames of

trajectory based on merging distance cutoff (54) .After aligning each representative structure of mutants and wild type, we sought to compare the DNA conformational changes with respect to Amsacrine in each complex. Results from the two mutants clearly shows the loss of intercalation state of Amsacrine partially (in case of E571K and completely (in case of R487K) as seen in figure 13 which shows the detailed picture of DNA cleavage site.

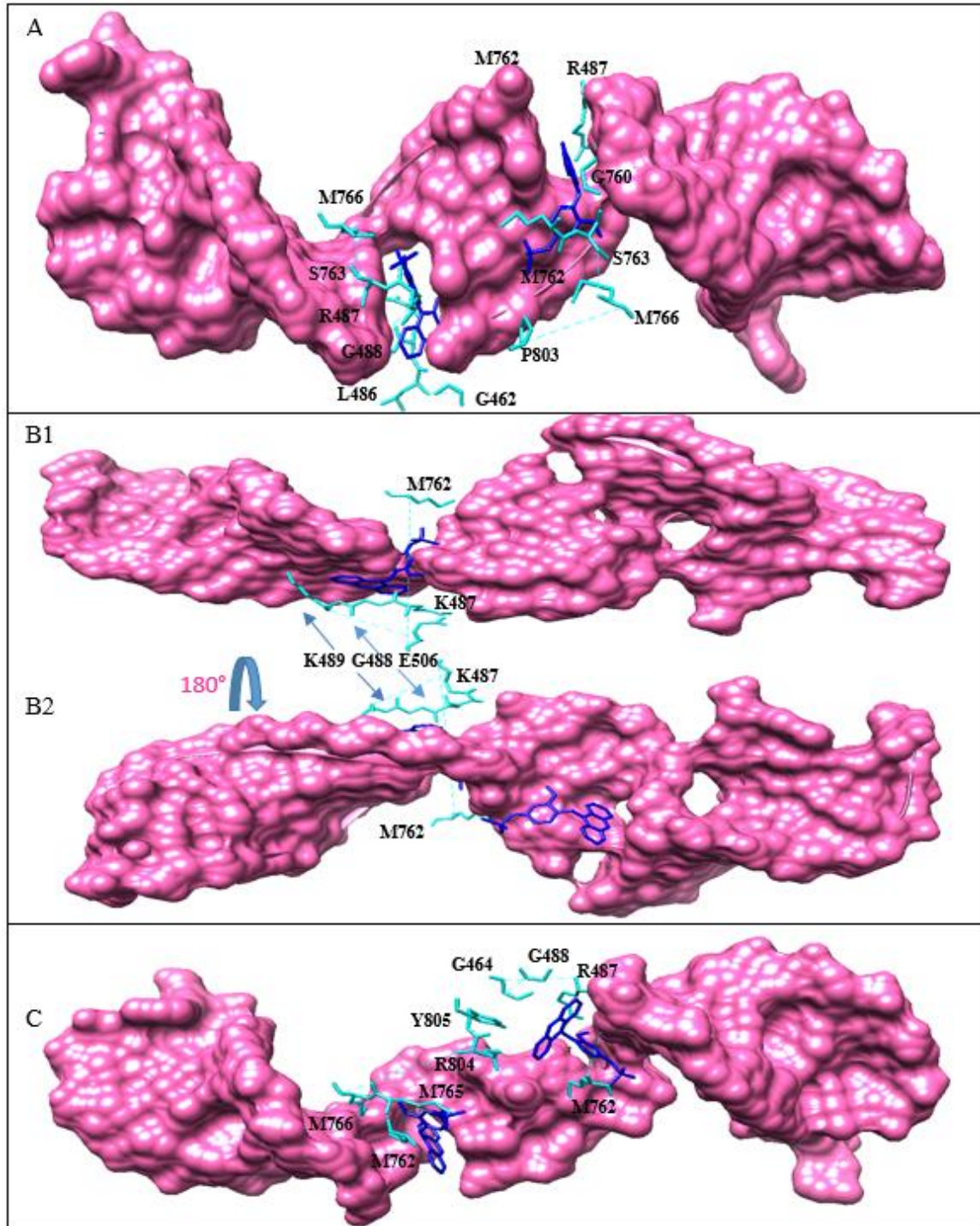


Figure 13. Amsacrine-DNA intercalation Changes of the R487 (B1, B2) and E571K(C) Mutations Compared to Wild Type (A).R487K. B1 and B2 represent the front and rear views of DNA showing the two-ligand intercalation changes. All three complexes represent 3Å^o cutoff distance from the ligand.

3.3.4 Enzyme protein C α RMSF analysis. Enzyme protein C α RMSF analysis indicated significant conformational changes in both mutants compared to wild type enzyme. The Root Mean Square Fluctuation (RMSF) is useful for detecting local changes along the protein chain. (RMSF) Diagrams of each binding site of the three complexes were combined in one diagram for comparison purpose (Figure 14). Results clearly shows that for the most part, R487K mutation reflected the highest fluctuation pattern compared to E571K mutation, which in turn was higher than WT level (figure 14). This clearly indicates the significant conformational changes in protein structure upon mutations, which contributes to the weakening effect of the mutation. Furthermore, the dominant fluctuation pattern in both binding sites was consist with the secondary structure distribution of the enzyme structure where loops and turns are exhibiting the highest dynamic effects compared to alpha strands.

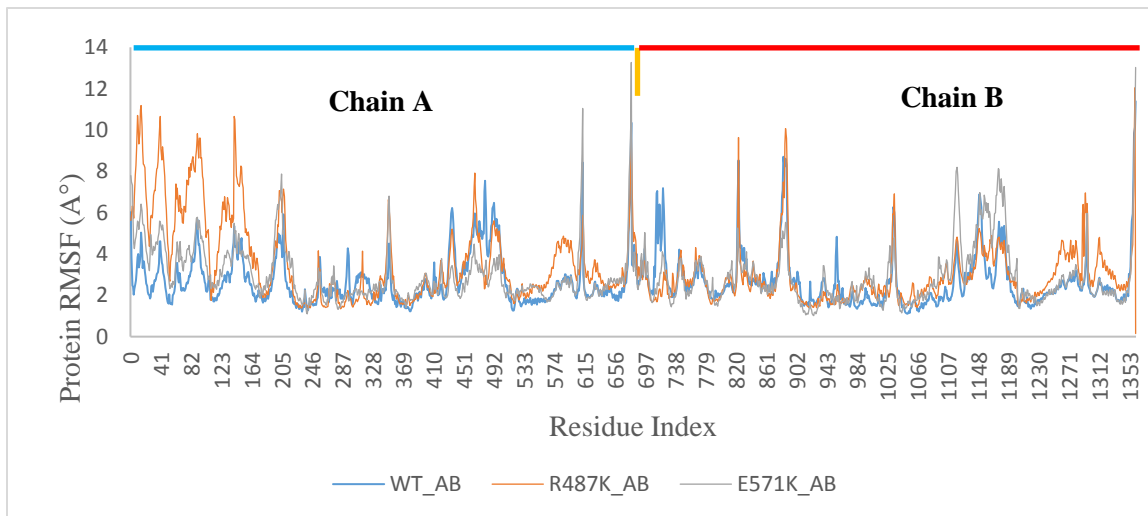


Figure 14. Protein C α RMSF diagrams of hTop2 α WT and mutants upon Amsacrine Binding. Residue from 1 to 645 represent the chain (A) of enzyme while residue 646 to 1330 belongs to chain (B).

3.3.5 Ligand conformational change (L-RMSF). Ligand conformational change indicated different configurations and higher intensities in two mutants compared to wild type. Ligand RMSF shows the ligands dynamic fluctuations with respect to protein broken down by atomic contribution of ligand molecule. It gives insights about the entropic contribution endured by the ligand during protein interaction. According to our ligand RMSF comparison diagram, the general pattern of fluctuation is significantly higher for the mutants compared to the wild type. More importantly, R487K mutant showed higher ligand fluctuation than E571K mutant (Figure 15). Another worth mentioning is the region of the Amsacrine molecule exhibiting higher fluctuation. Obviously, the highest fluctuations are seen in the first and the last part of L-RMSF plot, which corresponds, to the 3-methoxy group of m-AMSA and the 4'-amino-methanesulfon-m-anisidide head group, which are loosely connected groups. However, unexpectedly, another high fluctuation was observed at the middle of the plot, which correspond, to the third ring of acridine moiety in Amsacrine responsible for active intercalation inside DNA grove.

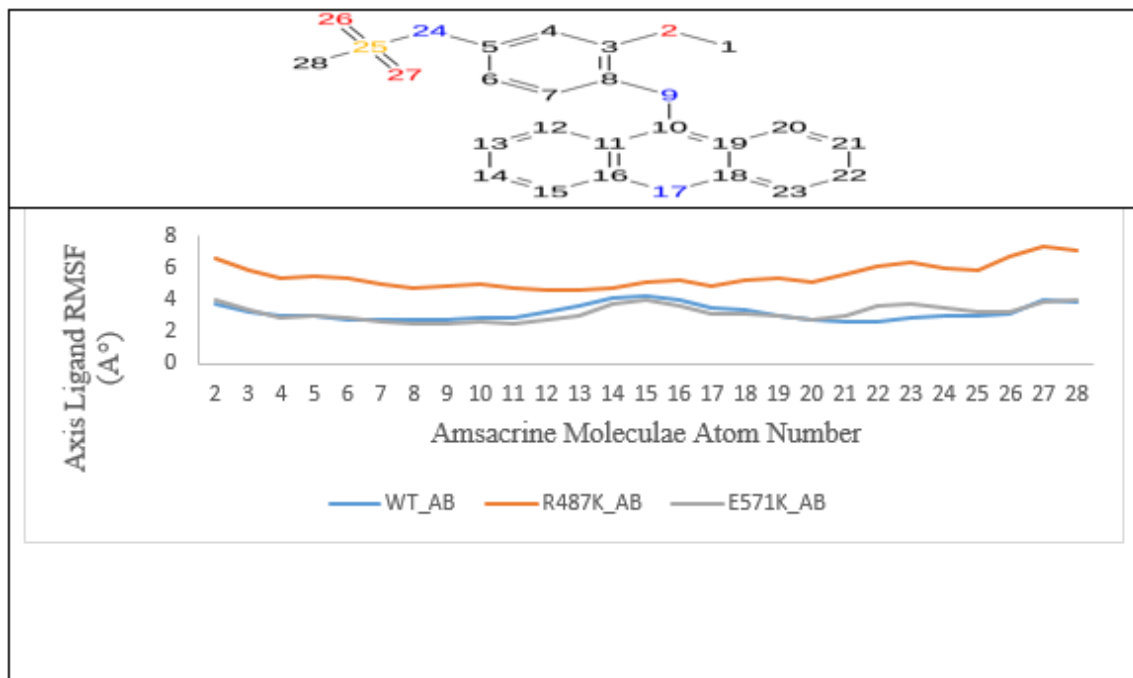


Figure 15. Average ligand RMSF for the three complexes. Complexes were aligned and superimposed using Maestro software.

3.4 Discussion and Conclusion

Previous study identified two point mutations (R487K and E571K) of human Top2 α in leukemia cell line (90). The vivo essays conferred more than 100-fold and 25-fold resistance to Amsacrine for R487K and E571K respectively. Reduced cleavable complex formation was identified to be the resistance mechanism. However, detailed molecular and structural mechanisms underlying this resistance remains to be elusive. We have applied homology modeling and MD simulations to mechanically understand mutational impact on the complex structure and stability.

Our MM-GBSA binding data indicated the significant weakening of Amsacrine binding affinities toward two mutants compared to wild type as seen in (table 4). The binding energy decrease caused by R487K mutation is larger than that by E571K, indicating that R487K can cause higher fold of drug resistance than E571K by a bigger reduction of the ternary complex formation. This fold change order is consistent with the experimental result, which indicated 100 and 25 fold drug resistance for R487K and E571K respectively. (95) When decomposing the overall ligand binding into ligand-DNA (LD) and ligand-protein (LP) interactions, we observed different contribution pattern for these two mutants. In R487K mutation, a $\Delta\Delta G$ value of 17.7 kcal/mol in LP suggested significant impairment of ligand interaction with protein TOP2 α . This is likely the direct impact of the mutation on the protein's ability to form intermolecular interaction with Amsacrine, because R487 is one of the major contributors to Amsacrine protein interaction in the wild type(86). This also emphasizes the role of Amsacrine molecule head group in forming the ternary complex (85). On other hand, $\Delta\Delta G$ of LD in R487K (i.e. 10.4 kcal/mol) is much lower than change in LP (i.e. 17.7 kcal/mol), indicating that ligand-DNA interaction contributes less than ligand-protein interaction to overall ligand binding energy decrease. In E571K, decrease of LP (5.6 kcal/mol) is much smaller than decrease of LD (11.0 kcal/mol), indicating that change of ligand-DNA interaction plays bigger role in the overall decrease of the ligand binding energy. This might be explained by the fact that E571K is located far away from the ligand-protein binding site and thus cause smaller perturbation on ligand-protein interaction. When comparing R487 with E571, the larger LP weakening in R487 is consistent with higher fold resistance compared to E571K.

Another significant impact of the mutations envisioned through our MD simulations were the Amsacrine-DNA intercalation changes as can be seen from the most abundant structures of mutants and WT DNA (Figure 13A). For example, the Amsacrine Molecule moiety was diffused away and relocated to be outside the DNA binding groove as seen in E571K (figure 13C) . As such, Amsacrine inhibitory effect was lost because both intercalating ability and protein binding were abolished and Top2a might be re-ligated and thus recovered. This agrees the previously published experimental studies that established the role of Acridine moiety in Amsacrine to anchor it into the DNA groove. (83,85,87)

The mutations also lead to the changes of ligand-protein binding poses, which can be seen in the ligand 2D diagram in (Figure S3) and (Table 5). The most significant changes can be observed in R487K chain A and B where protein established new contacts with ligands in certain regions while lost some in other regions. Likewise, the binding poses comparisons indicated the significant changes in ligand binding pose with respect to protein which clearly can be seen in chain B of WT and two mutants Figure S3. These results is consistent with the role of Amsacrine as an enzyme poison (85) in addition to a DNA intercalator.

The protein RMSF profiles further showed the changes of protein dynamics due to the mutations. In both mutants, RMSF diagram fluctuation intensity was higher compared in WT enzyme. Although this RMSF profiles from on crystal structure of a lesioned DNA with Amsacrine were DNA was pre-nicked with Top2 and cleaved; it clearly shows larger fluctuation of mutant protein structure can cause disruption in network of residues at Amsacrine binding site as seen in Figure 13. More importantly, the fluctuation was

observed higher in R487K than E571k which was higher than WT. This was also supported by the RMSF averages which also was in agreement with the previous order. It appears that the larger protein fluctuation might be required for the normal function of the enzyme. Our data showed the active role of two key residues ARG487 and GLU571 in maintaining protein backbone integrity and subsequent propagation of the conformational change conferred by these two mutations on protein structure and dynamics (96).

This phenomenon was further pictured via examining the L-RMSF results, which measures ligand configurational changes in respect to receptor. Results were indicating the unique pattern and higher magnitude of conformational changes in R487K compared to WT and E571K mutant (Figure 15). Moreover, regions in Amsacrine molecule of high fluctuation were mainly the 3-methoxy group and the 4'-amino-methanesulfon-m-anisidide head groups. The fact that these groups are the major contributors in Amsacrine binding to protein, a higher fluctuation in these groups can negatively affect the ligand-protein affinity. This is in fact another advantage of MD simulation which characterizes mutational impact between protein and ligand, since ligand conformational orientation is essential for proper binding pose and determines the success of intercalation.

Computational tools enabled us to understand the how mutations lead to resistance through energy calculations and other MD simulation parameters. The two mutants resulted in binding affinity weakening of Ligand-DNA-Protein complexes of two mutants in consistent manner with the in vivo fold resistance results .More importantly, larger drug resistance of R487K than E571K was caused by larger weakening of ligand protein interaction which agrees with the established Amsacrine inhibitory mechanism which emphasize the crucial role of protein in maintaining ternary complex with ligand.

For both mutants, weakening of ligand- DNA interaction also contributed to destabilization of the ternary complex, a ligand moved out of intercalation was observed in R487K and E571K could destabilize the ternary complex due to intercalation loss. Furthermore, MD simulation method could detect the significant changes in binding poses and 2D interaction diagrams, which also contributed to resistance .MD simulation, could prioritizes and characterizes the most significant mutation quantitatively and qualitatively. This is crucial for future drug design of effective ligands to counteract these mutations. (97)

References

- [1] Basak, S.C. and Majumdar, S. (2015) The Importance of Rigorous Statistical Practice in the Current Landscape of QSAR Modelling. *Current Computer-Aided Drug Design*, **11**, 2-4.
- [2] Le Anh Vu¹, P.T.C.Q., Nguyen Thuy Huong³. (2015) In silico Drug Design: Prospective for Drug Lead Discovery. *International Journal of Engineering Science Invention*, **4**, 60-70.
- [3] Jorgensen, W.L., Maxwell, D.S. and TiradoRives, J. (1996) Development and testing of the OPLS all-atom force field on conformational energetics and properties of organic liquids. *Journal of the American Chemical Society*, **118**, 11225-11236.
- [4] Li, J., Abel, R., Zhu, K., Cao, Y., Zhao, S. and Friesner, R.A. (2011) The VSGB 2.0 model: A next generation energy model for high resolution protein structure modeling. *Proteins-Structure Function and Bioinformatics*, **79**, 2794-2812.
- [5] Friesner, R.A., Murphy, R.B., Repasky, M.P., Frye, L.L., Greenwood, J.R., Halgren, T.A., Sanschagrin, P.C. and Mainz, D.T. (2006) Extra precision glide: Docking and scoring incorporating a model of hydrophobic enclosure for protein-ligand complexes. *Journal of Medicinal Chemistry*, **49**, 6177-6196.
- [6] Ballantyne, J.C. and Mao, J. (2003) Opioid therapy for chronic pain. *N. Engl. J. Med.*, **349**, 1943-1953.
- [7] McQuay, H., Moore, A. and Justins, D. (1997) Treating acute pain in hospital. *BMJ*, **314**, 1531-1535.
- [8] Sullivan, M.D. and Howe, C.Q. (2013) Opioid therapy for chronic pain in the United States: promises and perils. *Pain*, **154 Suppl 1**, S94-100.
- [9] Pasternak, G.W. (2014) Opiate pharmacology and relief of pain. *J. Clin. Oncol.*, **32**, 1655-1661.
- [10] Pasternak, G.W. and Pan, Y.X. (2013) Mu Opioids and Their Receptors: Evolution of a Concept. *Pharmacol Rev*, **65**, 1257-1317.
- [11] Ling, G.S., Spiegel, K., Lockhart, S.H. and Pasternak, G.W. (1985) Separation of opioid analgesia from respiratory depression: evidence for different receptor mechanisms. *J. Pharmacol. Exp. Ther.*, **232**, 149-155.
- [12] Ling, G.S., MacLeod, J.M., Lee, S., Lockhart, S.H. and Pasternak, G.W. (1984) Separation of morphine analgesia from physical dependence. *Science*, **226**, 462-464.
- [13] Ling, G.S., Spiegel, K., Nishimura, S.L. and Pasternak, G.W. (1983) Dissociation of morphine's analgesic and respiratory depressant actions. *Eur. J. Pharmacol.*, **86**, 487-488.
- [14] Ahlbeck, K. (2011) Opioids: a two-faced Janus. *Curr. Med. Res. Opin.*, **27**, 439-448.

- [15] Tafelski, S., Beutlhauser, T., Bellin, F., Reuter, E., Fritzsche, T., West, C. and Schaefer, M. (2016) Incidence of constipation in patients with outpatient opioid therapy. *Schmerz*, **30**, 158-165.
- [16] Raehal, K.M., Walker, J.K. and Bohn, L.M. (2005) Morphine side effects in beta-arrestin [2 knockout mice. *J. Pharmacol. Exp. Ther.*, **314**, 1195-1201.
- [17] Manchikanti, L., Helm, S., 2nd, Fellows, B., Janata, J.W., Pampati, V., Grider, J.S. and Boswell, M.V. (2012) Opioid epidemic in the United States. *Pain Physician*, **15**, ES9-38.
- [18] Volkow, N.D., Frieden, T.R., Hyde, P.S. and Cha, S.S. (2014) Medication-assisted therapies--tackling the opioid-overdose epidemic. *N. Engl. J. Med.*, **370**, 2063-2066.
- [19] Compton, W.M. and Volkow, N.D. (2006) Major increases in opioid analgesic abuse in the United States: concerns and strategies. *Drug Alcohol Depend.*, **81**, 103-107.
- [20] Mogil, J.S., Ritchie, J., Smith, S.B., Strasburg, K., Kaplan, L., Wallace, M.R., Romberg, R.R., Bijl, H., Sarton, E.Y., Fillingim, R.B. *et al.* (2005) Melanocortin-1 receptor gene variants affect pain and mu-opioid analgesia in mice and humans. *J. Med. Genet.*, **42**, 583-587.
- [21] McDonald, J. and Lambert, D. (2005) Opioid receptors. *Continuing Education in Anaesthesia, Critical Care & Pain*, **5**, 22-25.
- [22] Violin, J.D. and Lefkowitz, R.J. (2007) Beta-arrestin-biased ligands at seven-transmembrane receptors. *Trends Pharmacol. Sci.*, **28**, 416-422.
- [23] Tidgewell, K., Groer, C.E., Harding, W.W., Lozama, A., Schmidt, M., Marquam, A., Hiemstra, J., Partilla, J.S., Dersch, C.M., Rothman, R.B. *et al.* (2008) Herkinorin analogues with differential beta-arrestin-2 interactions. *J. Med. Chem.*, **51**, 2421-2431.
- [24] Groer, C.E., Schmid, C.L., Jaeger, A.M. and Bohn, L.M. (2011) Agonist-directed interactions with specific beta-arrestins determine mu-opioid receptor trafficking, ubiquitination, and dephosphorylation. *J. Biol. Chem.*, **286**, 31731-31741.
- [25] Raehal, K.M., Schmid, C.L., Groer, C.E. and Bohn, L.M. (2011) Functional selectivity at the mu-opioid receptor: implications for understanding opioid analgesia and tolerance. *Pharmacol. Rev.*, **63**, 1001-1019.
- [26] Kelly, E. (2013) Efficacy and ligand bias at the mu-opioid receptor. *Br. J. Pharmacol.*, **169**, 1430-1446.
- [27] Chen, Y., Mestek, A., Liu, J., Hurley, J.A. and Yu, L. (1993) Molecular cloning and functional expression of a mu-opioid receptor from rat brain. *Mol. Pharmacol.*, **44**, 8-12.
- [28] Eppler, C.M., Hulmes, J.D., Wang, J.B., Johnson, B., Corbett, M., Luthin, D.R., Uhl, G.R. and Linden, J. (1993) Purification and partial amino acid sequence of a mu opioid receptor from rat brain. *J. Biol. Chem.*, **268**, 26447-26451.
- [29] Thompson, R.C., Mansour, A., Akil, H. and Watson, S.J. (1993) Cloning and pharmacological characterization of a rat mu opioid receptor. *Neuron*, **11**, 903-913.

- [30] Wang, J.B., Imai, Y., Eppler, C.M., Gregor, P., Spivak, C.E. and Uhl, G.R. (1993) Mu opiate receptor: cDNA cloning and expression. *Proc. Natl. Acad. Sci. U. S. A.*, **90**, 10230-10234.
- [31] Pasternak, G.W. (2004) Multiple opiate receptors: deja vu all over again. *Neuropharmacology*, **47 Suppl 1**, 312-323.
- [32] Manglik, A., Kruse, A.C., Kobilka, T.S., Thian, F.S., Mathiesen, J.M., Sunahara, R.K., Pardo, L., Weis, W.I., Kobilka, B.K. and Granier, S. (2012) Crystal structure of the mu-opioid receptor bound to a morphinan antagonist. *Nature*, **485**, 321-U170.
- [33] Reiter, E., Ahn, S., Shukla, A.K. and Lefkowitz, R.J. (2012) In Insel, P. A., Amara, S. G. and Blaschke, T. F. (eds.), *Annual Review of Pharmacology and Toxicology, Vol 52*, Vol. 52, pp. 179-197.
- [34] Xu, J., Xu, M., Brown, T., Rossi, G.C., Hurd, Y.L., Inturrisi, C.E., Pasternak, G.W. and Pan, Y.X. (2013) Stabilization of the mu-Opioid Receptor by Truncated Single Transmembrane Splice Variants through a Chaperone-like Action. *J Biol Chem*, **288**, 21211-21227.
- [35] Lu, Z., Xu, J., Rossi, G.C., Majumdar, S., Pasternak, G.W. and Pan, Y.X. (2015) Mediation of opioid analgesia by a truncated 6-transmembrane GPCR. *J. Clin. Invest.*
- [36] Majumdar, S., Grinnell, S., Le Rouzic, V., Burgman, M., Polikar, L., Ansonoff, M., Pintar, J., Pan, Y.X. and Pasternak, G.W. (2011) Truncated G protein-coupled mu opioid receptor MOR-1 splice variants are targets for highly potent opioid analgesics lacking side effects. *Proc. Natl. Acad. Sci. U. S. A.*, **108**, 19778-19783.
- [37] Majumdar, S., Subrath, J., Le Rouzic, V., Polikar, L., Burgman, M., Nagakura, K., Ocampo, J., Haselton, N., Pasternak, A.R., Grinnell, S. *et al.* (2012) Synthesis and evaluation of aryl-naloxamide opiate analgesics targeting truncated exon 11-associated mu opioid receptor (MOR-1) splice variants. *J. Med. Chem.*, **55**, 6352-6362.
- [38] Schuller, A.G., King, M.A., Zhang, J., Bolan, E., Pan, Y.X., Morgan, D.J., Chang, A., Czick, M.E., Unterwald, E.M., Pasternak, G.W. *et al.* (1999) Retention of heroin and morphine-6 beta-glucuronide analgesia in a new line of mice lacking exon 1 of MOR-1. *Nat. Neurosci.*, **2**, 151-156.
- [39] Pan, Y.X., Xu, J., Xu, M., Rossi, G.C., Matulonis, J.E. and Pasternak, G.W. (2009) Involvement of exon 11-associated variants of the mu opioid receptor MOR-1 in heroin, but not morphine, actions. *Proc. Natl. Acad. Sci. U. S. A.*, **106**, 4917-4922.
- [40] Majumdar, S., Grinnell, S., Le Rouzic, V., Burgman, M., Polikar, L., Ansonoff, M., Pintar, J., Pan, Y.X. and Pasternak, G.W. (2011) Truncated G protein-coupled mu opioid receptor MOR-1 splice variants are targets for highly potent opioid analgesics lacking side effects. *P Natl Acad Sci USA*, **108**, 19778-19783.

- [41] Majumdar, S., Subrath, J., Le Rouzic, V., Polikar, L., Burgman, M., Nagakura, K., Ocampo, J., Haselton, N., Pasternak, A.R., Grinnell, S. *et al.* (2012) Synthesis and Evaluation of Aryl-Naloxamide Opiate Analgesics Targeting Truncated Exon 11-Associated mu Opioid Receptor (MOR-1) Splice Variants. *Journal of Medicinal Chemistry*, **55**, 6352-6362.
- [42] Zhang, J., Yang, J., Jang, R. and Zhang, Y. (2015) GPCR-I-TASSER: A Hybrid Approach to G Protein-Coupled Receptor Structure Modeling and the Application to the Human Genome. *Structure*, **23**, 1538-1549.
- [43] Magrane, M. and Consortium, U. (2011) UniProt Knowledgebase: a hub of integrated protein data. *Database : the journal of biological databases and curation*, **2011**, bar009.
- [44] Sastry, G.M., Adzhigirey, M., Day, T., Annabhimoju, R. and Sherman, W. (2013) Protein and ligand preparation: parameters, protocols, and influence on virtual screening enrichments. *Journal of computer-aided molecular design*, **27**, 221-234.
- [45] Harder, E., Damm, W., Maple, J., Wu, C., Reboul, M., Xiang, J.Y., Wang, L., Lupyran, D., Dahlgren, M.K., Knight, J.L. *et al.* (2016) OPLS3: A Force Field Providing Broad Coverage of Drug-like Small Molecules and Proteins. *Journal of Chemical Theory and Computation*, **12**, 281-296.
- [46] Friesner, R.A., Banks, J.L., Murphy, R.B., Halgren, T.A., Klicic, J.J., Mainz, D.T., Repasky, M.P., Knoll, E.H., Shelley, M., Perry, J.K. *et al.* (2004) Glide: A new approach for rapid, accurate docking and scoring. 1. Method and assessment of docking accuracy. *Journal of Medicinal Chemistry*, **47**, 1739-1749.
- [47] Lyman, E., Higgs, C., Kim, B., Lupyran, D., Shelleys, J.C., Farid, R. and Voth, G.A. (2009) A Role for a Specific Cholesterol Interaction in Stabilizing the Apo Configuration of the Human A(2A) Adenosine Receptor. *Structure*, **17**, 1660-1668.
- [48] Mark, P. and Nilsson, L. (2001) Structure and dynamics of the TIP3P, SPC, and SPC/E water models at 298 K. *Journal of Physical Chemistry A*, **105**, 9954-9960.
- [49] Zhang, J., Hou, Y., Wang, Y., Wang, C. and Zhang, X. (2012) The LBFGS quasi-Newtonian method for molecular modeling prion AGAAAAGA amyloid fibrils. *Natural Science*, **04**, 1097-1108.
- [50] Ikeguchi, M. (2004) Partial rigid-body dynamics in NPT, NPAT and NP gamma T ensembles for proteins and membranes. *Journal of Computational Chemistry*, **25**, 529-541.
- [51] Bailey, A.G. and Lowe, C.P. (2009) MILCH SHAKE: An Efficient Method for Constraint Dynamics Applied to Alkanes. *Journal of Computational Chemistry*, **30**, 2485-2493.
- [52] Shan, Y.B., Klepeis, J.L., Eastwood, M.P., Dror, R.O. and Shaw, D.E. (2005) Gaussian split Ewald: A fast Ewald mesh method for molecular simulation. *Journal of Chemical Physics*, **122**.

- [53] Stuart, S.J., Zhou, R.H. and Berne, B.J. (1996) Molecular dynamics with multiple time scales: The selection of efficient reference system propagators. *Journal of Chemical Physics*, **105**, 1426-1436.
- [54] Kevin J. Bowers, E.C., Huafeng Xu, Ron O. Dror, Michael P. Eastwood,, Brent A. Gregersen, J.L.K., Istvan Kolossvary, Mark A. Moraes, Federico D. Sacerdoti, and John K. Salmon, Y.S., David E. Shaw. (2006) Scalable Algorithms for Molecular Dynamics Simulations on Commodity Clusters.
- [55] Jakubik, J., El-Fakahany, E.E. and Dolezal, V. (2015) Towards predictive docking at aminergic G-protein coupled receptors. *Journal of Molecular Modeling*, **21**.
- [56] Wu, C., Scott, J. and Shea, J.E. (2012) Binding of Congo red to amyloid protofibrils of the Alzheimer A β ₉₋₄₀ peptide probed by molecular dynamics simulations. *Biophys. J.*, **103**, 550-557.
- [57] Wu, C., Bowers, M.T. and Shea, J.E. (2011) On the origin of the stronger binding of PIB over thioflavin T to protofibrils of the Alzheimer amyloid- β peptide: a molecular dynamics study. *Biophys. J.*, **100**, 1316-1324.
- [58] Wu, C., Biancalana, M., Koide, S. and Shea, J.E. (2009) Binding modes of thioflavin-T to the single-layer beta-sheet of the peptide self-assembly mimics. *J. Mol. Biol.*, **394**, 627-633.
- [59] Wu, C., Wang, Z.X., Lei, H.X., Duan, Y., Bowers, M.T. and Shea, J.E. (2008) The Binding of Thioflavin T and Its Neutral Analog BTA-1 to Protofibrils of the Alzheimer's Disease Ab(16-22) Peptide Probed by Molecular Dynamics Simulations. *J. Mol. Biol.*, **384**, 718-729.
- [60] Wu, C., Lei, H.X., Wang, Z.X., Zhang, W. and Duan, Y. (2006) Phenol red interacts with the protobril-like oligomers of an amyloidogenic hexapeptide NFGAIL through both hydrophobic and aromatic contacts. *Biophys. J.*, **91**, 3664-3672.
- [61] Duan, Y., Wu, C., Chowdhury, S., Lee, M.C., Xiong, G., Zhang, W., Yang, R., Cieplak, P., Luo, R., Lee, T. *et al.* (2003) A point-charge force field for molecular mechanics simulations of proteins based on condensed-phase quantum mechanical calculations. *J. Comput. Chem.*, **24**, 1999-2012.
- [62] Xu, J., Xu, M., Hurd, Y.L., Pasternak, G.W. and Pan, Y.X. (2009) Isolation and characterization of new exon 11-associated N-terminal splice variants of the human mu opioid receptor gene. *Journal of neurochemistry*, **108**, 962-972.
- [63] Lu, Z., Xu, J., Rossi, G.C., Majumdar, S., Pasternak, G.W. and Pan, Y.X. (2015) Mediation of opioid analgesia by a truncated 6-transmembrane GPCR. *The Journal of clinical investigation*, **125**.
- [64] Grinnell, S.G., Majumdar, S., Narayan, A., Le Rouzic, V., Ansonoff, M., Pintar, J.E. and Pasternak, G.W. (2014) Pharmacologic Characterization in the Rat of a Potent Analgesic Lacking Respiratory Depression, IBNtxA. *J Pharmacol Exp Ther*, **350**, 710-718.

- [65] Convertino, M., Samoshkin, A., Viet, C.T., Gauthier, J., Li Fraine, S.P., Sharif-Naeini, R., Schmidt, B.L., Maixner, W., Diatchenko, L. and Dokholyan, N.V. (2015) Differential Regulation of 6-and 7-Transmembrane Helix Variants of mu-Opioid Receptor in Response to Morphine Stimulation. *PLoS One*, **10**.
- [66] Z. Salamon, S.C., E. Varga, H.I. Yamamura, V.J. Hruba, G. Tollin. (2000) Plasmon Resonance Studies of Agonist/Antagonist Binding to the Human δ -Opioid Receptor: New Structural Insights into Receptor-Ligand Interactions. *Biophys J*, **79**, 2463-2474.
- [67] Sagara T1, E.H., Okamura M, Fujii I, Shimohigashi Y, Kanematsu K. (1996) Ligand recognition in mu opioid receptor: experimentally based modeling of mu opioid receptor binding sites and their testing by ligand docking. *Bioorganic & Medicinal Chemistry*, **4**, 2151-2166.
- [68] Eguchi, M. (2004) Recent advances in selective opioid receptor agonists and antagonists. *Medicinal research reviews*, **24**, 182-212.
- [69] Cui, X., Yeliseev, A. and Liu, R. (2013) Ligand interaction, binding site and G protein activation of the mu opioid receptor. *Eur J Pharmacol*, **702**, 309-315.
- [70] Gentilucci, L., Tolomelli, A., De Marco, R. and Artali, R. (2012) Molecular docking of opiates and opioid peptides, a tool for the design of selective agonists and antagonists, and for the investigation of atypical ligand-receptor interactions. *Curr. Med. Chem.*, **19**, 1587-1601.
- [71] Mansour, A., Taylor, L.P., Fine, J.L., Thompson, R.C., Hoversten, M.T., Mosberg, H.I., Watson, S.J. and Akil, H. (1997) Key residues defining the mu-opioid receptor binding pocket: a site-directed mutagenesis study. *J. Neurochem.*, **68**, 344-353.
- [72] Noori, H.R., Mucksch, C. and Urbassek, H.M. (2014) A structural feature of the non-peptide ligand interactions with mice mu-opioid receptors. *Curr. Comput. Aided Drug Des.*, **10**, 354-360.
- [73] Mansour, A., Taylor, L.P., Fine, J.L., Thompson, R.C., Hoversten, M.T., Mosberg, H.I., Watson, S.J. and Akil, H. (1997) Key residues defining the mu-opioid receptor binding pocket: A site-directed mutagenesis study. *Journal of neurochemistry*, **68**, 344-353.
- [74] Serohijos, A.W.R., Yin, S., Ding, F., Gauthier, J., Gibson, D.G., Maixner, W., Dokholyan, N.V. and Diatchenko, L. (2011) Structural Basis for mu-Opioid Receptor Binding and Activation. *Structure*, **19**, 1683-1690.
- [75] Cui, X., Yeliseev, A. and Liu, R. (2013) Ligand interaction, binding site and G protein activation of the mu opioid receptor. *European Journal of Pharmacology*, **702**, 309-315.
- [76] Sencanski, M. (2011) Modeling the ligand specific mu- and delta-opioid receptor conformations (vol 76, pg 1247, 2011). *Journal of the Serbian Chemical Society*, **76**, 1453-1454.
- [77] Huang, W., Manglik, A., Venkatakrisnan, A.J., Laeremans, T., Feinberg, E.N., Sanborn, A.L., Kato, H.E., Livingston, K.E., Thorsen, T.S., Kling, R.C. *et al.* (2015) Structural insights into micro-opioid receptor activation. *Nature*, **524**, 315-321.

- [78] Venkatakrisnan, A.J., Deupi, X., Lebon, G., Tate, C.G., Schertler, G.F. and Babu, M.M. (2013) Molecular signatures of G-protein-coupled receptors. *Nature*, **494**, 185-194.
- [79] Wheatley, M., Wootten, D., Conner, M.T., Simms, J., Kendrick, R., Logan, R.T., Poyner, D.R. and Barwell, J. (2012) Lifting the lid on GPCRs: the role of extracellular loops. *British Journal of Pharmacology*, **165**, 1688-1703.
- [80] Kmiecik, S., Jamroz, M. and Kolinski, M. (2014) Structure Prediction of the Second Extracellular Loop in G-Protein-Coupled Receptors. *Biophys J*, **106**, 2408-2416.
- [81] Waldhoer, M., Bartlett, S.E. and Whistler, J.L. (2004) Opioid receptors. *Annual Review of Biochemistry*, **73**, 953-990.
- [82] Nitiss, J.L. (2009) Targeting DNA topoisomerase II in cancer chemotherapy. *Nature reviews. Cancer*, **9**, 338-350.
- [83] E.Graves*, R.M.W.a.D. (1989) Thermodynamiiics of the interactions of m-AMSA and o-AMSA with nucleic acids: influence of ionic strength and DNA base composition. *Nucleic acids research*, **17**, 9933.
- [84] Marsh, K.L., Willmore, E., Tinelli, S., Cornarotti, M., Meczes, E.L., Capranico, G., Fisher, L.M. and Austin, C.A. (1996) Amsacrine-promoted DNA cleavage site determinants for the two human DNA topoisomerase II isoforms alpha and beta. *Biochemical Pharmacology*, **52**, 1675-1685.
- [85] Ketron, A.C., Denny, W.A., Graves, D.E. and Osheroff, N. (2012) Amsacrine as a Topoisomerase II Poison: Importance of Drug-DNA Interactions. *Biochemistry*, **51**, 1730-1739.
- [86] Farsani, F.M., Ganjalikhany, M.R., Dehbashi, M., Naeini, M.M. and Vallian, S. (2016) Structural basis of DNA topoisomerase II-alpha (Top2-alpha) inhibition: a computational analysis of interactions between Top2-alpha and its inhibitors. *Medicinal Chemistry Research*, **25**, 1250-1259.
- [87] Jangir, D.K., Dey, S.K., Kundu, S. and Mehrotra, R. (2012) Assessment of amsacrine binding with DNA using UV-visible, circular dichroism and Raman spectroscopic techniques. *Journal of Photochemistry and Photobiology B-Biology*, **114**, 38-43.
- [88] Dong, K.C. and Berger, J.M. (2007) Structural basis for gate-DNA recognition and bending by type IIA topoisomerases. *Nature*, **450**, 1201-U1204.
- [89] Shahid, M., Sobia, E., Singh, A., Malik, A., Khan, H.M., Jonas, D. and Hawkey, P.M. (2009) Beta-lactams and Beta-lactamase-inhibitors in current- or potential-clinical practice: A comprehensive update. *Critical Reviews in Microbiology*, **35**, 81-108.
- [90] Patel, S., Keller, B.A. and Fisher, L.M. (2000) Mutations at arg486 and glu571 in human topoisomerase II alpha confer resistance to amsacrine: Relevance for antitumor drug resistance in human cells. *Molecular Pharmacology*, **57**, 784-791.
- [91] Thakur, D.S. (2011) Topoisomerase II inhibitors in cancer treatment. *international journal of pharamceutical sciences and nanotechnology*, **3**, 1173.

- [92] Wu, C.-C., Li, T.-K., Farh, L., Lin, L.-Y., Lin, T.-S., Yu, Y.-J., Yen, T.-J., Chiang, C.-W. and Chan, N.-L. (2011) Structural Basis of Type II Topoisomerase Inhibition by the Anticancer Drug Etoposide. *Science*, **333**, 459-462.
- [93] Jacobson, M.P., Pincus, D.L., Rapp, C.S., Day, T.J.F., Honig, B., Shaw, D.E. and Friesner, R.A. (2004) A hierarchical approach to all-atom protein loop prediction. *Proteins-Structure Function and Bioinformatics*, **55**, 351-367.
- [94] Jacobson, M.P., Friesner, R.A., Xiang, Z. and Honig, B. (2002) On the Role of the Crystal Environment in Determining Protein Side-chain Conformations. *Journal of Molecular Biology*, **320**, 597-608.
- [95] Michael Hinds, K.D., Janice Mayes, Elizabeth Altschuler, Ruud Jansen, Fred D. Ledley, and Leonard A. Zwelling. (1991) Identification of a Point Mutation in the Topoisomerase II Gene from a Human Leukemia Cell Line Containing an Amsacrine-resistant Form of Topoisomerase III. [*CANCER RESEARCH*, **51**, 4729-4731.
- [96] Borders, C.L., Broadwater, J.A., Bekeny, P.A., Salmon, J.E., Lee, A.S., Eldridge, A.M. and Pett, V.B. (1994) A Structural Role For Arginine In Proteins - Multiple Hydrogen-Bonds To Backbone Carbonyl Oxygens. *Protein Science*, **3**, 541-548.
- [97] Champoux, J.J. (2001) DNA TOPOISOMERASES: Structure, Function, and Mechanism. *Annu. Rev. Biochem*, **70**, 369-413.

Appendix A

Supporting Material (Chapter 2)

Table S1

Glide XP docking score (units: kcal/mol).

	hMOR-1	hMOR-G2	hMOR-G1
Morphine	-3.4	-2.7	-3.0
IBNtxA	-3.3	-4.1	-5.4

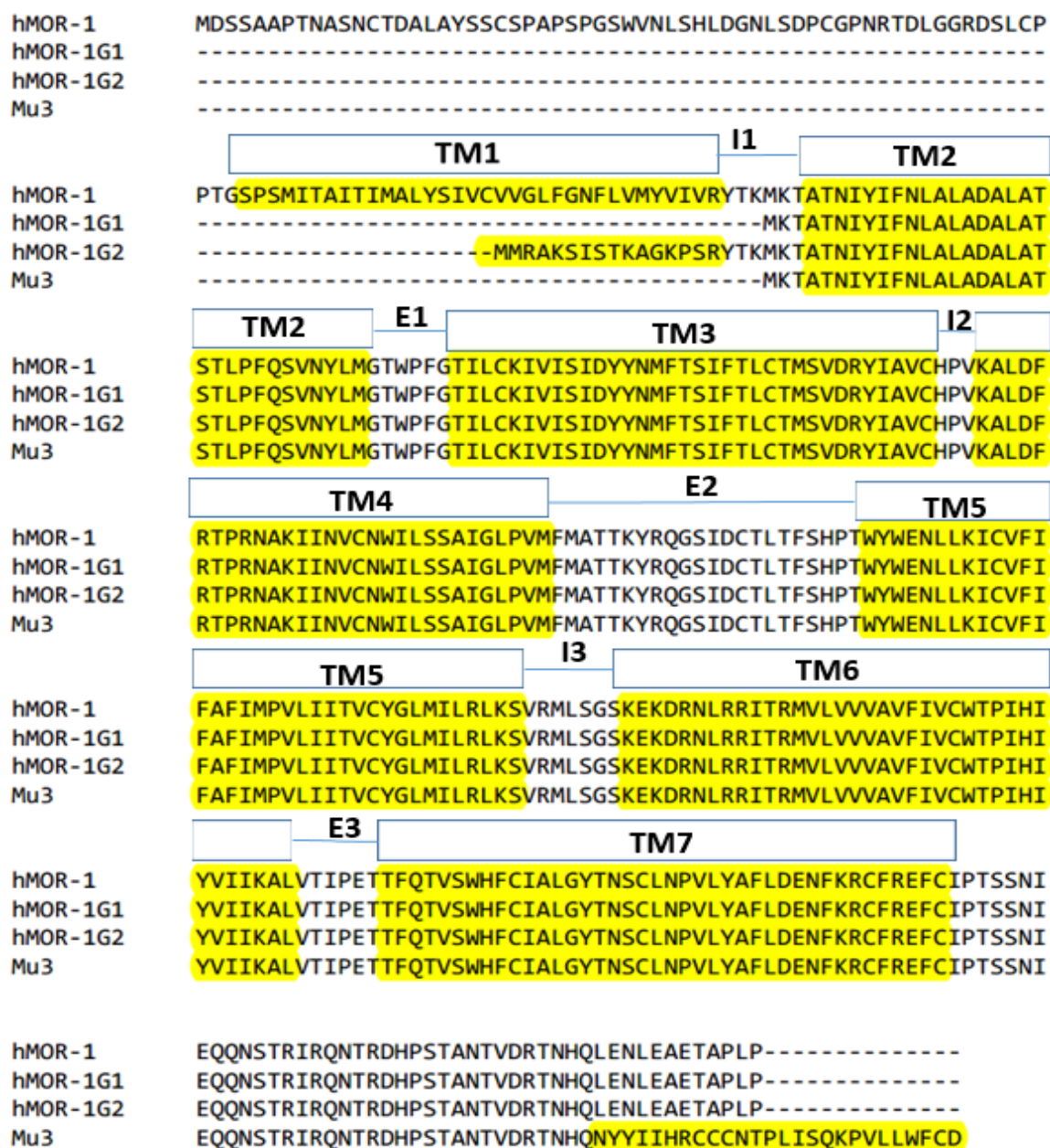


Figure S1. Sequences of full-length and truncated variants of human MOR-1 (hMOR-1). Rectangular boxes refer to the Trans membranes helices. The yellow highlight represents the amino acids sequences for each transmembrane domain. The intracellular (I1-I3) and extracellular loops (E1-E3) connecting the Trans membranes are illustrated as threads labeled according to loop location.

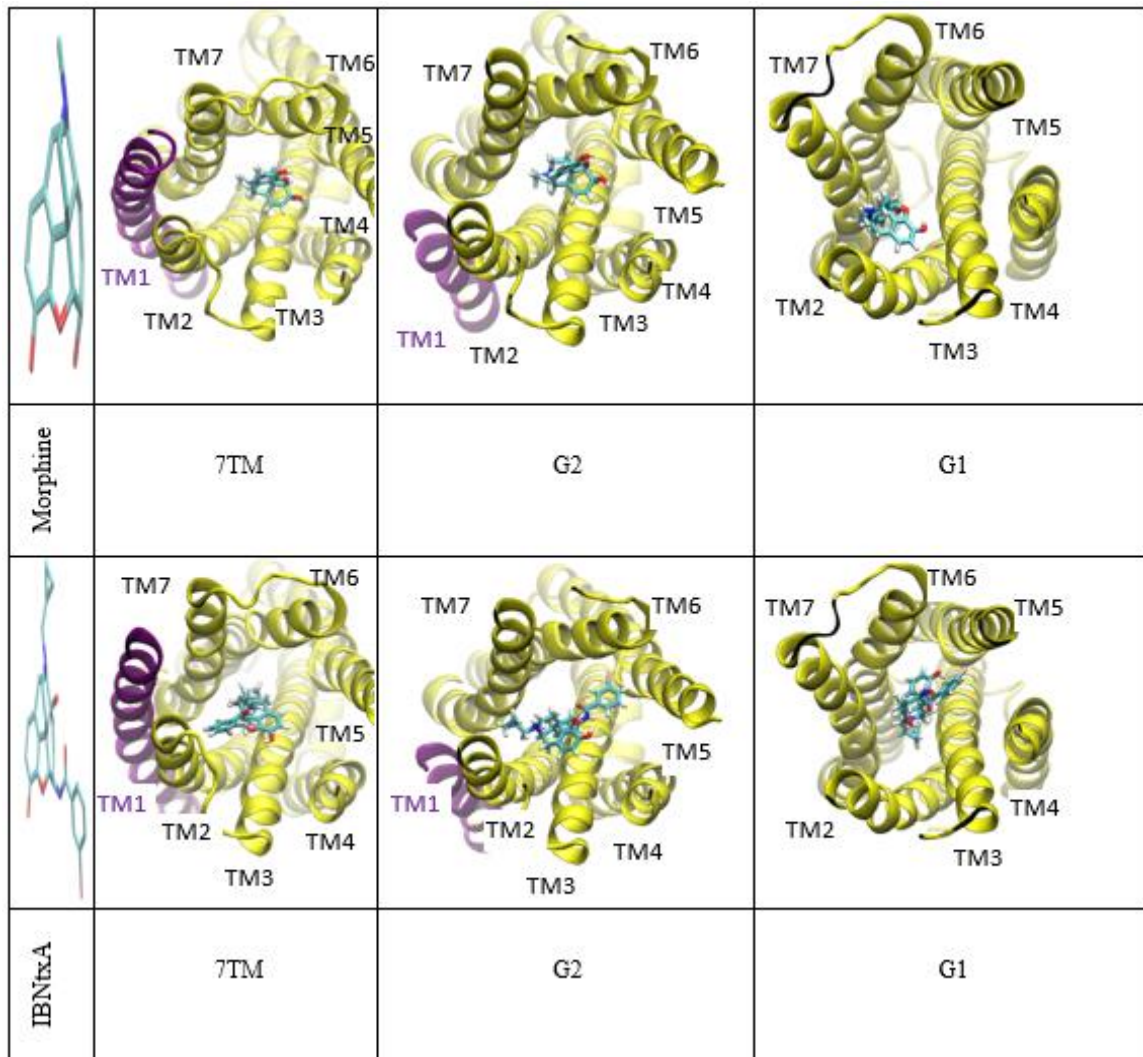


Figure S2. 3D-structures of morphine, IBNtxA, and their complexes with 7TM, G2 and G1 hMOR-1 receptors obtained from Glide XP docking. TM1 is colored in purple.

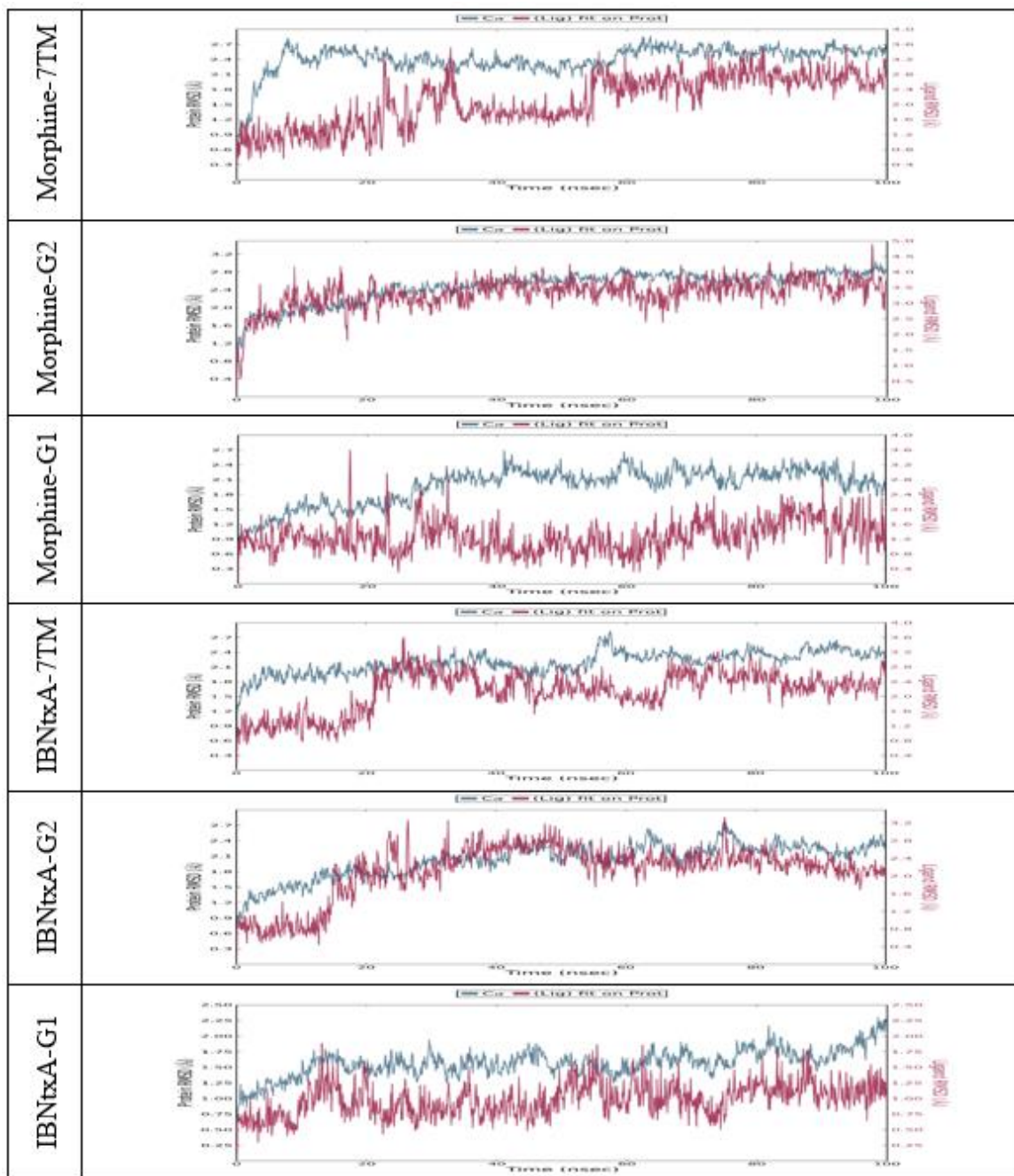


Figure S3. Root Mean Square Deviation (RMSD) of protein-Ligand complexes against simulation time. α -RMSD is measured using the initial frame as reference, while the ligand fit on protein RMSD refer to in place RMSD of ligand when protein is aligned.

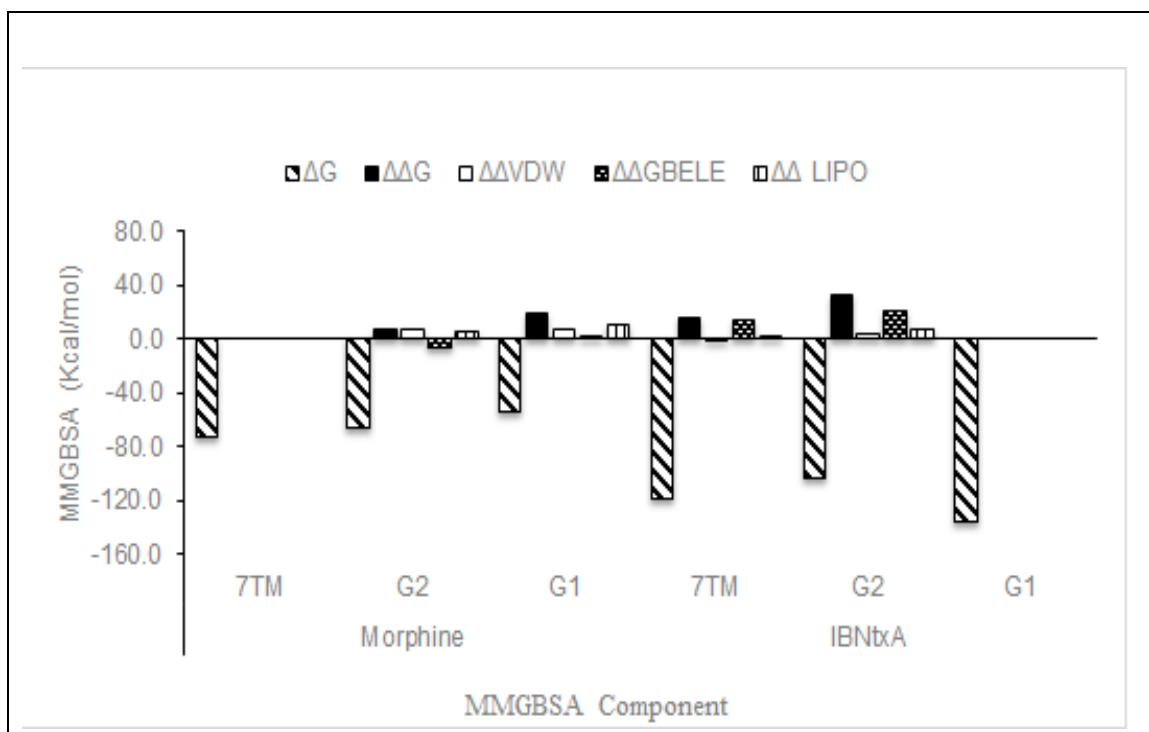


Figure s4. MMGBSA binding energies of both Morphine and IBNtxA complexes with three different receptors. The above columns represent the different components of MM-GBSA binding energy (kcal/mol).

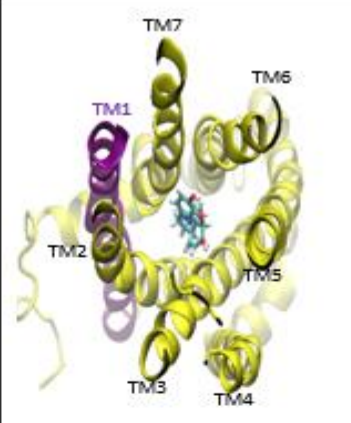
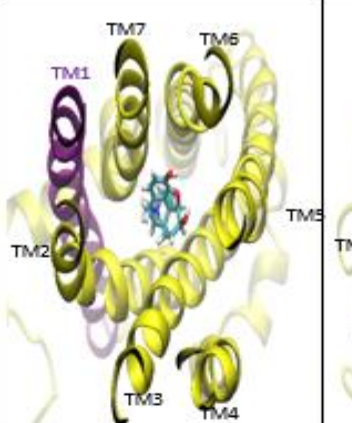
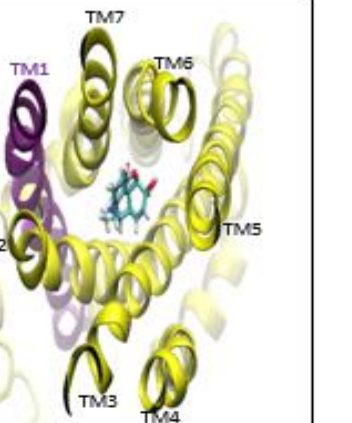
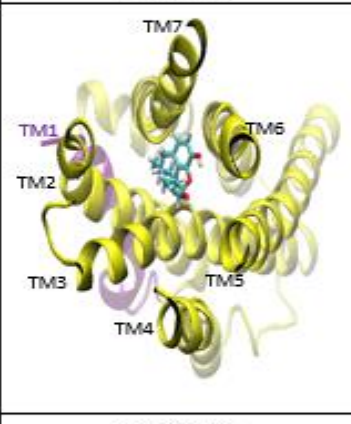
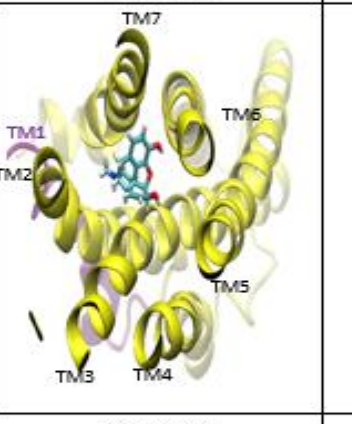
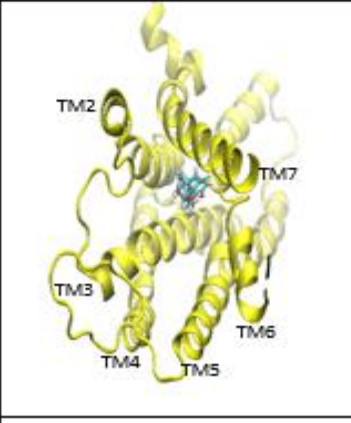
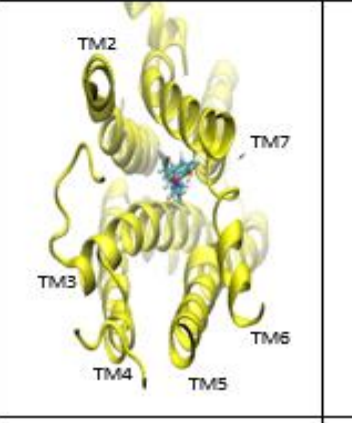
7TM-morphine			
	A (59%)	B (38%)	C (2%)
	G2-morphine		
D (78%)		E (21%)	
G1-morphine			
	F (73%)	G (26%)	

Figure S5. Representative receptor-morphine structures of top structural families from the clustering analysis. Abundance is annotated. For all structures, the extracellular and intracellular loops were truncated for clarity. The abundance is annotated.

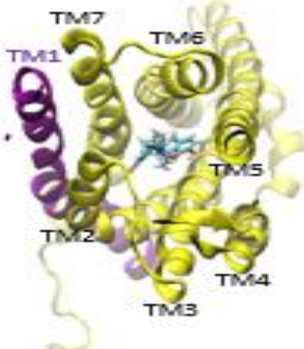
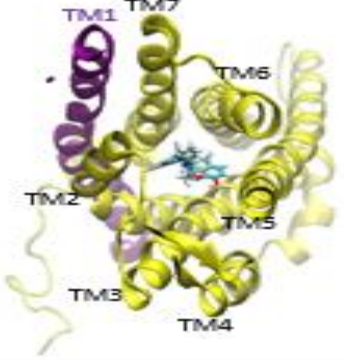
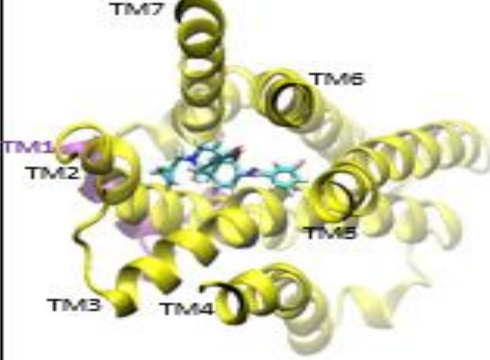
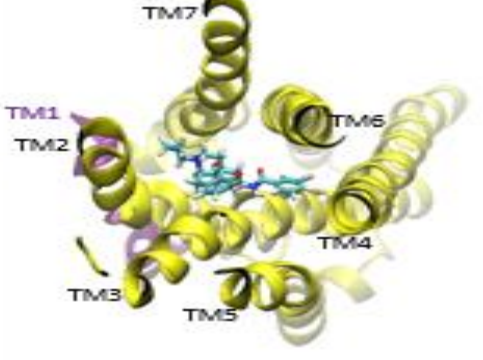
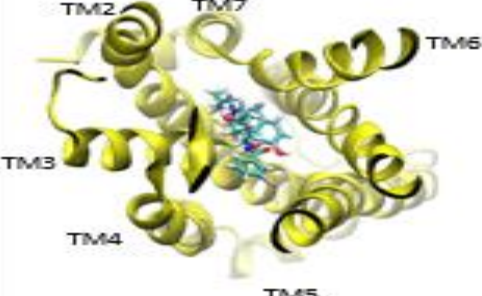
7TM-IBNtxA		
	A (78.2%)	B (21.7%)
G2-IBNtxA		
	C (93.7%)	D (6.2%)
G1-IBNtxA		
	E (100%)	

Figure S6. Representative receptor-IBNtxA structures of top Complexes structural families from the clustering analysis. Abundance is annotated.

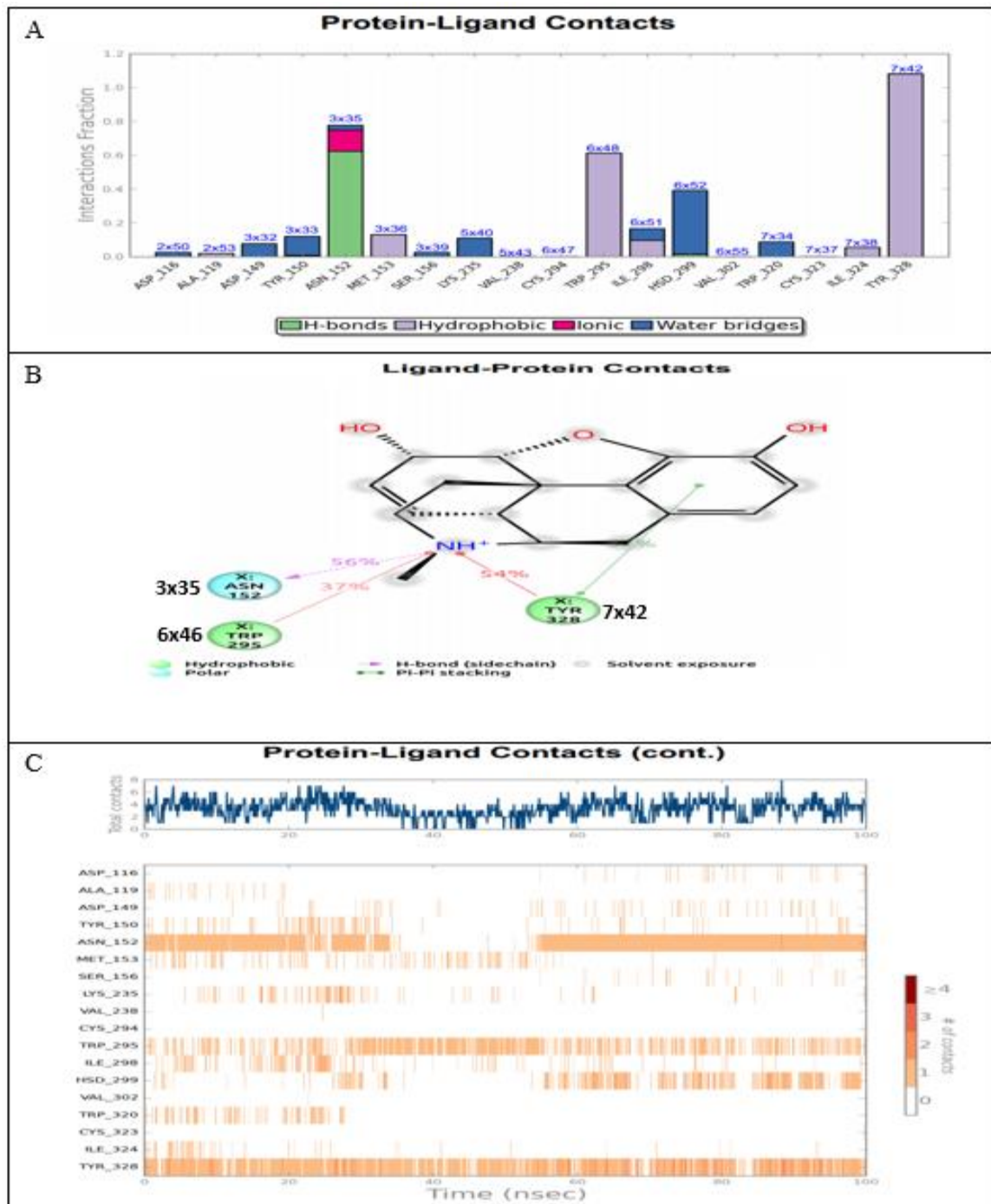


Figure S7. Contacts of Morphine to wild type receptor (hMOR-1). The genetic numbering is annotated for each interacting residue. A: Interactions fraction over the MD trajectory. B: Illustrates interactions persist more than 30% of simulation time. C: The ligand protein contacts over the MD trajectory.

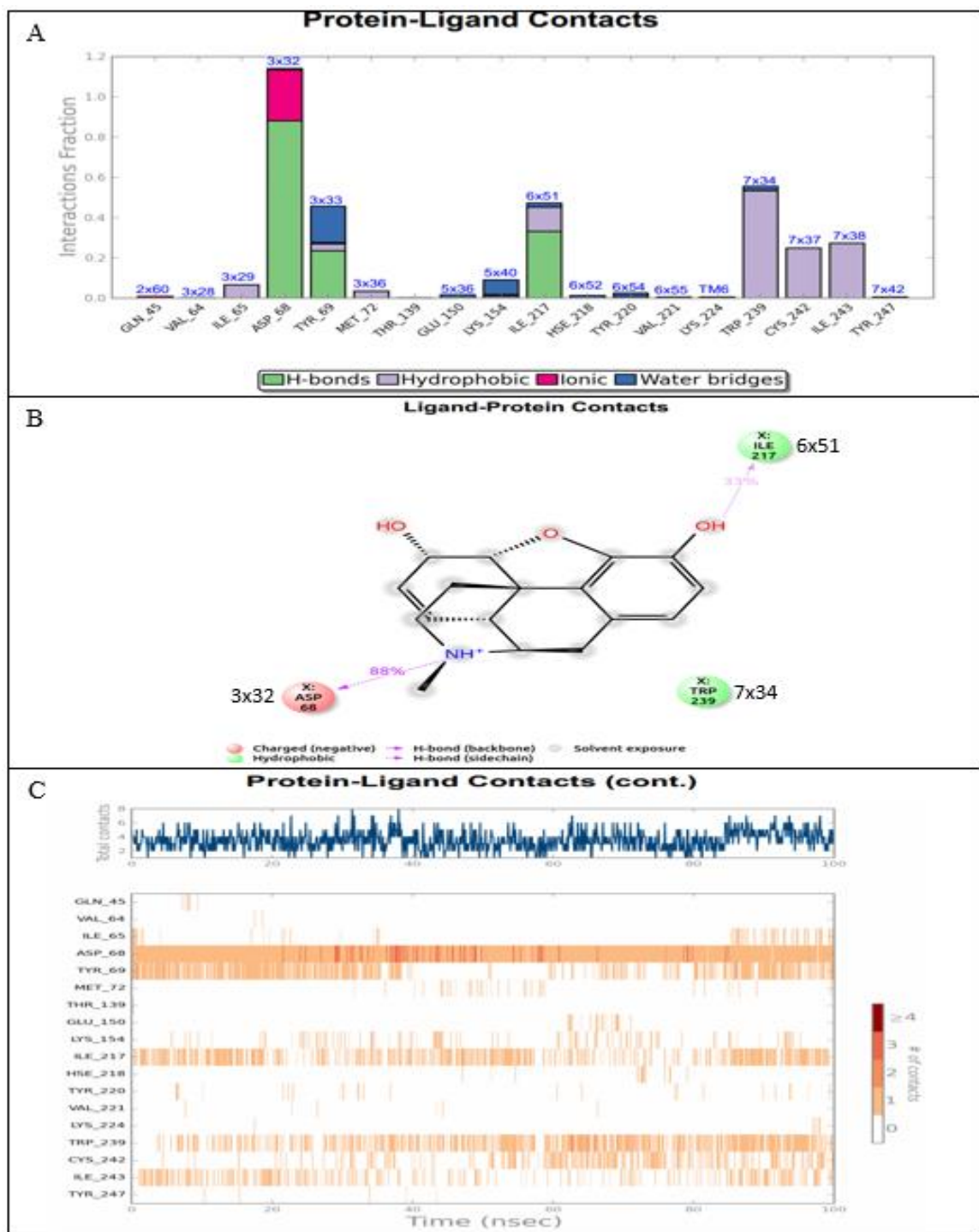


Figure S8. 2D profile data of Morphine binding with G2 splice variant receptor

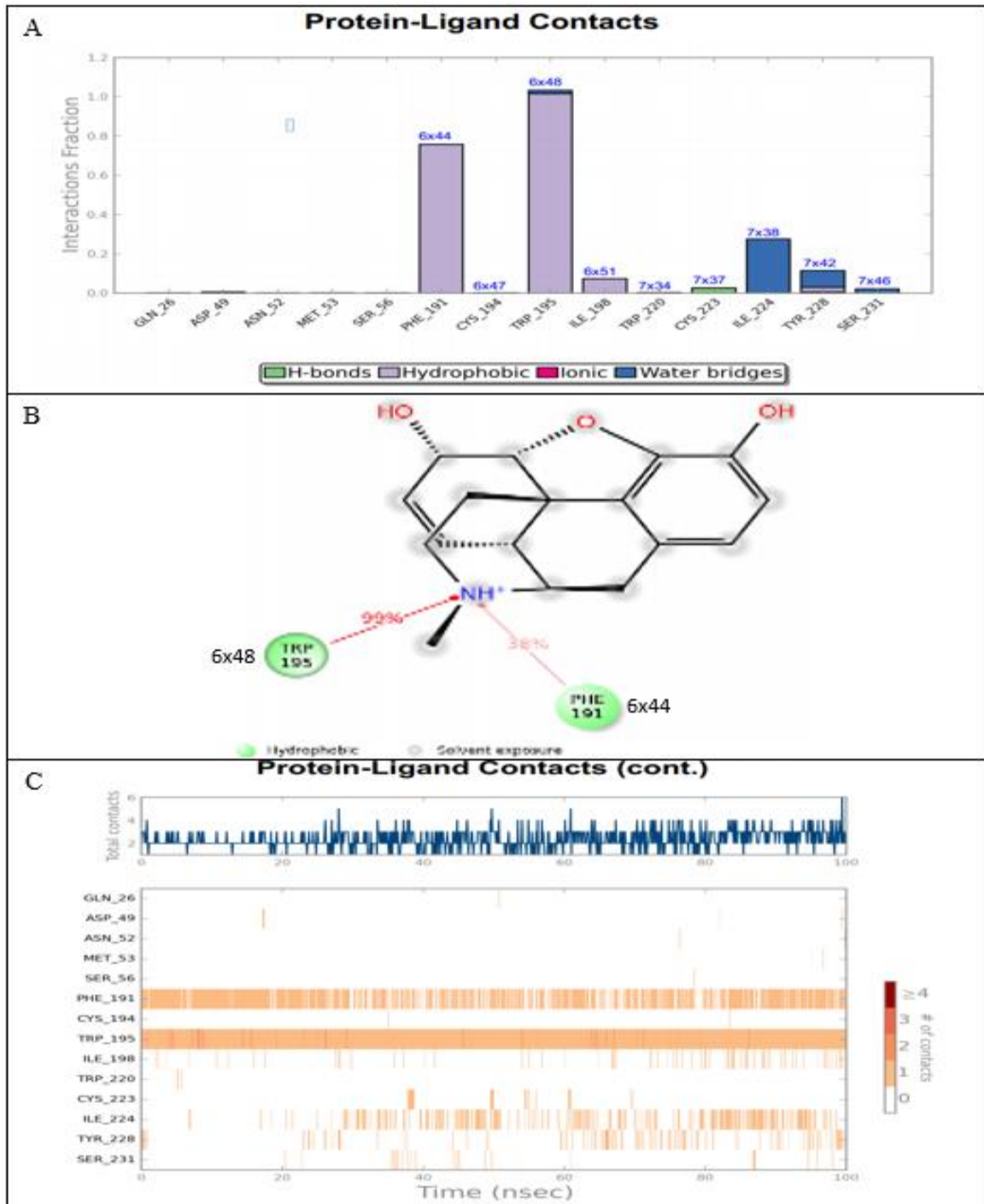


Figure S9. 2D profile data of Morphine binding with G1 splice variant receptor

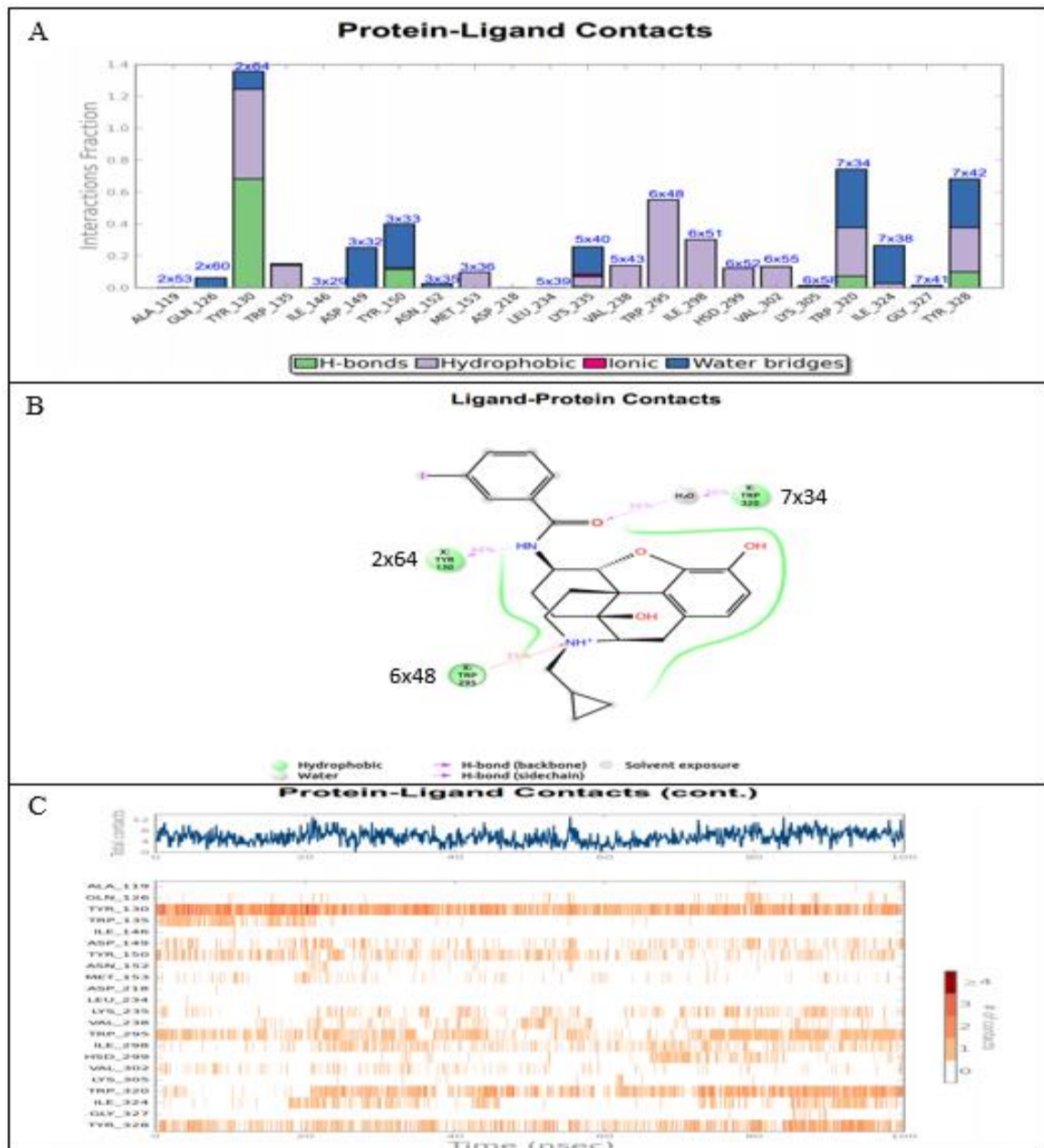


Figure S10. 2D profile data of IBNtxA binding to wild type receptor (MOR-1).

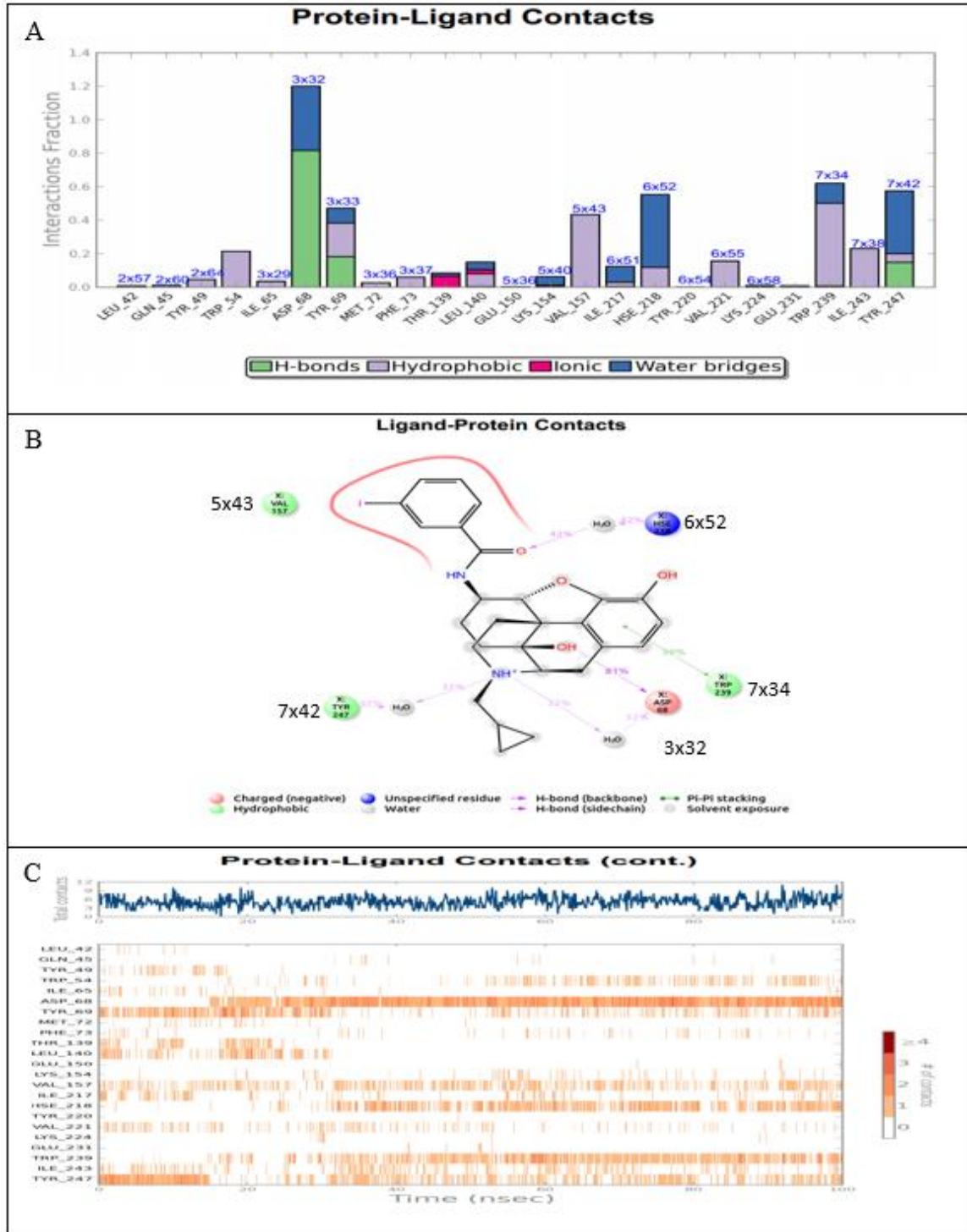


Figure S11. 2D profile data of IBNtxA with G2 splice variant receptor.

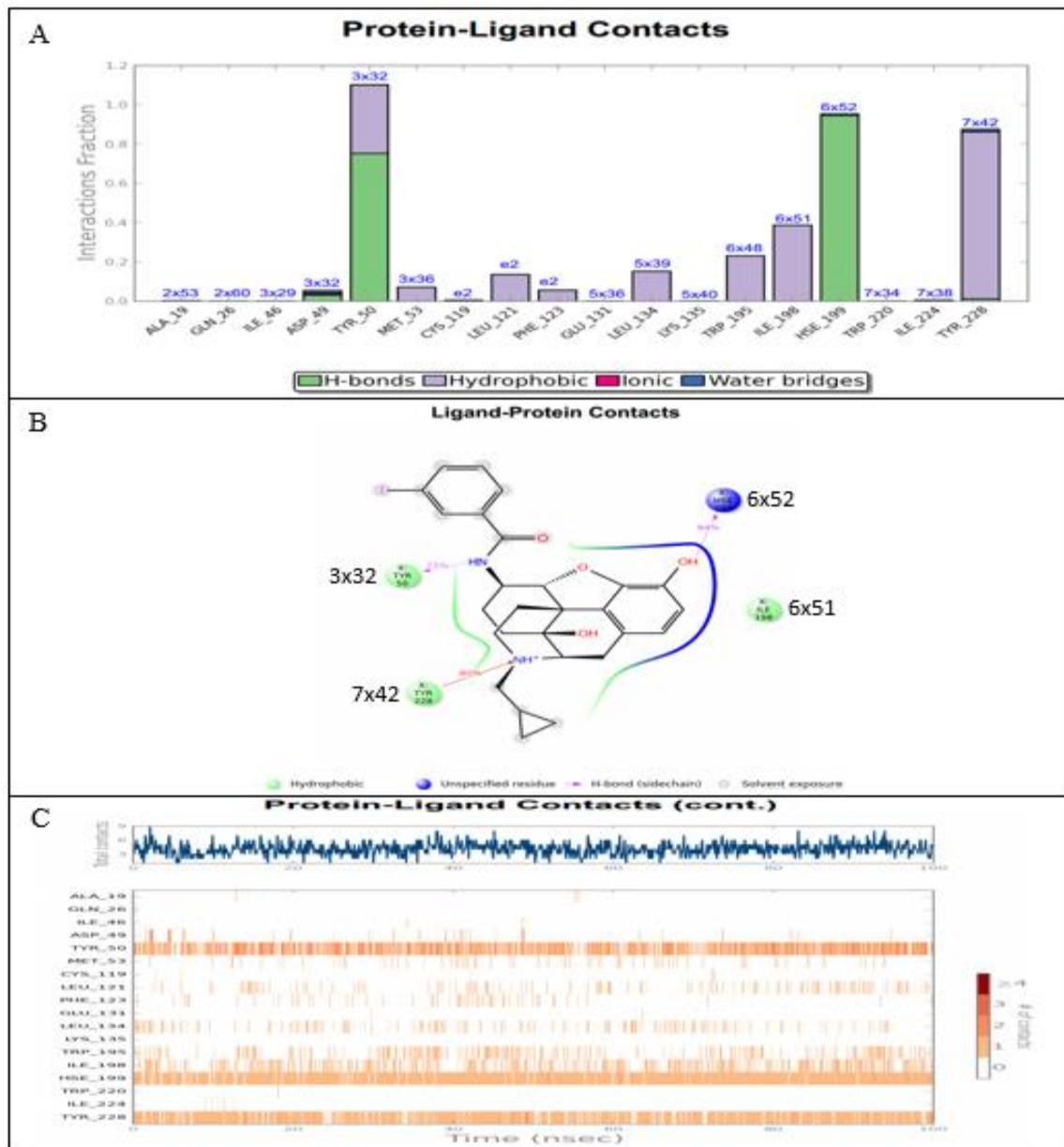


Figure S12. 2D profile data of IBNtxA with G1 splice variant receptor

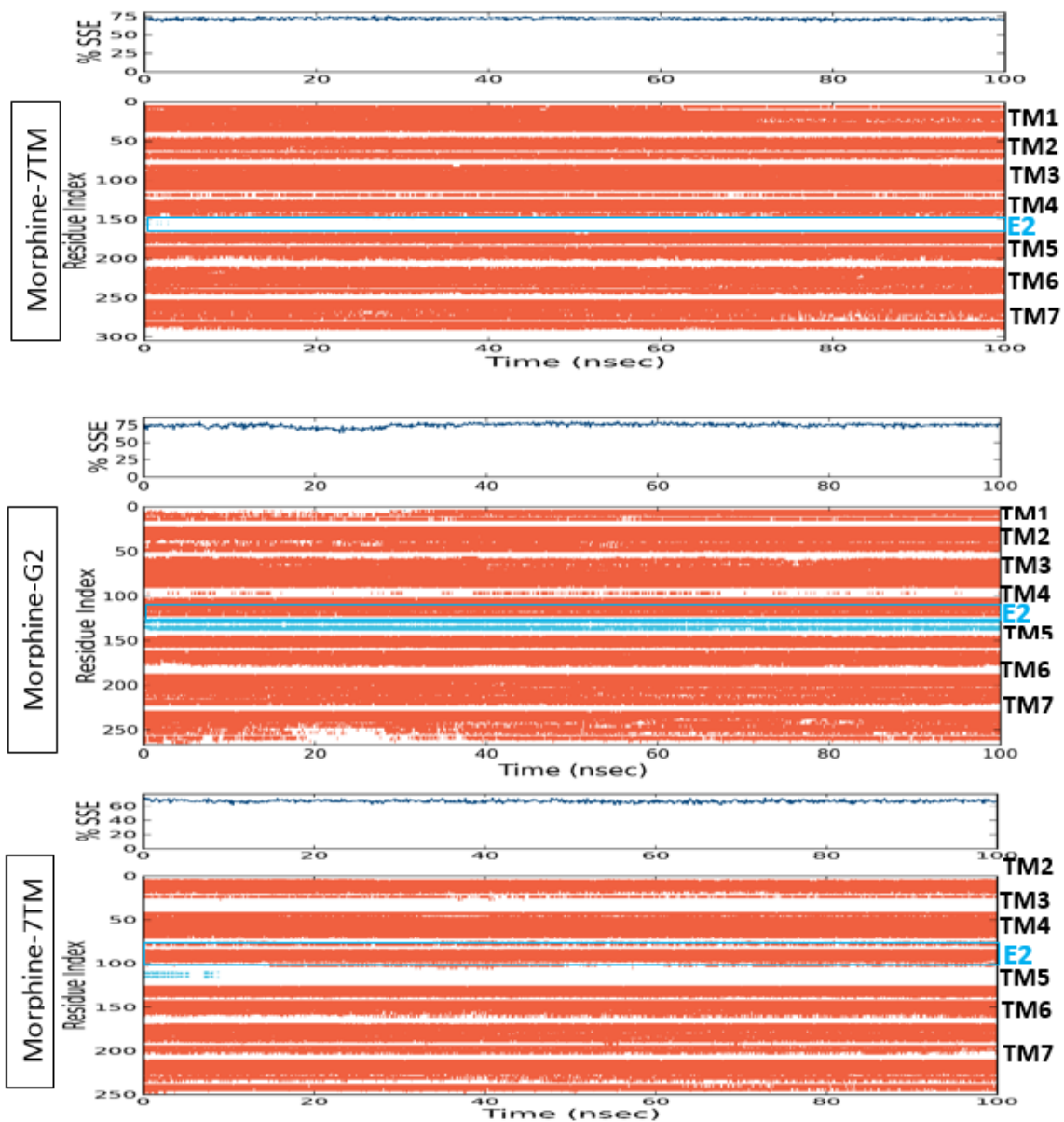


Figure S13. Secondary structure elements over the simulation time for Morphine with three receptors.

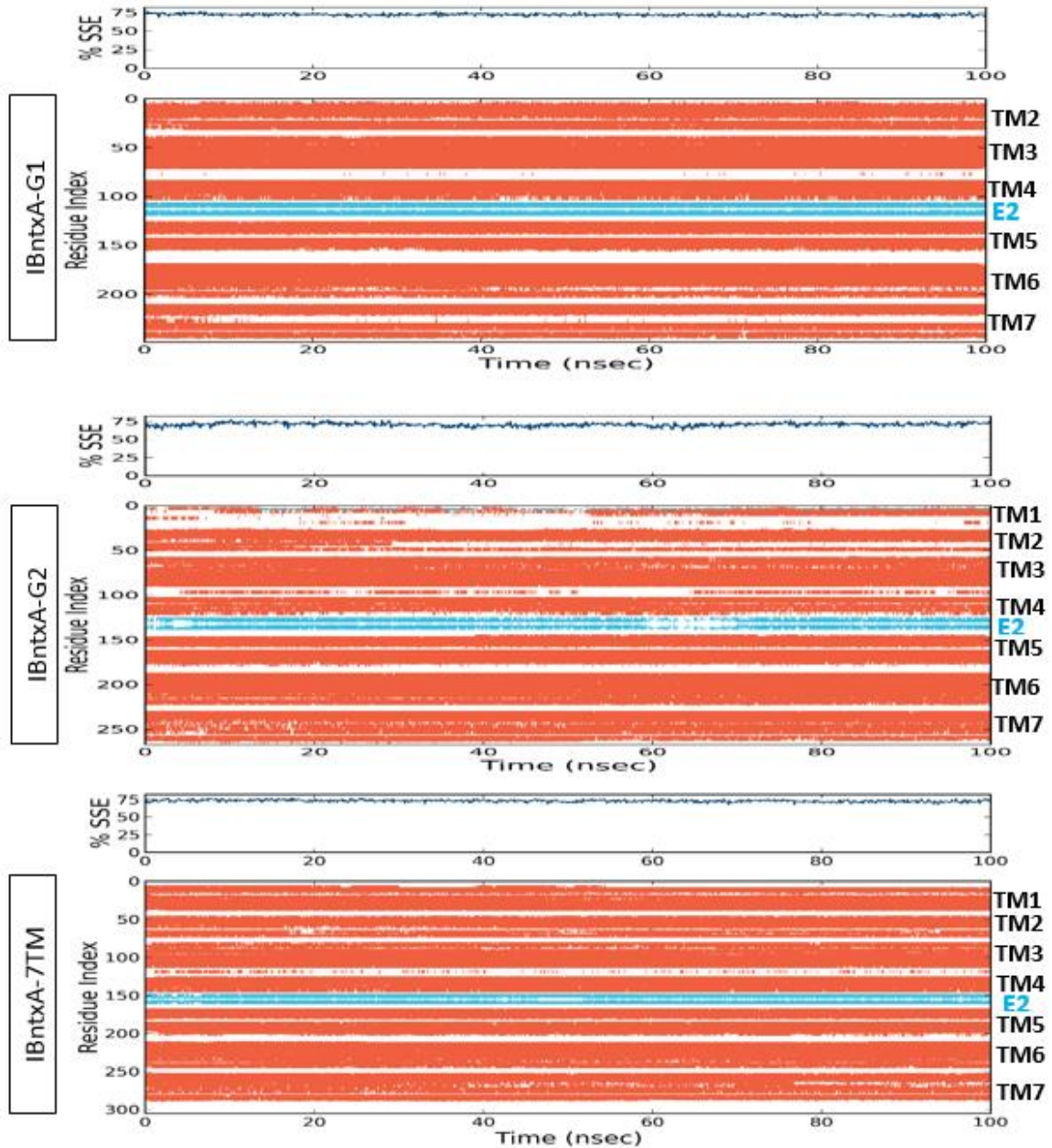


Figure S14. Secondary structure elements over the simulation time for IbntxA with three receptors.

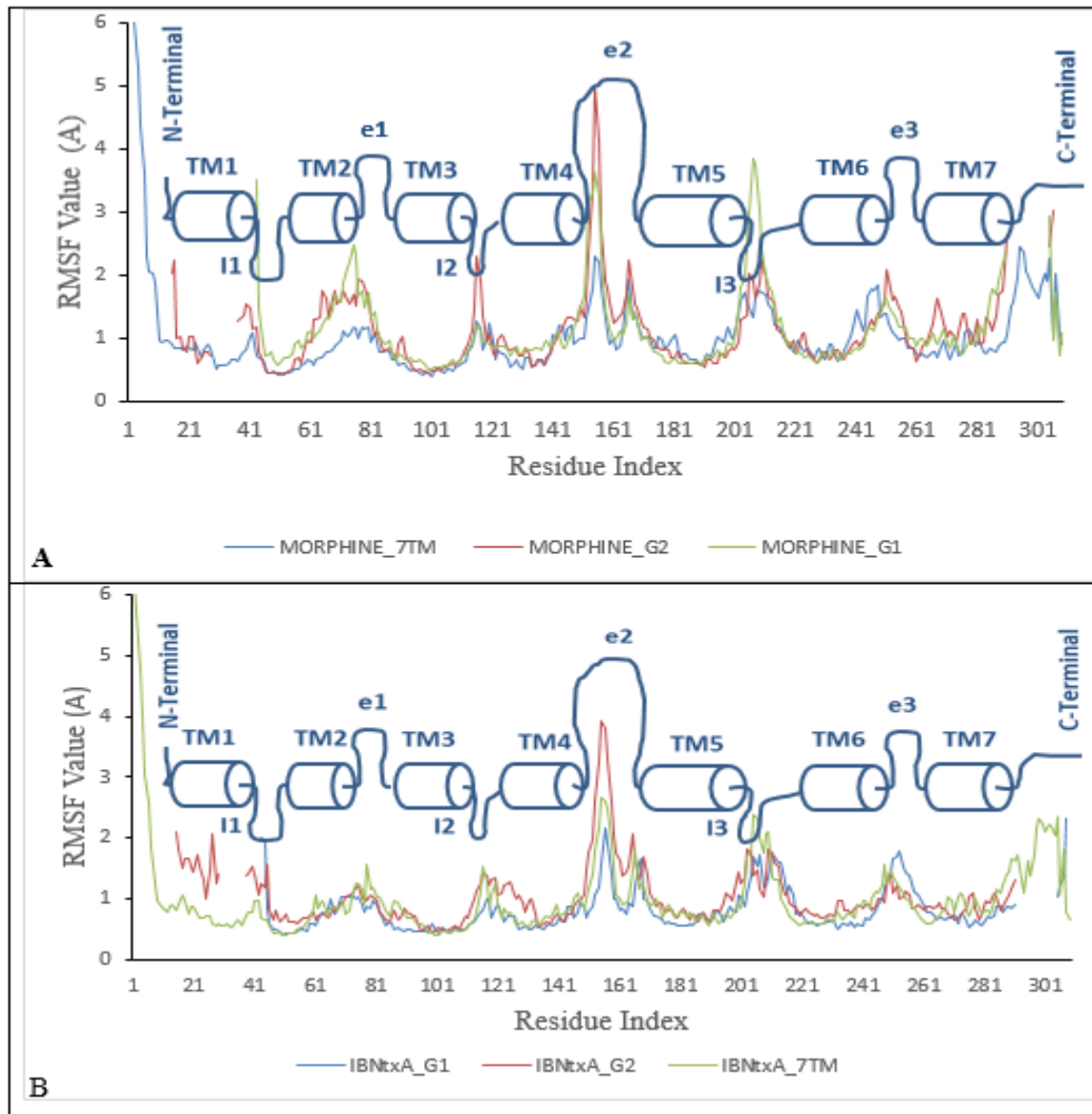


Figure S15. Figure S. RMSF diagrams of receptor Protein C- α . Diagram (A): Morphine-7tm-G2-G1 protein C- α RMSFs comparisons. Diagram (B): IBNtxA-7TM-G1-G2 protein C- α RMSFs comparisons. The residue index is shown for the full length wild type MOR-1 receptor. In case of G1 receptor, the RMSF diagram starts at the TM2 skipping TM1 as result of truncation.

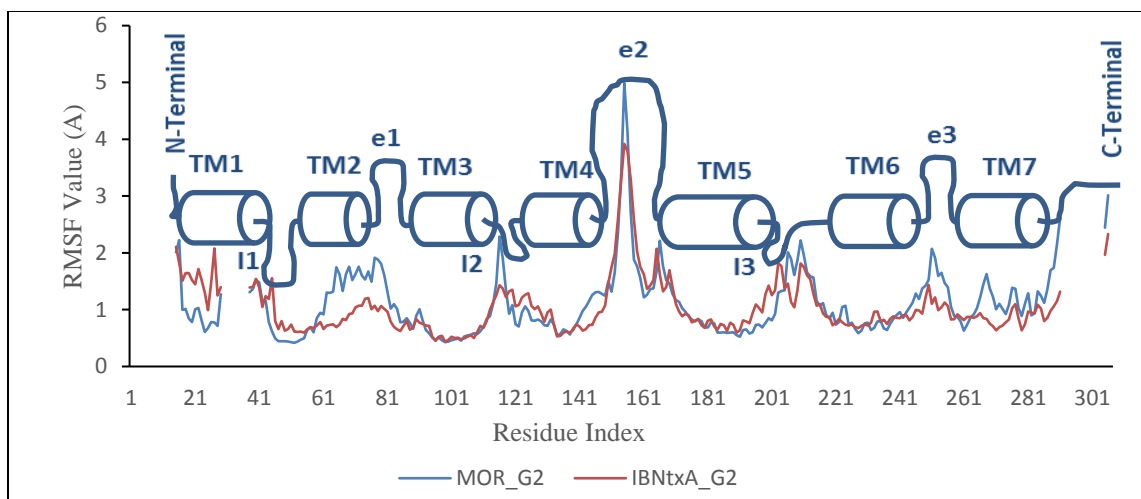


Figure S16. RMSF diagram of receptor Protein C- α . Figures G2 Receptor Interaction with both IBNtxA and Morphine Comparisons.

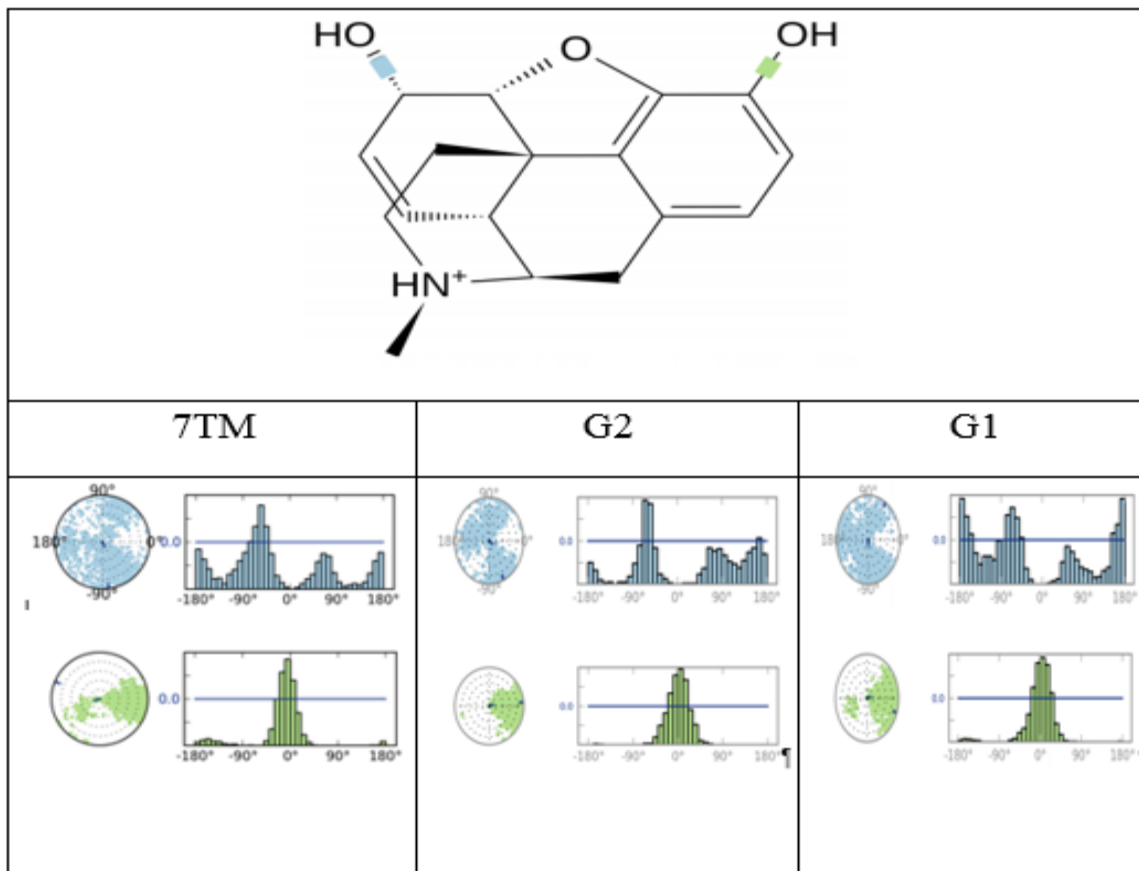


Figure S17. Ligand torsion profile of Morphine binding to three different receptors.

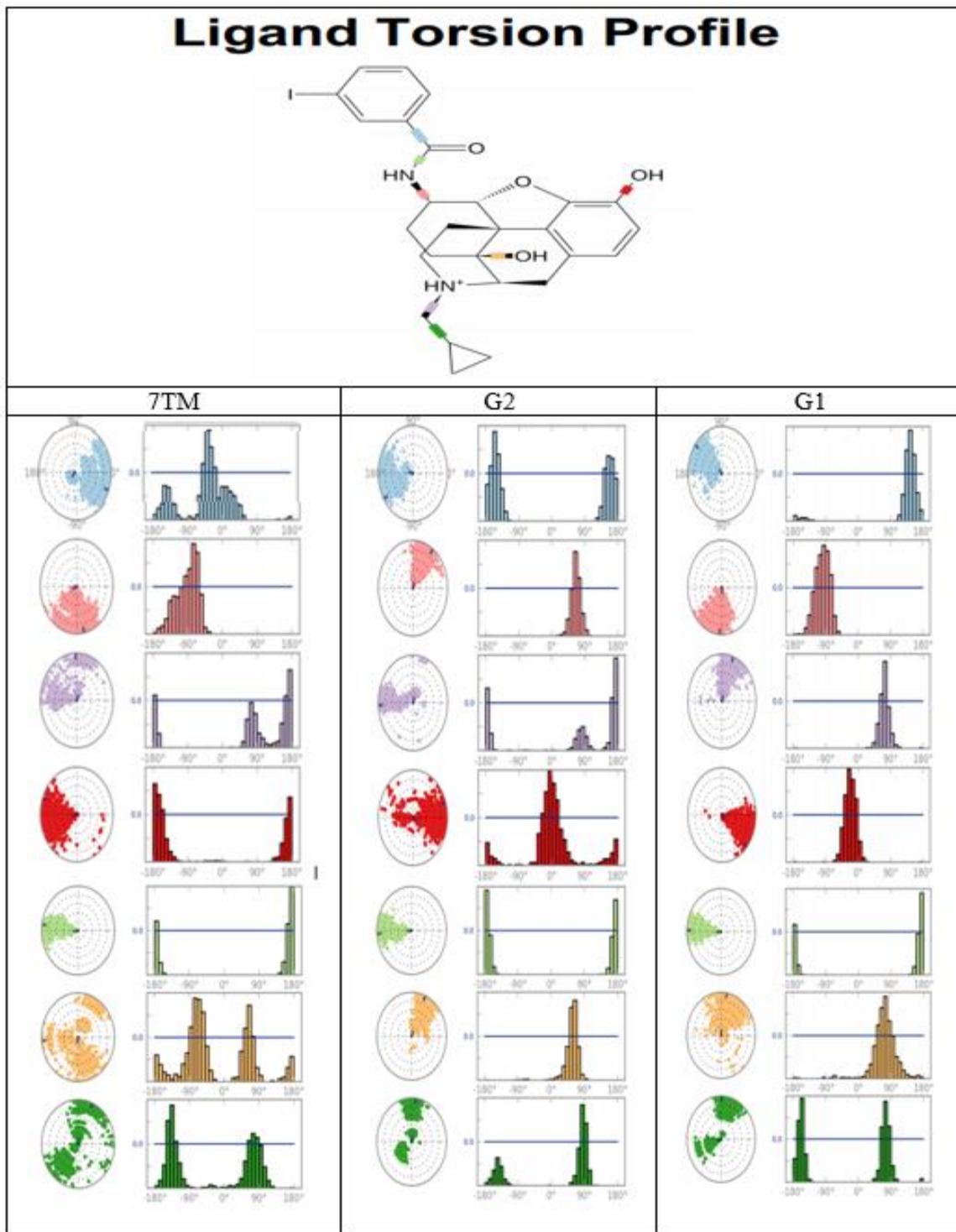


Figure S18. Ligand torsion profile of IBNtxA when binding to three different receptors.

Appendix B

Supporting Material (Chapter 3)

Table S1

MM-GBSA binding energies of Amsacrine to hTop2 α WT and two mutants.

	LD-A	LP-A	LPD-A	LD-B	LP-B	LPD-B
WT	-36.73 \pm 3.85	-32.73 \pm 3.32	-71.81 \pm 3.74	-27.15 \pm 2.61	-32.60 \pm 3.34	-60.93 \pm 4.37
R487K	-24.00 \pm 4.03	-15.07 \pm 3.31	-39.13 \pm 4.2	-18.99 \pm 9.23	-14.81 \pm 11.03	-34.82 \pm 8.7
E571K	-20.99 \pm 5.1	-21.99 \pm 7.13	-42.85 \pm 6.57	-20.73 \pm 2.83	-32.15 \pm 4.37	-53.50 \pm 6.4

LD: Ligand-DNA complex, **LP:** Ligand-Protein complex, **LPD:** Ligand-Protein-DNA complex.

A&B: refers to the two binding sites.

Table S2

Decomposition of MM-GBSA binding energies of Amsacrine to hTop2 α WT and two mutants

ΔG Type	WT						R487K						E571K					
	LDP-A	LD-A	LP-A	LDP-B	LD-B	LP-B	LDP-A	LD-A	LP-A	LDP-B	LD-B	LP-B	LDP-A	LD-A	LP-A	LDP-B	LD-B	LP-B
¹ ΔG	-71.81	-36.7	-32.7	-60.93	-27.2	-32.6	-39.13	-24	-15.1	-34.82	-19	-14.8	-42.85	-21	-22	-53.5	-20.7	-32.2
² $\Delta\Delta G$	0	0	0	0	0	0	32.68	12.73	17.67	26.11	8.16	17.78	28.96	15.73	10.75	7.44	6.42	0.44
³ ΔVDW	-60.46	-37.6	-22.4	-52.23	-30.1	-21.9	-51.14	-33.1	-18.1	-33.89	-22	-11.9	-44.11	-28.6	-15.6	-48.68	-26.5	-22.3
$\Delta\Delta VDW$	0	0	0	0	0	0	9.32	4.51	4.34	18.34	8.11	9.94	16.35	8.98	6.85	3.55	3.6	-0.39
⁴ $\Delta LIPO$	-25.53	-8.59	-16.5	-26.18	-7.28	-18.6	-5.57	-0.89	-4.67	-11.54	-3.41	-8.13	-16.25	-2.58	-13.7	-21.86	-2.91	-18.9
$\Delta\Delta LIPO$	0	0	0	0	0	0	19.96	7.7	11.8	14.64	3.87	10.5	9.28	6.01	2.81	4.32	4.37	-0.31
⁵ $\Delta GBELE$	14.18	9.4	6.16	17.49	10.21	7.89	17.57	9.963	7.68	10.61	6.4	5.24	17.51	10.18	7.25	17.05	8.66	9.05
$\Delta\Delta GBELE$	0	0	0	0	0	0	3.39	0.563	1.52	-6.88	-3.81	-2.65	3.33	0.78	1.09	-0.44	-1.55	1.16

¹ ΔG : MM-GBSA binding energy (Complex – Receptor – Ligand).

² $\Delta\Delta G$: relative binding energy with reference to WT complex.

³ ΔVDW : Change of van der Waals energy (vdW + Pi-pi stacking + Self-contact correction) in gas phase upon complex formation

⁴ $\Delta LIPO$: Change of lipophilic term (Lipophilic energy) upon complex formation.

⁵ $\Delta GBELE$: Change of electrostatic interactions (GB/Generalized Born electrostatic solvation energy + ELE/Coulomb energy + Hydrogen-bonding) upon complex formation.

LD: Ligand-DNA only Interaction, LP: Ligand-Protein only Interaction, LPD: Ligand-Protein-DNA interaction

A&B: refers to the two binding sites.

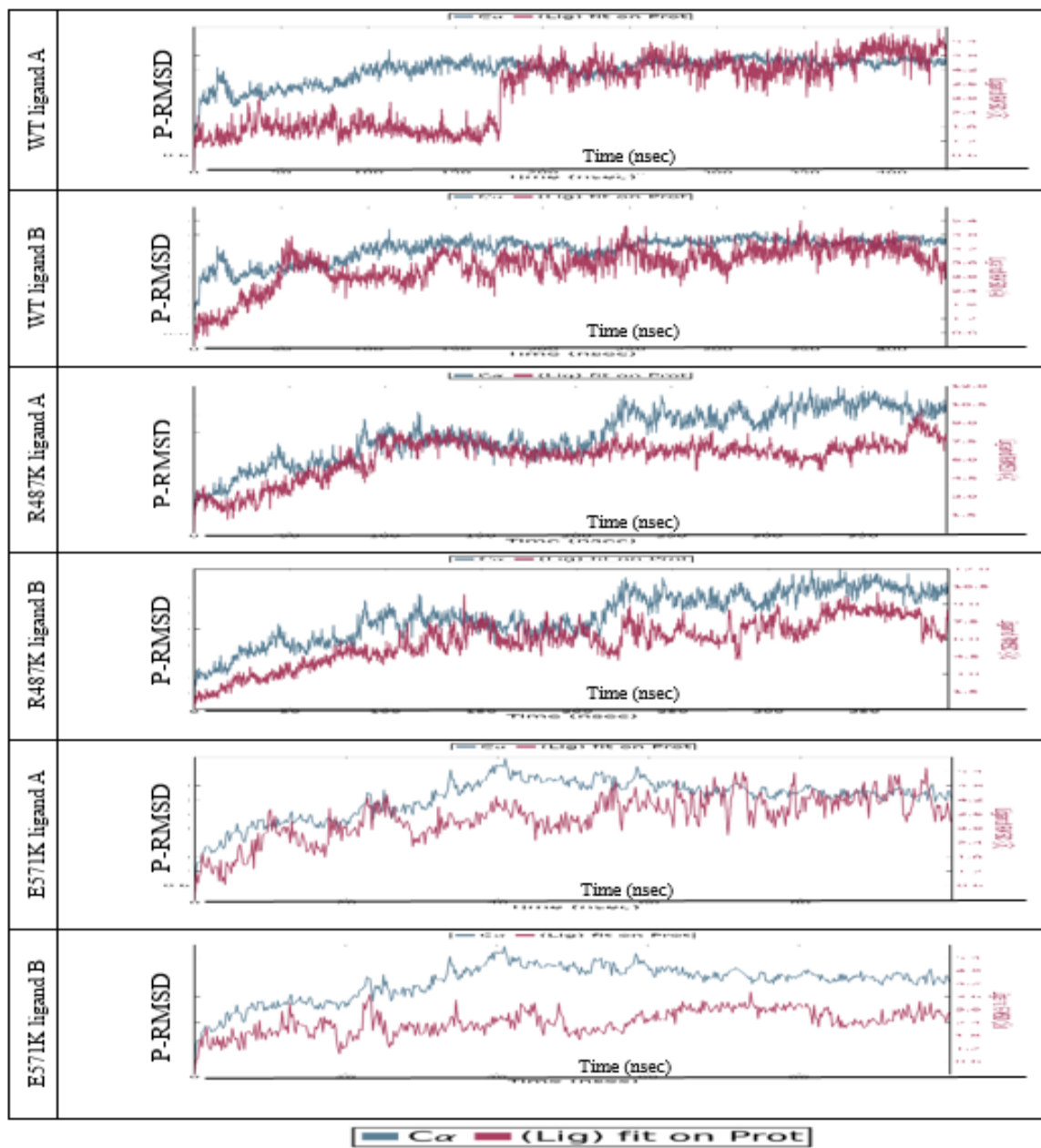


Figure S1. Root Mean Square Deviation (RMSD) of Amsacrine-Enzyme complexes against simulation time. C α -RMSD is measured using the initial frame as reference, while the ligand fit on protein RMSD refer to in place RMSD of ligand when protein is aligned.

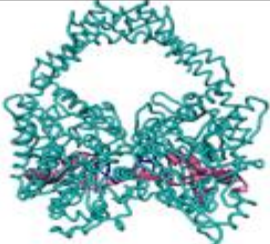
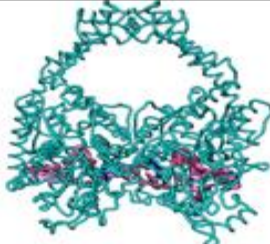
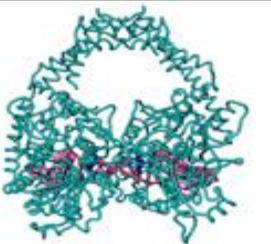
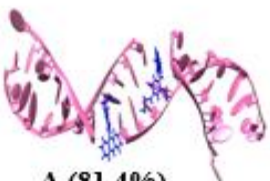




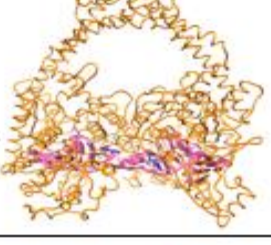
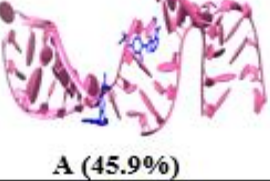
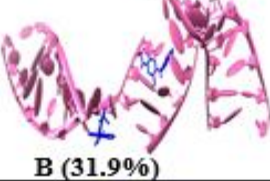
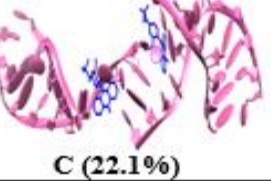
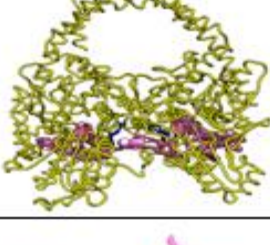
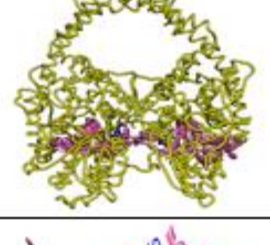
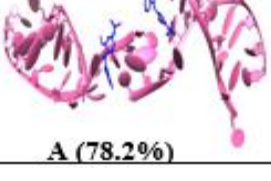
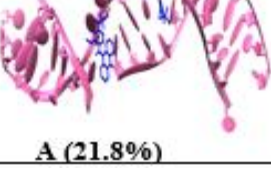
WT-Complex			
WT-DNA	 A (81.4%)	 B (14.2%)	 C (3.6%)
R487K-Complex			
R487K-DNA	 A (45.9%)	 B (31.9%)	 C (22.1%)
E571K-Complex			
E571K-DNA	 A (78.2%)	 A (21.8%)	

Figure S2. Representative hTOP2 α -Amsacrine structures of top structural families from the clustering analysis. Abundance is annotated.

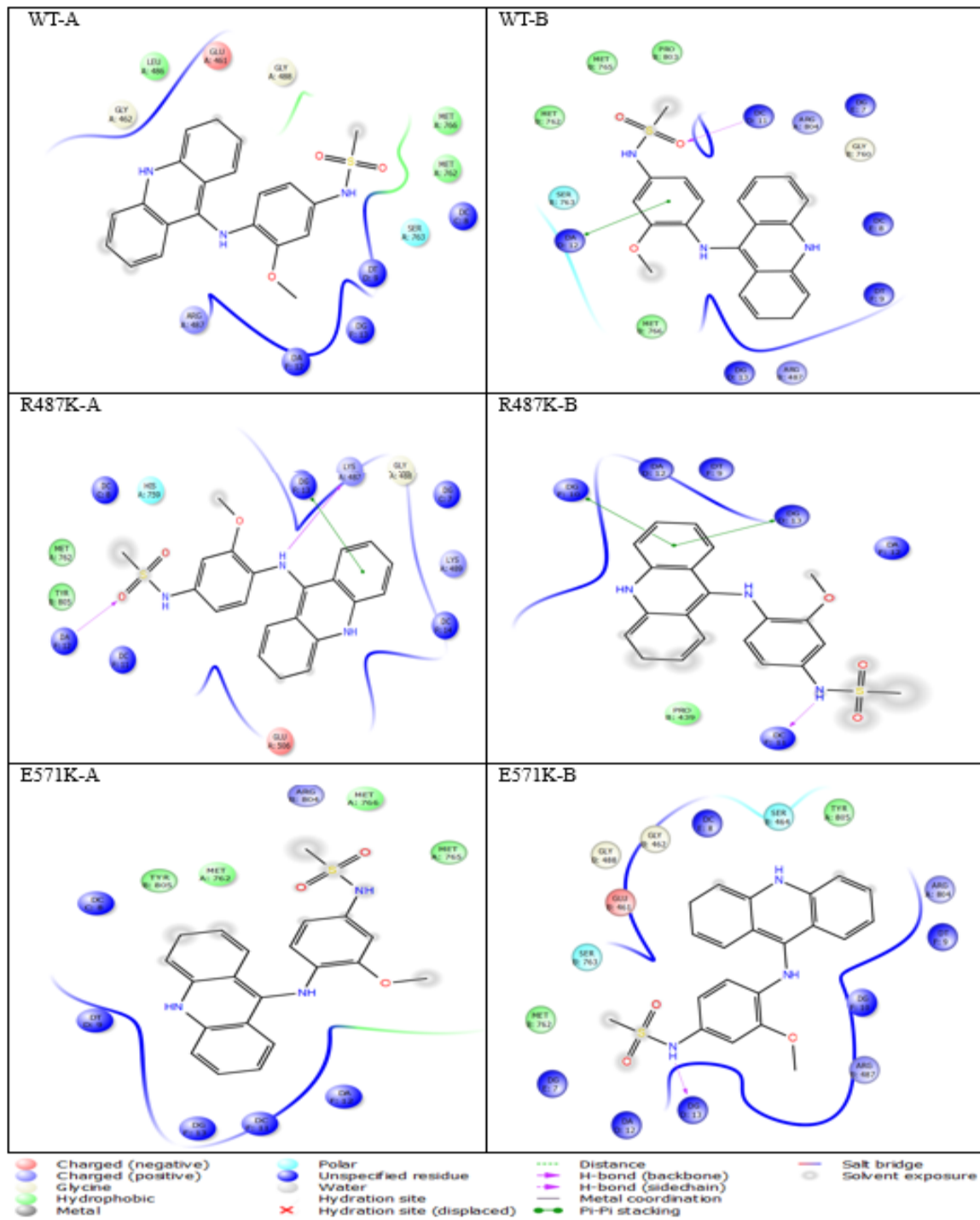


Figure S3. 2D interaction diagrams of Amsacrine with hTOP2 α WT and mutants. All complexes were aligned and superimposed using Maestro software.

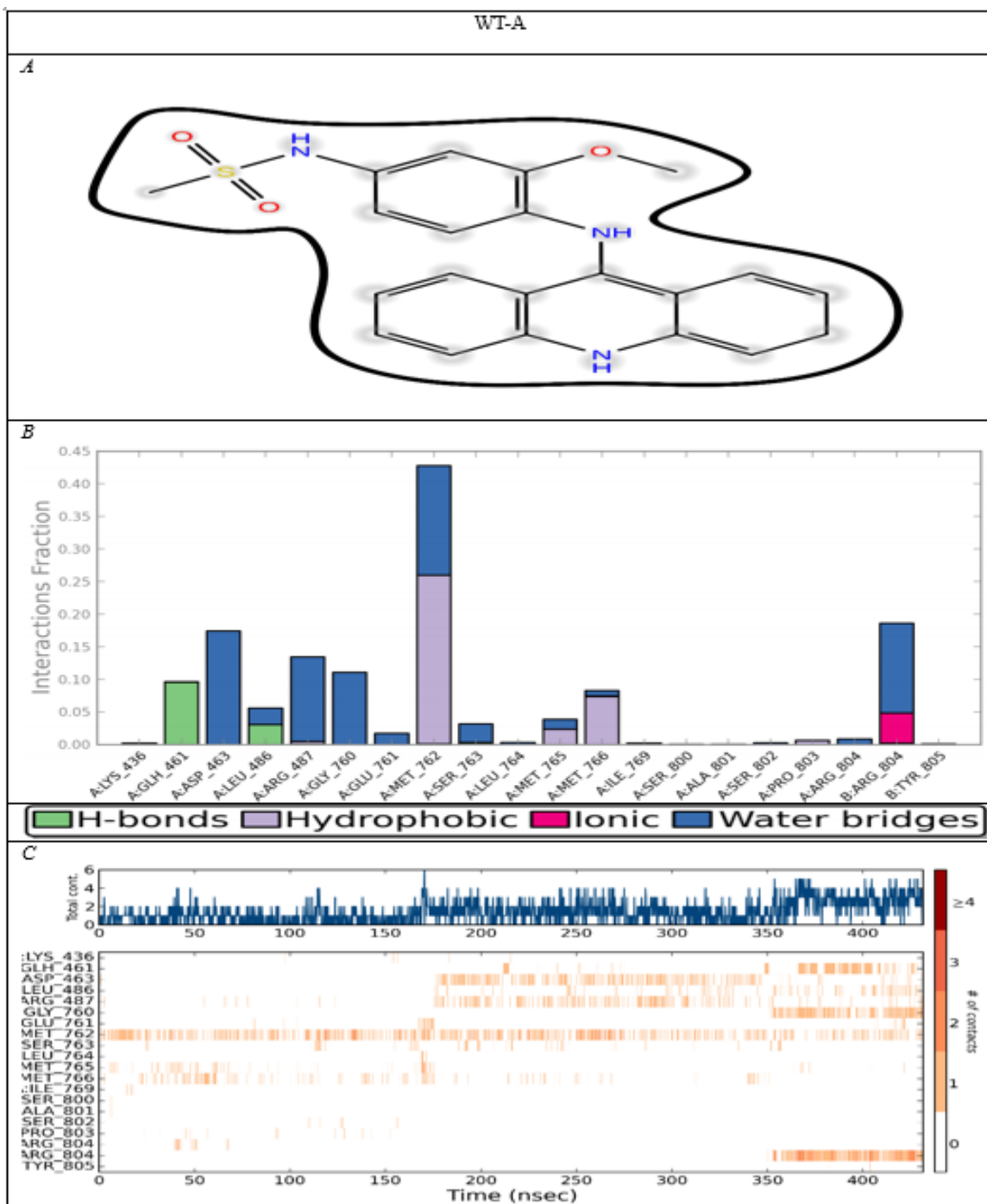


Figure S4. 2D profile data of Amsacrine binding to WT hTop2 α Chain A. (A) Interactions occurring more than 30% of simulation time. (B) protein interactions with ligands throughout simulation time. (C) Timeline representations of interactions and contacts.

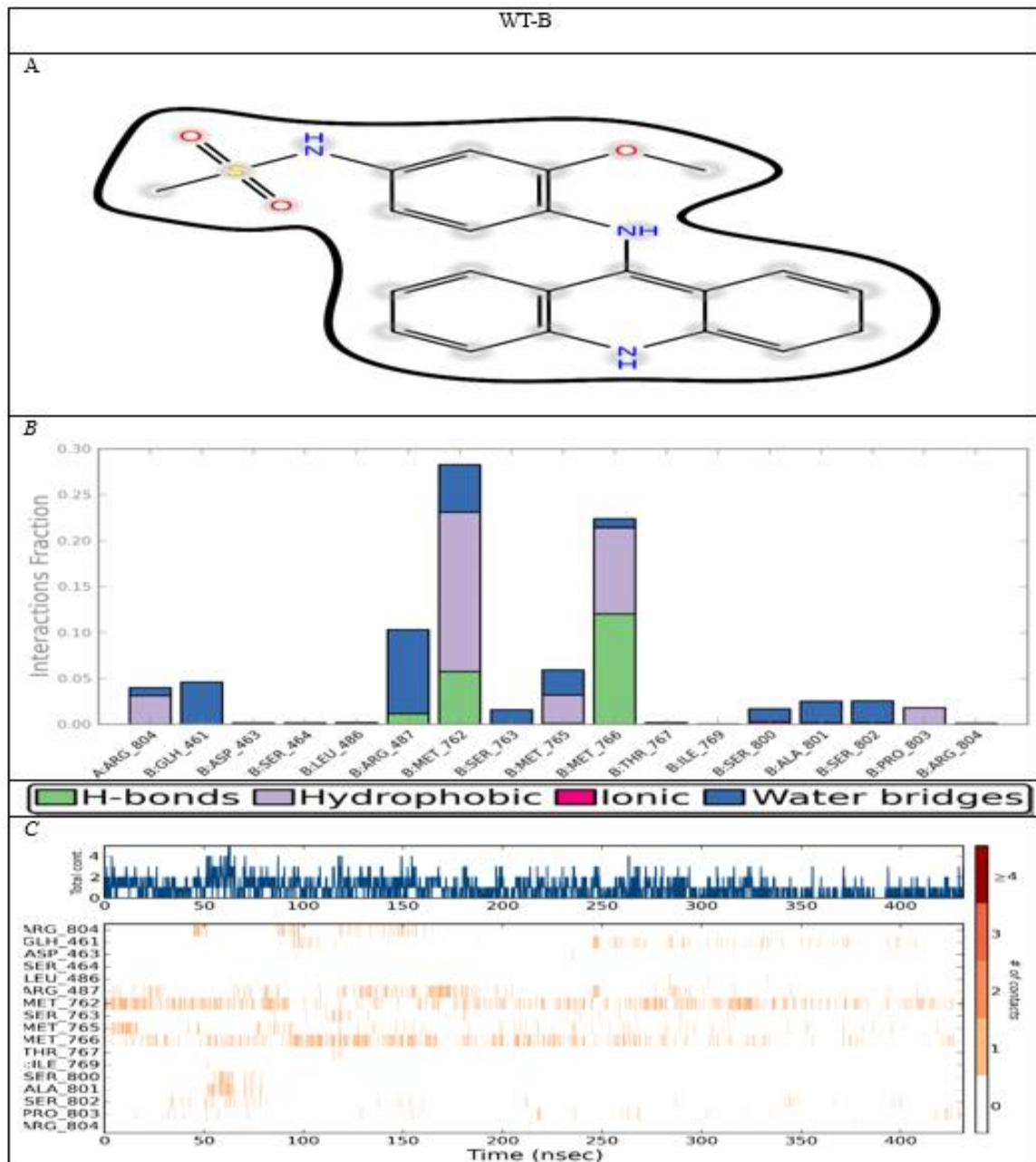


Figure S5. 2D profile data of Amsacrine binding to WT hTop2 α Chain B. (A) interactions occurring more than 30% of simulation time. (B) protein interactions with ligands throughout simulation time. (C) Timeline representations of interactions and contacts.

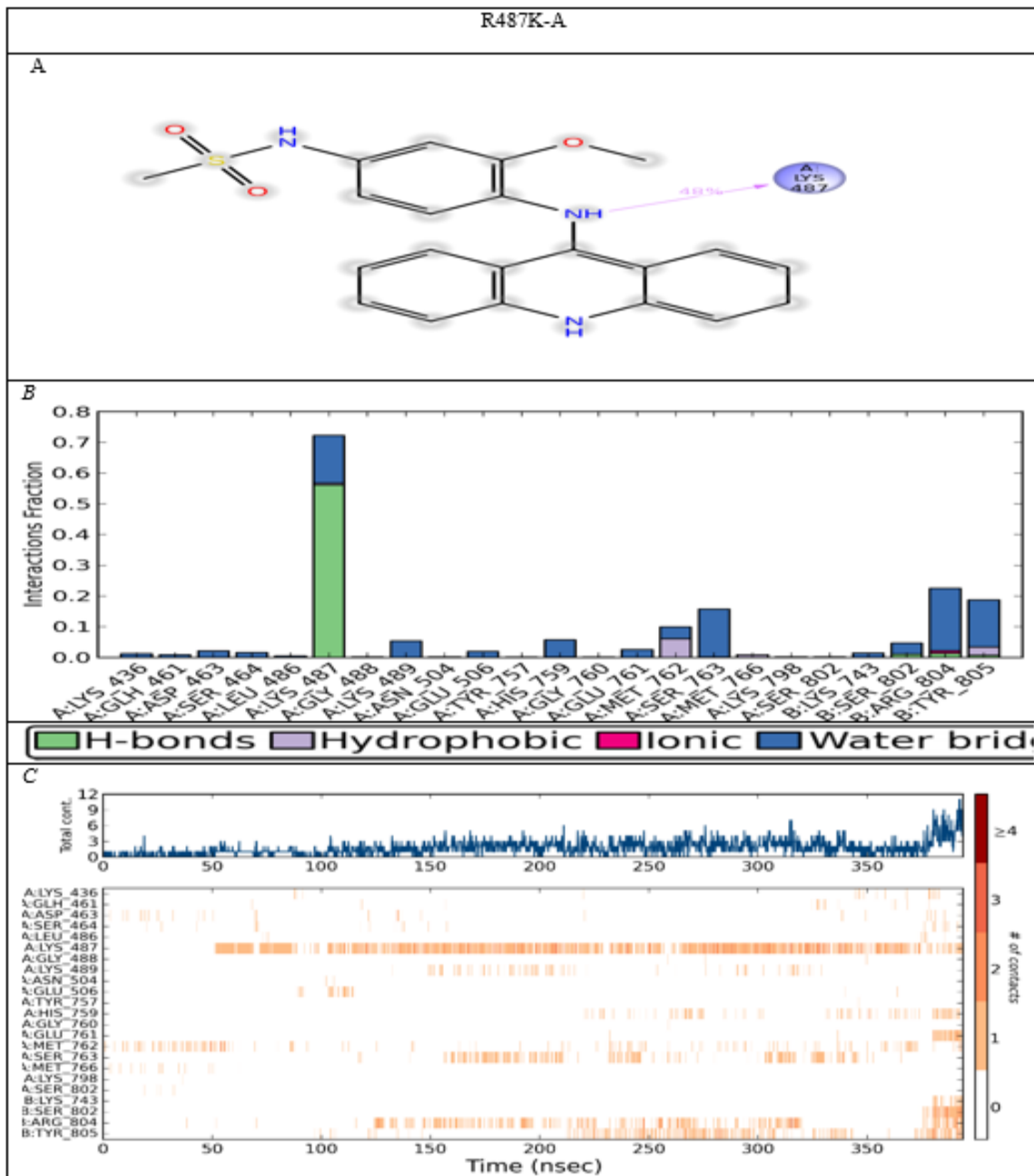


Figure S6. 2D profile data of Amsacrine binding to R487K mutant Chain A. (A) interactions occurring more than 30% of simulation time. (B) protein interactions with ligands throughout simulation time. (C) timeline representations of interactions and contacts.

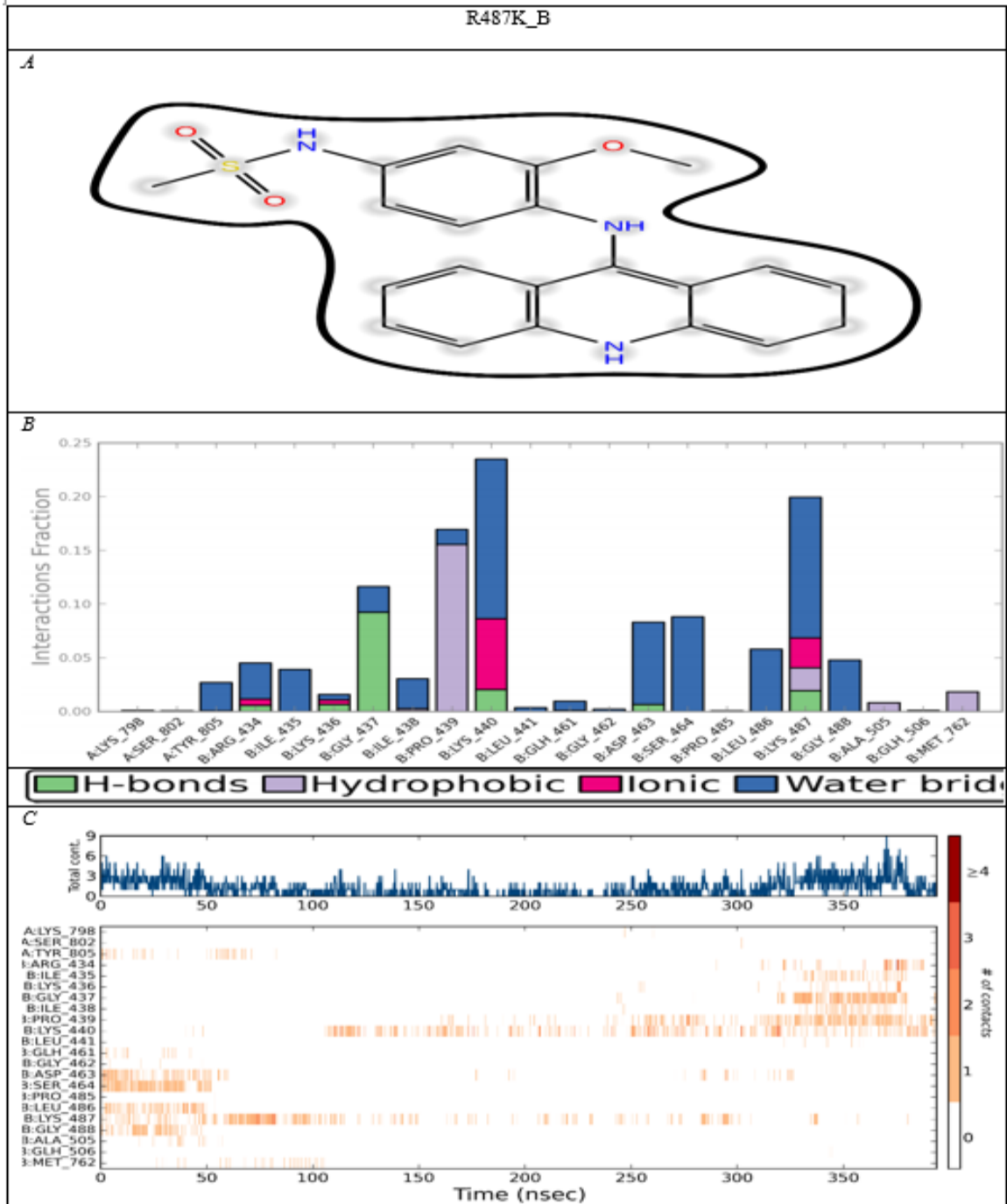


Figure S7. 2D profile data of Amsacrine binding to R487K mutant Chain B. (A) interactions occurring more than 30% of simulation time. (B) protein interactions with ligands throughout simulation time. (C) Timeline representations of interactions and contacts.

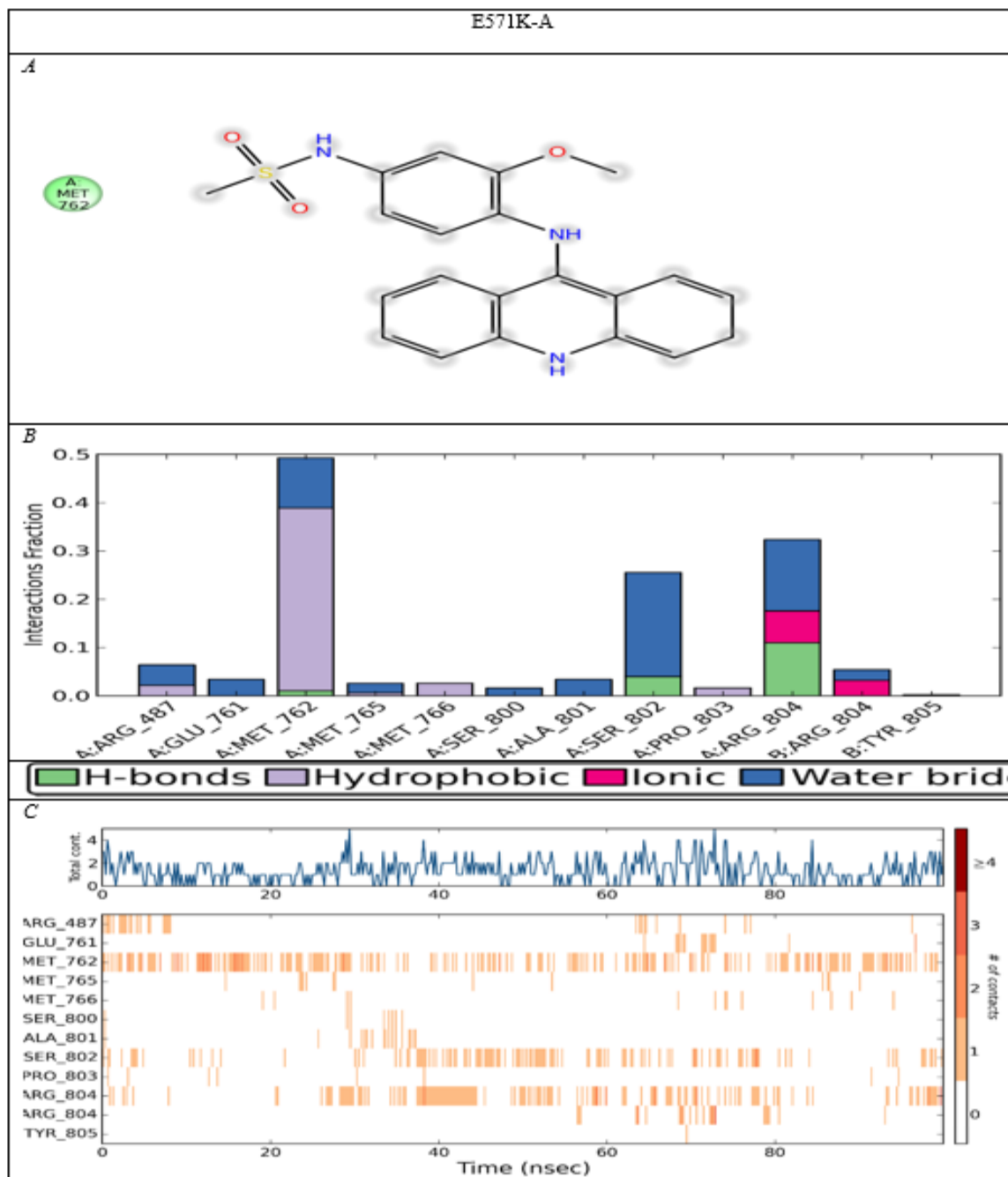


Figure S8. 2D profile data of Amsacrine binding to E571K Chain A. (A) interactions occurring more than 30% of simulation time. (B) protein interactions with ligands throughout simulation time. (C) timeline representations of interactions and contacts.

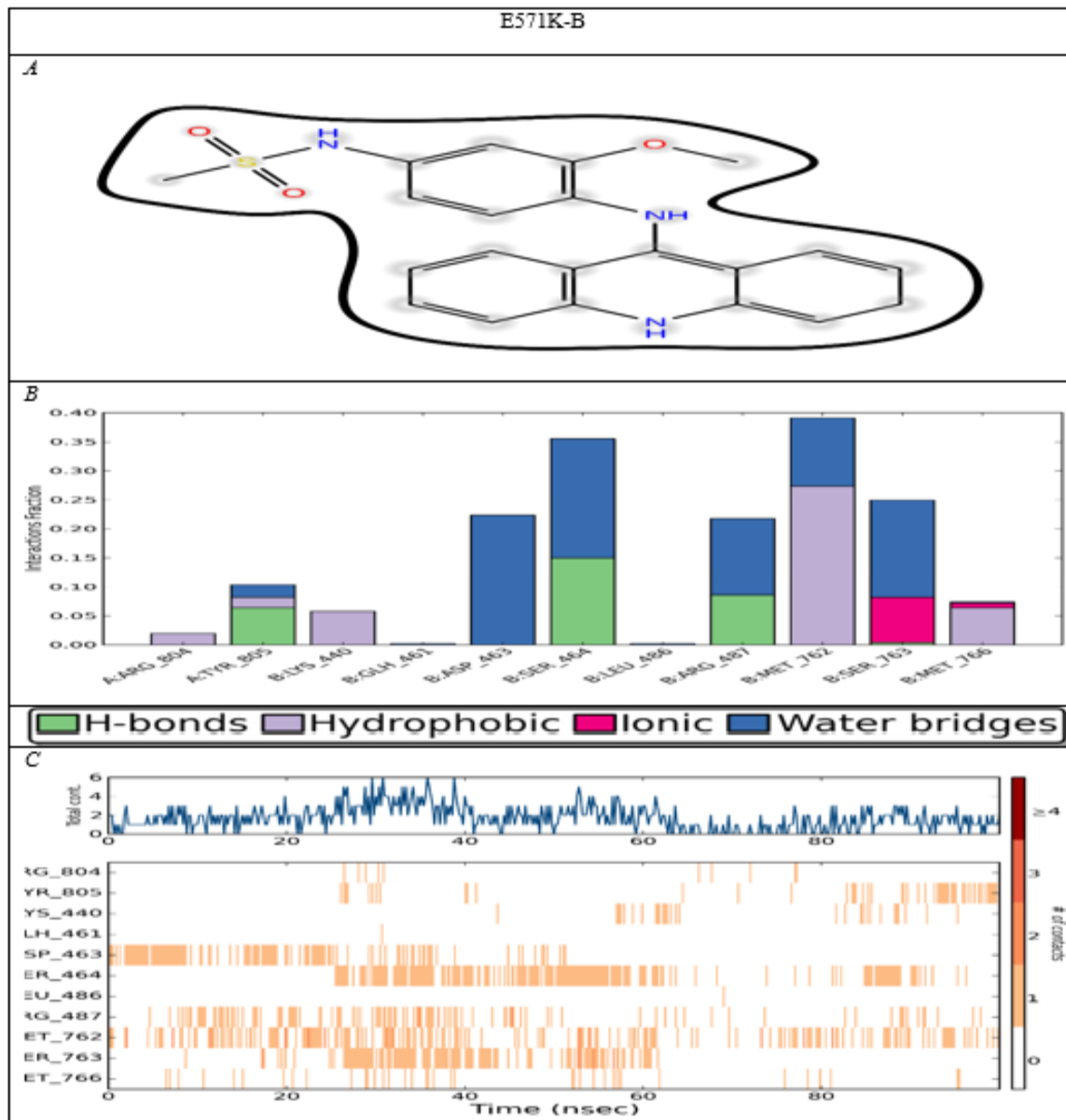


Figure S9. 2D profile data of Amsacrine binding to E571K Chain B. (A) interactions occurring more than 30% of simulation time. (B) protein interactions with ligands throughout simulation time. (C) timeline representations of interactions and contacts.

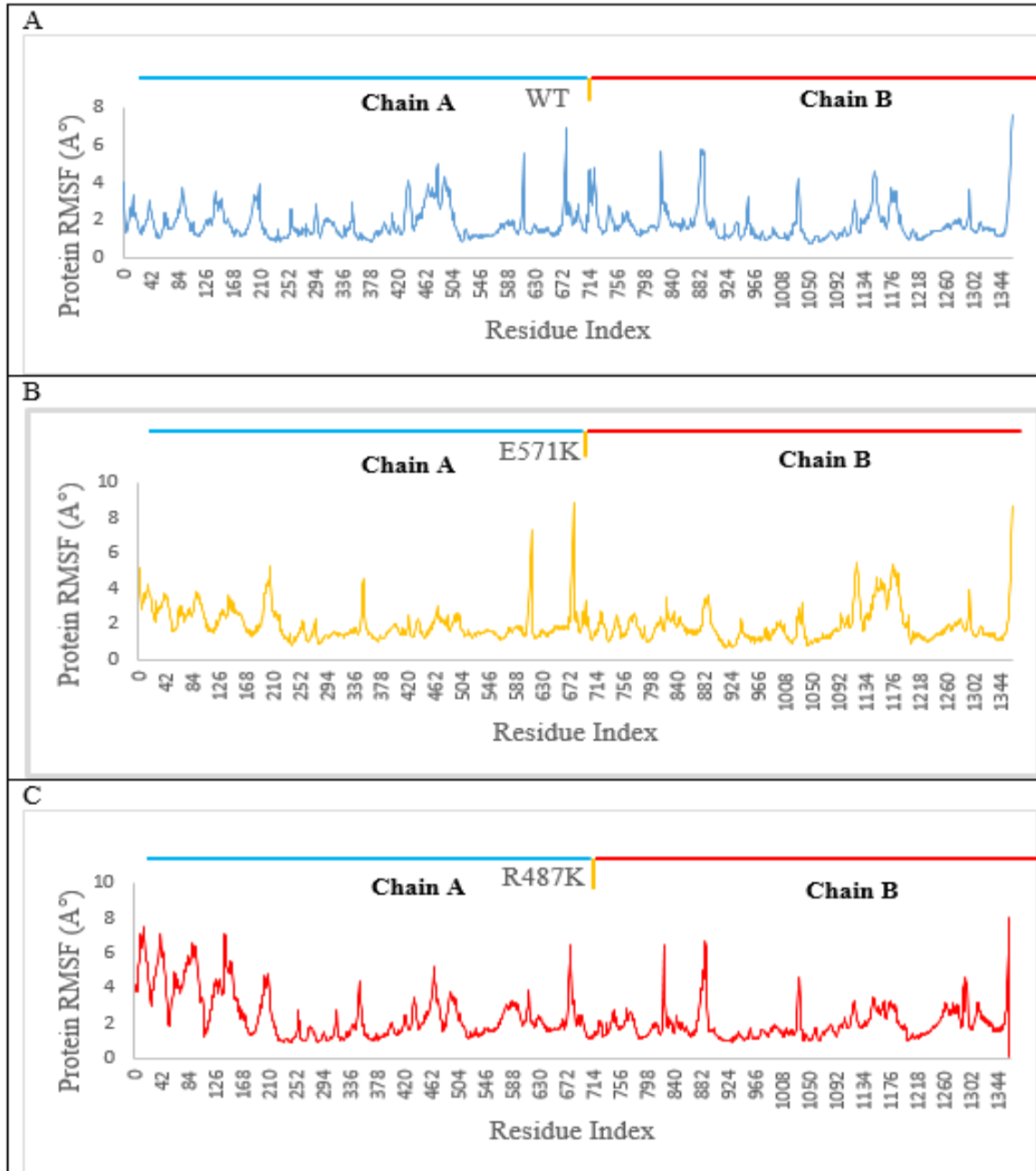


Figure S10. RMSF of hTop2 α WT and mutants in the complex with Amsacrine. Chain A sequence is: 0 - 678 .Chain B sequence is: 679 -1361.

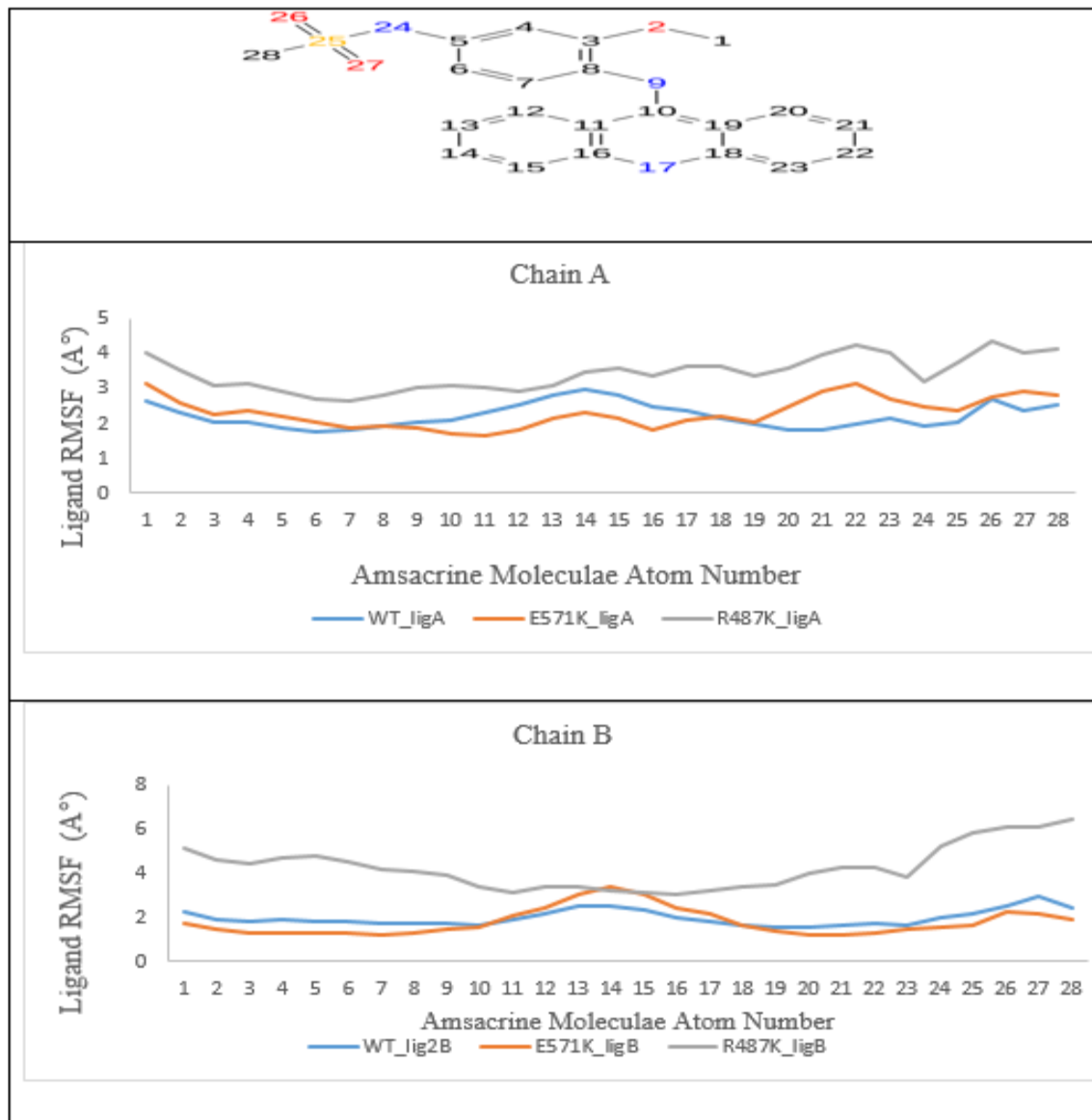


Figure S11. Ligand RMSF for the three complexes.

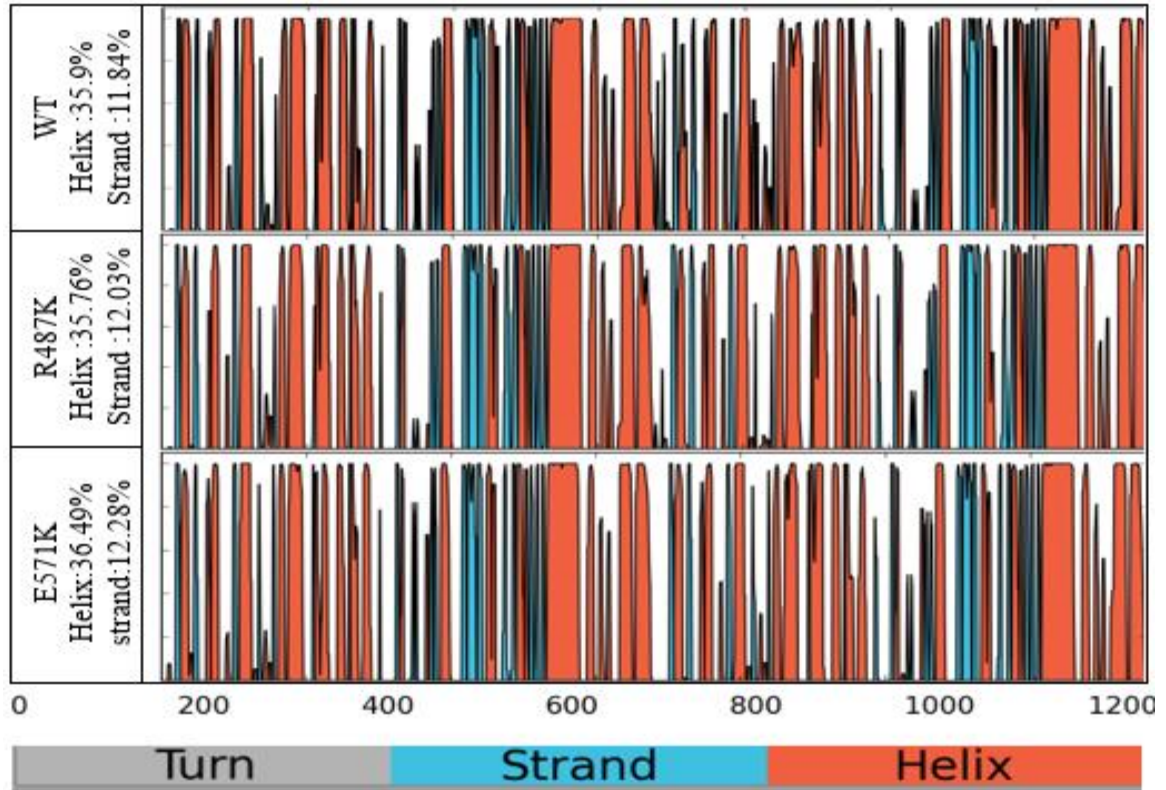


Figure S12. The secondary structure elements over the simulation time for the three complexes. All three complexes were aligned with Maestro software.

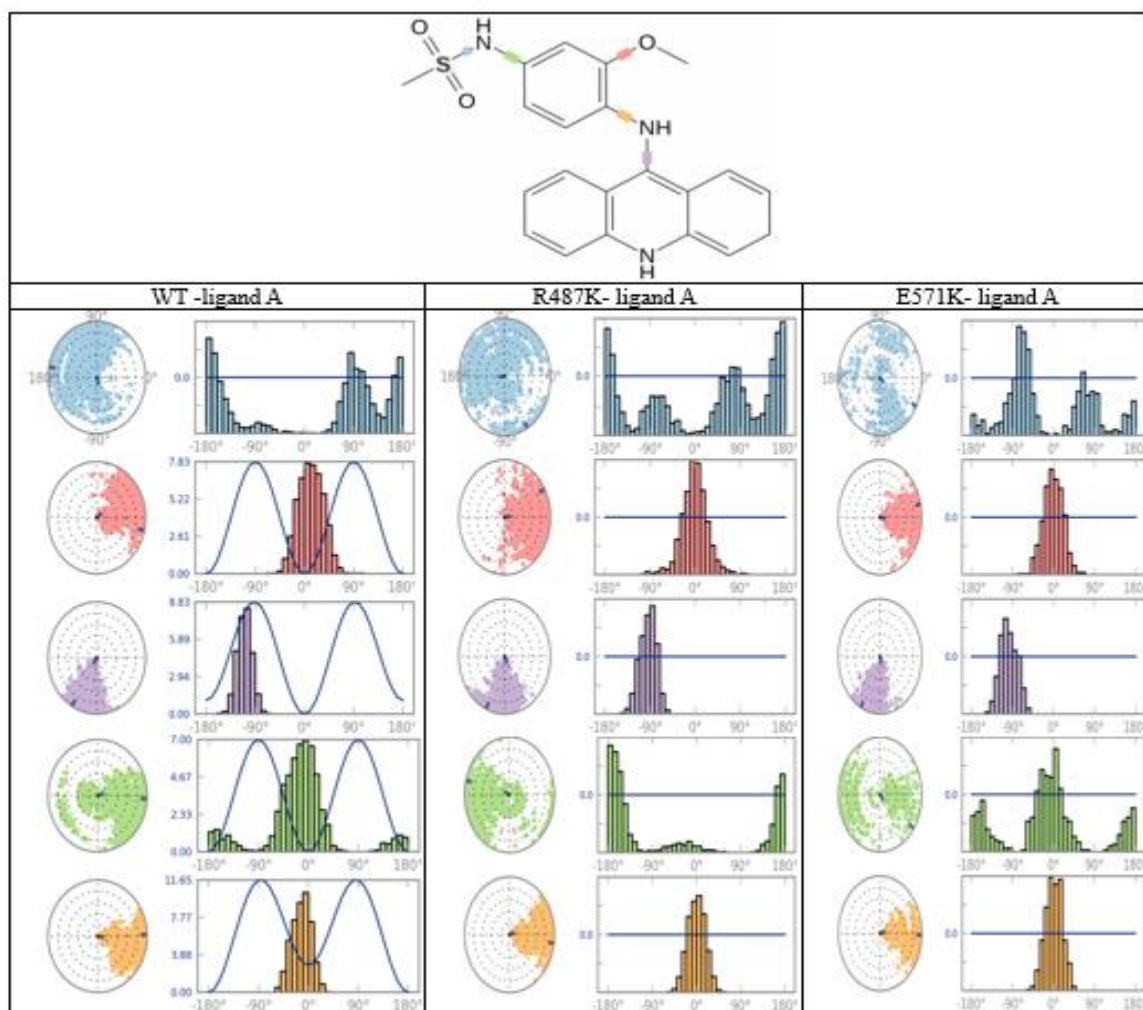


Figure S13. Ligand torsion profile of Amsacrine when binding to chain A of hTop2 α WT and mutants.

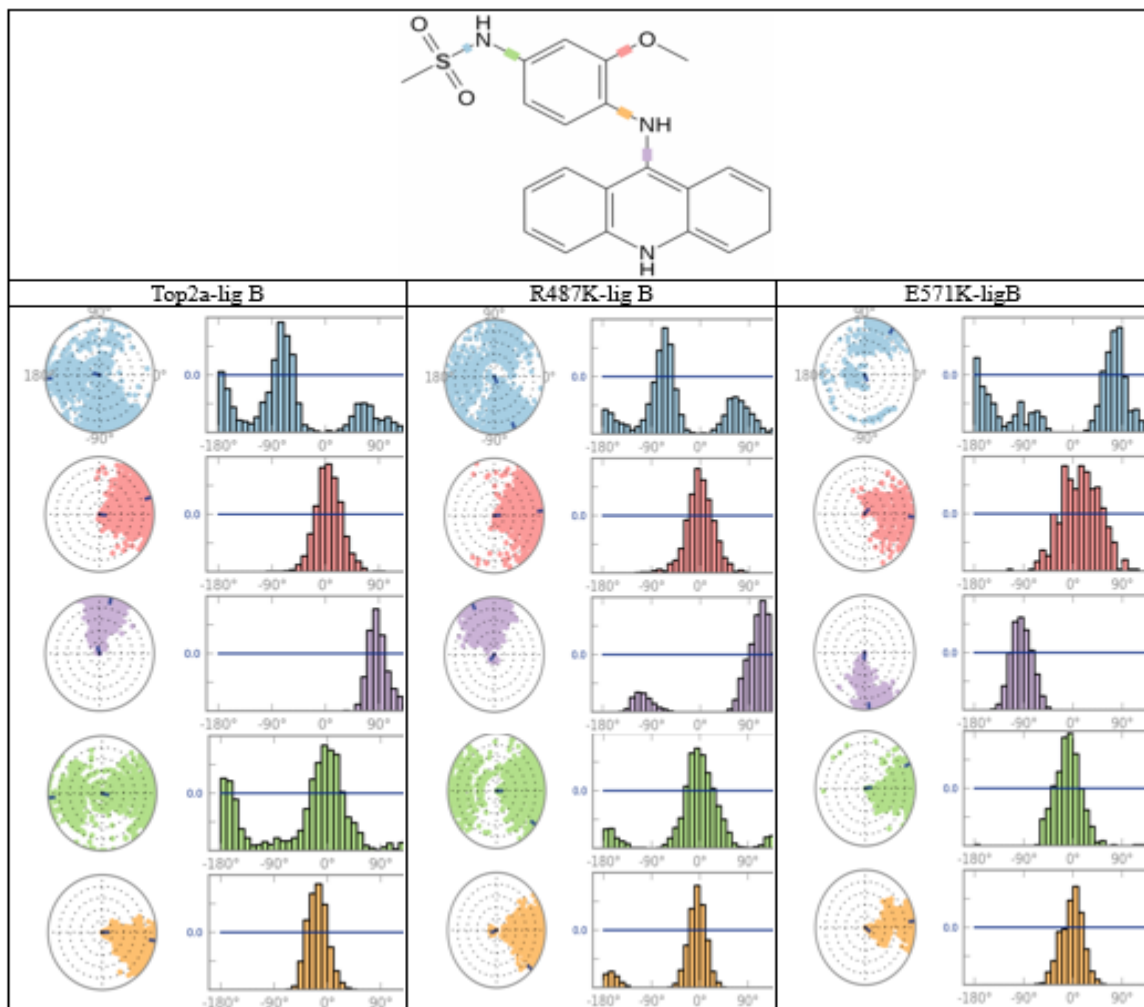


Figure S14. Ligand torsion profile of Amsacrine when binding to chain B of hTop2 α WT and mutants.